MIT-3944-5
MITNE-113

MASSACHUSETTS INSTITUTE OF TECHNOLOGY
DEPARTMENT OF NUCLEAR ENGINEERING
Cambridge , Massachusetts 02139

SOME APPLICATIONS OF GE(LI) GAMMA-RAY SPECTROSCOPY TO FUEL ELEMENT ASSAY

by
Yoshiyuti Hukai, N.C. Rasmussen, M.J. Driscoll

April, 1970

Contract AT (30-1)-3944
U.S. Atomic Energy Commission

MASSACHUSETTS INSTITUTE OF TECHNOLOGY

DEPARTMENT OF NUCLEAR ENGINEERING

Cambridge, Massachusetts

SOME APPLICATIONS OF GE(LI) GAMMA-RAY SPECTROSCOPY TO FUEL ELEMENT ASSAY

by

Yoshiyuti Hukai, N. C. Rasmussen, M. J. Driscoll

April, 1970

MIT – 3944 – 5

MITNE – 113

Contract AT(30-1)-3944

U. S. Atomic Energy Commission

DISTRIBUTION

MIT-3944-5 MITNE-113

AEC Research and Development Contract

U. S. Atomic Energy Commission, Headquarters
Division of Reactor Development and Technology
Reactor Physics Branch (2 copies)
Core Design Branch (1 copy)
Water Reactor Branch (1 copy)
Washington, D. C. 20545

U. S. Atomic Energy Commission
Savannah River Laboratory
Attn: B. C. Rusche
Aiken, South Carolina 29801 (1 copy)

AECL Chalk River Laboratory
Attn: C. Millar
Sheridan Park, Ontario, Canada (1 copy)

H. S. Potter, N. Y. Patent Group
U. S. Atomic Energy Commission
Brookhaven Office (1 copy
Upton, New York 11973 with 426 Form)

U. S. Atomic Energy Commission
Cambridge Office (2 copies)

ABSTRACT

It was the object of this work to study the gamma rays emitted by the products of the interaction of thermal neutrons with the nuclei of U-238, Th-232, U-235 and Pu-239 during and after irradiation and to explore some applications mainly to fuel element assay. An irradiation facility and a Ge(Li) detector cryostat were constructed for this purpose.

A new method of assaying a fuel rod containing a mixture of plutonium and uranium oxide, based on the difference in the observed yield of the fission products I-135 and Sr-92, has been developed.

The energies and intensities of the thermal neutron capture gamma rays for U-238 and Th-232 were determined. Four new lines have been found in the energy region previously unexplored for U-238. For Th-232, 66 certain lines were found, compared to 7 lines in the literature.

Many prompt gammas emitted by the highly excited fission products following the fission of U-235 and Pu-239 were resolved in the energy region above 1.4 MeV. For U-235 fissions, 57 lines were found, and for Pu-239, 51 certain lines were recorded. The use of prompt gammas for assaying fuel rods was investigated. An accuracy of about ± 7% was obtained for the analysis of U-238 content; ± 10% to ± 20% accuracy was obtained for U-235 analysis in the range of 1% to 2% enrichment; and ± 35% accuracy for the analysis of 0.25% Pu-enriched rods. It has been found that Ge(Li) detectors can be operated as fast neutron detectors and used to determine the relative neutron yield. With this method, the enrichment of uranium rods can be found with an accuracy of ± 1% to ± 2% in the range from 1% to 2% enrichment.

Finally, some considerations were given to the use of prompt gamma rays for measuring the initial conversion ratio C and the neutron yield parameter η.

ACKNOWLEDGMENTS

The work described in this report was made possible through the support of the M. I. T. Reactor Physics Project which is sponsored by the United States Atomic Energy Commission. This work has been performed primarily by the principal author, Y. Hukai, who has submitted the same report in partial fulfillment of the requirements for the Ph.D degree at M. I. T.

Overall direction of this work has been shared by Professors M. J. Driscoll and N. C. Rasmussen. The constructive advice of Professor Franklyn M. Clikeman on Ge(Li) detectors, the cryostat and the associated electronics is greatly appreciated. Appreciation is also extended to the following persons whose help and stimulating discussions during the many phases of this work were especially valuable: Dr. Victor J. Orphan, Dr. John Hamawi, Dr. Akira Watanabe, Dr. Thomas L. Harper, Mr. Albert Supple, Mrs. Bonnie Hites and Mr. Chuzo Takahata.

Greatly acknowledged are the assistance, patience and cooperation of the M. I. T. Reactor Machine Shop Staff, Radiation Protection Officers, Reactor Operation Personnel and the M. I. T. Computation Center. Thanks are extended also to Mrs. Mary Bosco for the typing of this report.

TABLE OF CONTENTS

TABLE OF CONTENTS (continued)

TABLE OF CONTENTS (continued)

TABLE OF CONTENTS (concluded)

LIST OF FIGURES

LIST OF FIGURES (continued)

LIST OF FIGURES (concluded)

LIST OF TABLES

LIST OF TABLES (concluded)

Chapter I

INTRODUCTION

The objective of the present work was to study the gamma rays emitted by the products of the interaction of thermal neutrons with the nuclei of U^{238}, Th^{232}, U^{235} and Pu^{239}, during and after irradiation, and to explore some applications concerned with Reactor Physics.

For this purpose, an irradiation facility was constructed and a high resolution Ge(Li) detector spectrometer was used. The experimental equipment is described in Chapter II.

The fission product gamma rays from the fission of U^{235} and Pu^{239} observable after the irradiation is over will be referred to as delayed gamma rays in this work. Those appearing during the bombardment by thermal neutrons (but not after) will be referred to as prompt gamma rays, even though some of these gamma rays may come from very short-lived fission products.

Due to the interest in burnup measurements, the analysis of delayed gamma rays with lifetimes from a few minutes to several years has been done extensively elsewhere (G1, O1, H1) and will not be a subject for further investigation here. But instead, an application of these gamma rays for the purpose of assaying fuel rods containing a mixture of plutonium and uranium is proposed. This method is based on the difference in yield of certain observable fission products of U^{235} and Pu^{239}. This subject is treated in Chapter III.

The study of prompt gamma rays coming from fuel elements is still far from exhausted and many results obtained in this work are unknown in the published literature. The study of prompt gamma rays may be divided into two distinct categories: those not involving the fission process, which is the case of the thermal neutron capture gamma rays for U^{238} and Th^{232}, and those involving fission which is the case for U^{235} and Pu^{239}. This separation is natural not only because of the presence of the prompt fission gamma rays but also because, together with the gamma rays, fast fission neutrons are emitted and this fact imposes extra problems of background reduction in obtaining the gamma spectra for these nuclei.

The capture gamma rays for U^{238} have been studied by Sheline et al. (S1) using a high resolution Ge(Li) detector, and in the low energy region by Maier (M1) using a diffraction spectrometer. Thus, the present results for U^{238} have mainly the purpose of confirming the data presented by those authors. For Th^{232}, Groshev (G2) and Burgov (G5) have studied the radiative capture gamma rays using magnetic Compton spectrometers and have reported up to seven lines. In the present work, with a spectrometer of about five times better resolution, 66 distinct lines have been found. The data for Th^{232} have importance for shielding calculations and for prompt activation analysis. For nuclear physicists, the radiative capture gamma rays together with (d, p) reaction data are useful for the study of the properties of the levels of Th^{233}, which is of particular interest because Th^{232} is the only naturally occuring isotope of Th. The results for U^{238} and Th^{232} are treated in the first part of Chapter IV.

For the cases of U^{235} and Pu^{239}, very little is available in the literature concerning their prompt gamma rays. Netter et al. (N1), using a time-of-flight technique, observed a 4.49-MeV gamma-ray line which they could assign as a prompt gamma ray from the absorption of a neutron by U^{235}. Bartholomew and Campion (B1) observed this line earlier and attributed it to the decay of Rb^{90}, which is a fission product. Greenwood (G3) has obtained the spectra of the prompt gamma rays for U^{235} and Pu^{239} using a NaI crystal, but no significant structure can be distinguished in his spectra above a few hundred keV. The lack of structure may be blamed on the background caused by fission neutrons interacting with the detector material. The present results show clearly more than fifty peaks for both U^{235} and Pu^{239} spread over the energy range above 1.4 MeV in the pair spectrometer gamma spectra. This subject is presented in the last part of Chapter IV.

Chapters V and VI treat two applications using prompt gamma rays. The first is the use of the prompt gamma rays for identification and assay of uranium fuel rods and rods containing a mixture of plutonium and uranium oxide; and the second, some considerations pertinent to the development of new techniques for measuring reactor physics parameters based on high resolution gamma-ray spectroscopy. A conceptual design for a gamma spectrometer operating with the M.I.T. Exponential Facility is also presented.

In Chapter VII, conclusions and recommendations are summarized.

The bibliography is given in Appendix A. Appendix B contains a description of computer code FUEL ASSAY, used in the method employing fission product decay gammas.

Chapter II

EXPERIMENTAL EQUIPMENT

2.1 INTRODUCTION

A permanent irradiation facility using the neutron beam port 4TH1 of the MIT Research Reactor is described in the next section. This facility is composed of two parts: the front facility closer to the reactor, followed by the rear facility using the same neutron beam.

The many advantages of using the triple coincidence mode for counting gamma rays of high energy (> 1.5 MeV) and the Compton suppression mode in the low energy portion (150 keV to 2.5 MeV) were demonstrated previously by Orphan (O2) and Harper (H2). Because of these advantages, in this present work the experiments involving prompt gamma rays were performed using the front facility which is equipped with a spectrometer with a fixed cryostat capable of counting gamma rays in either of these modes of operation.

On the other hand, fission product gamma rays require a high efficiency detector, and frequently a different geometry for irradiation and counting, so that a simple and movable cryostat with a large detector operating in the free mode was preferred. In this case, the rear irradiation facility was equipped and used for such delayed gamma-ray experiments.

2.2 DESCRIPTION

2.2.1 The Irradiation Facility

An overall top view of the irradiation facility is shown in Fig. 2.1. This is a permanent external irradiation facility which uses the neutron beam port 4TH1 of the MIT Research Reactor. It is composed of two basic parts: one, closer to the reactor wall, was designed by Harper (H2) as a part of the research for his doctoral thesis on capture gamma yield determination and it is an improved version of a spectrometer previously designed by V. J. Orphan (O2) two years before; the other, connected behind Harper's facility but using the same neutron beam, was designed by the principal author, and it is primarily used for irradiation of lattice fuel rods and large samples.

The neutrons from the reactor core are scattered by a graphite plug, 3-7/8 inches in diameter and 40 inches long, placed inside the 4TH1 tangential through-port next to the reactor core; the resulting scattering source forms the neutron beam for the external irradiation facility. The positioning of this graphite plug was optimized to have a maximum neutron flux available at the sample positions in the external irradiation facility. A steel collimator, tipped by a protective cadmium sleeve encased in aluminum cladding, reduces the neutron beam diameter to 3-1/2 inches upon exit from the port. This collimator, by reducing the diameter of the beam port, lowers the epithermal and fast neutron background in the area of the gamma detector by several orders of magnitude.

In order to avoid excessive detector background due to scattering of beam gammas by the sample being irradiated, a 1-1/2-inch-long lead

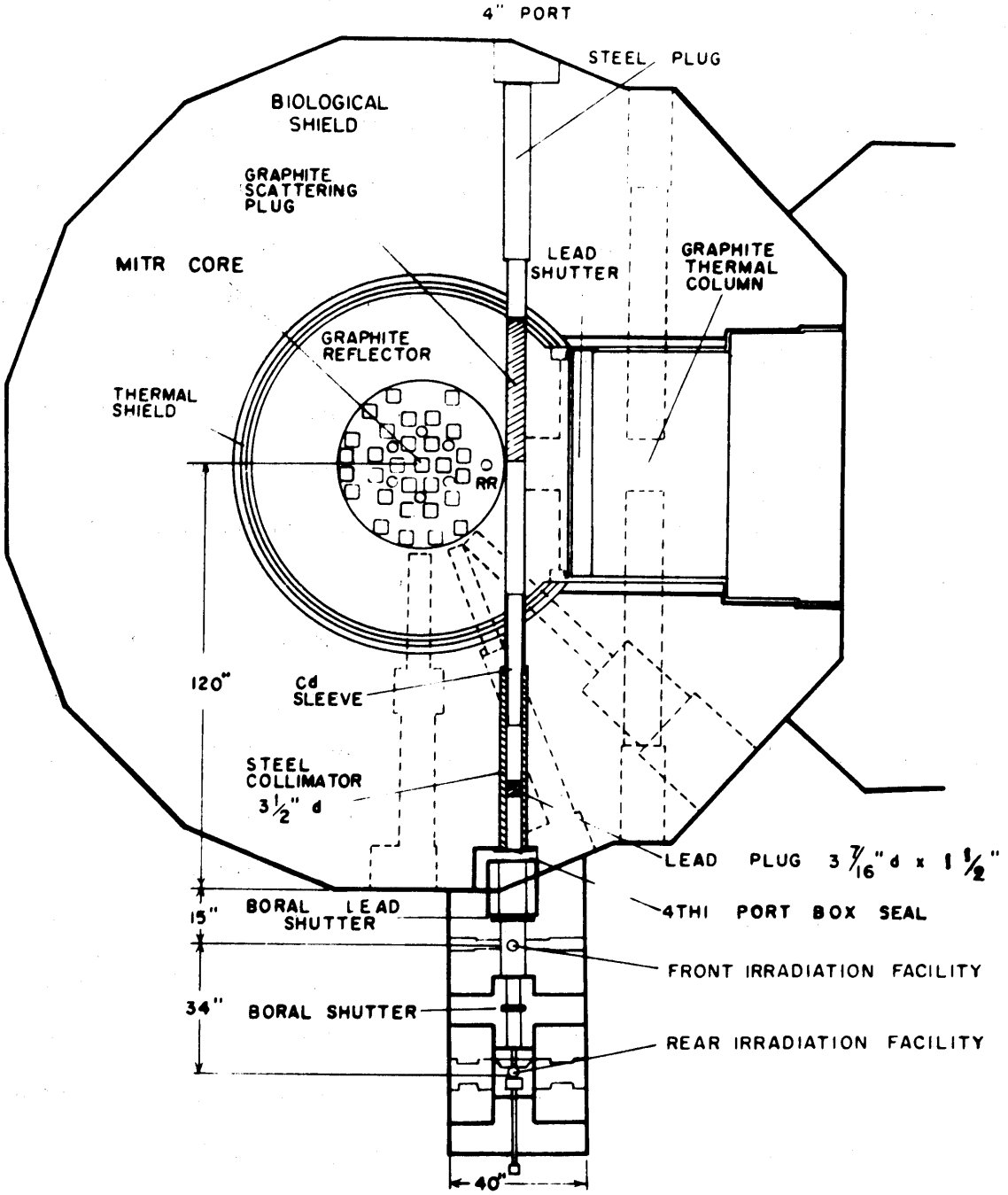

FIG. 2.1 TOP VIEW OF MITR CORE AND 4THI IRRADIATION FACILITY

plug clad in 1/16-inch-thick aluminum was placed 19 inches into the steel collimator. This plug was originally 2-3/4 inches long during Harper's experiments, but its length was reduced to 1-1/2 inches in order to increase by a factor of two the neutron flux at the irradiation facility without increasing excessively the gamma dose from the reactor. The beam port is sealed by a 1/8-inch-thick aluminum plate to prevent radioactive argon gas from escaping through the port.

A more detailed plan view of the irradiation facility is shown in Fig. 2.2. The primary shielding material used is heavy concrete, with masonite and boral used to thermalize and capture stray neutrons. Lead is used for shielding and collimation of gamma rays in most of the access ports of the facility. The thermal neutron beam coming from the reactor port can be interrupted at two distinct places preceding each of the two irradiation positions by two back-to-back boral plates of 1/4-inch thickness. A detailed description of the front facility is given by Harper in reference H2. The rear facility, although primarily designed for irradiation of fuel rods, is flexible enough for carrying out many kinds of experiments involving prompt and delayed gamma rays, gamma-gamma coincidence and neutron transmission. Basically, it has a central chamber in the form of a 10-inch square, 3 inches high, with five access ports. It is equipped with a V-notch holder that can keep the fuel rod under irradiation in a position aligned with the side collimators and the detector. The fuel rod is irradiated standing vertically on the floor, and may be of any reasonable height. It can be scanned continuously over a length of 21-1/2 inches, which is the height of the neutron beam above the reactor building main floor.

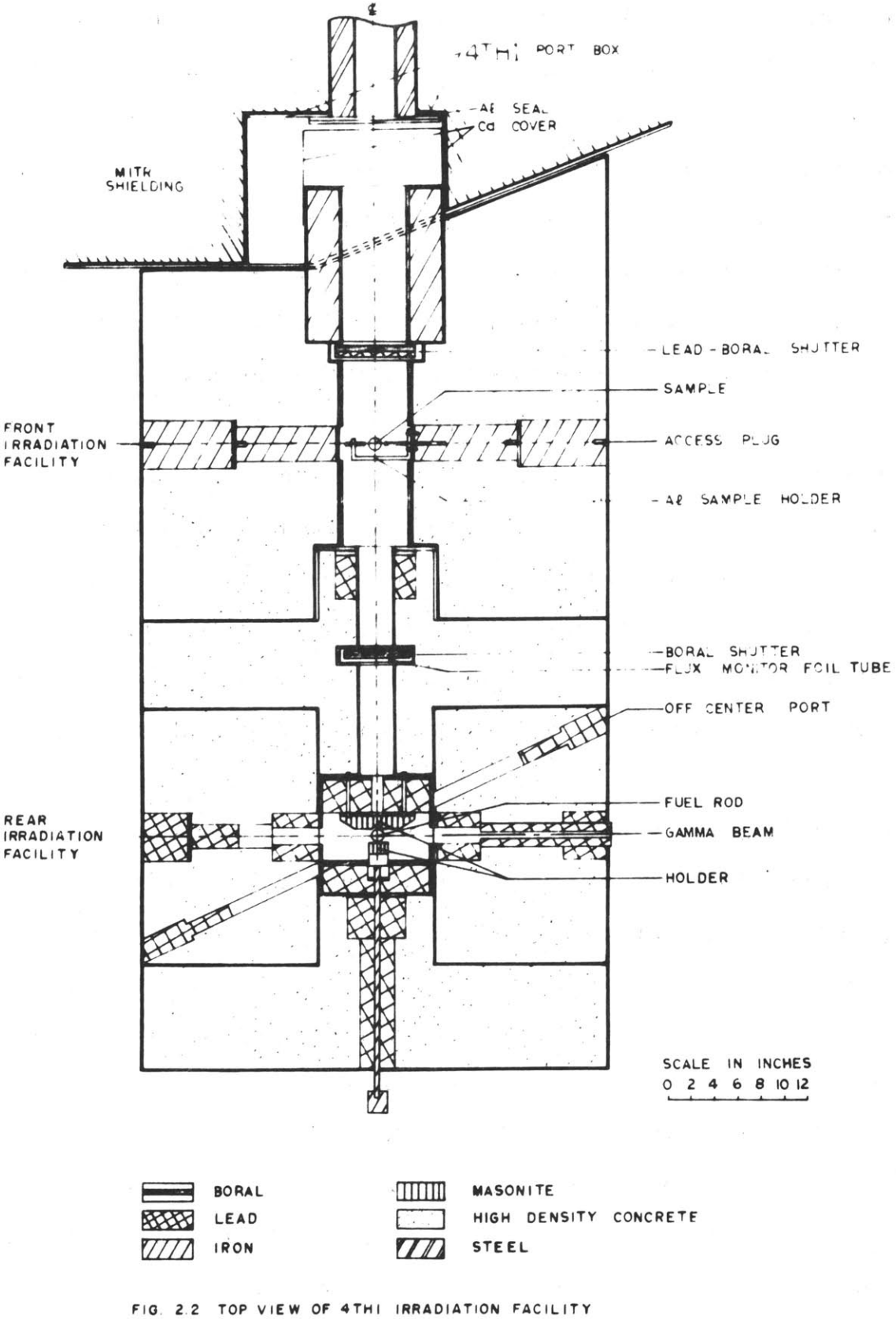

FIG. 2.2 TOP VIEW OF 4THI IRRADIATION FACILITY

Figure 2.3 shows how the irradiation is performed in both irradiation positions: (a) for the front facility, and (b) for the rear facility. At the front facility, the sample is inserted into the irradiation position through one of the side access ports, and the gamma rays coming from the sample are collimated vertically by a set of lead collimators with 1-inch-diameter holes topped by a replaceable 6-1/2-inch-long lead segment. A segment with an opening of 3/4 inch was used throughout this present work. The shielding along the gamma-ray flight path was varied according to the requirements set for each experiment, as described in Chapter IV. This shielding was necessary to protect the Ge(Li) detector either from the thermal or the fast neutrons, or both.

The detector and the surrounding NaI(Tl) annulus of the spectrometer located at the front facility are placed inside a gamma-ray shield of 5 inches of steel plus 3/4 inch of lead built by Atomium Corporation, which has been described by Hanson (H4). This shield casket serves also as a rigid base for positioning the Ge(Li) detector and the surrounding sodium crystals accurately with respect to one another and to the collimated gamma-ray beam emerging from the sample which is 96 cm below. The aluminum sample holder, as shown in Fig. 2.3(a), is attached to a boral-tipped steel plug, and an accurate positioning of that access plug insures that the holder and the sample are positioned in a reproducible geometry.

In this work, all the experiments involving prompt gamma rays were performed at the front facility, with the exception of the measurements of fission neutron yield which, while they also involved prompt gammas, were performed at the rear facility. All the irradiations for

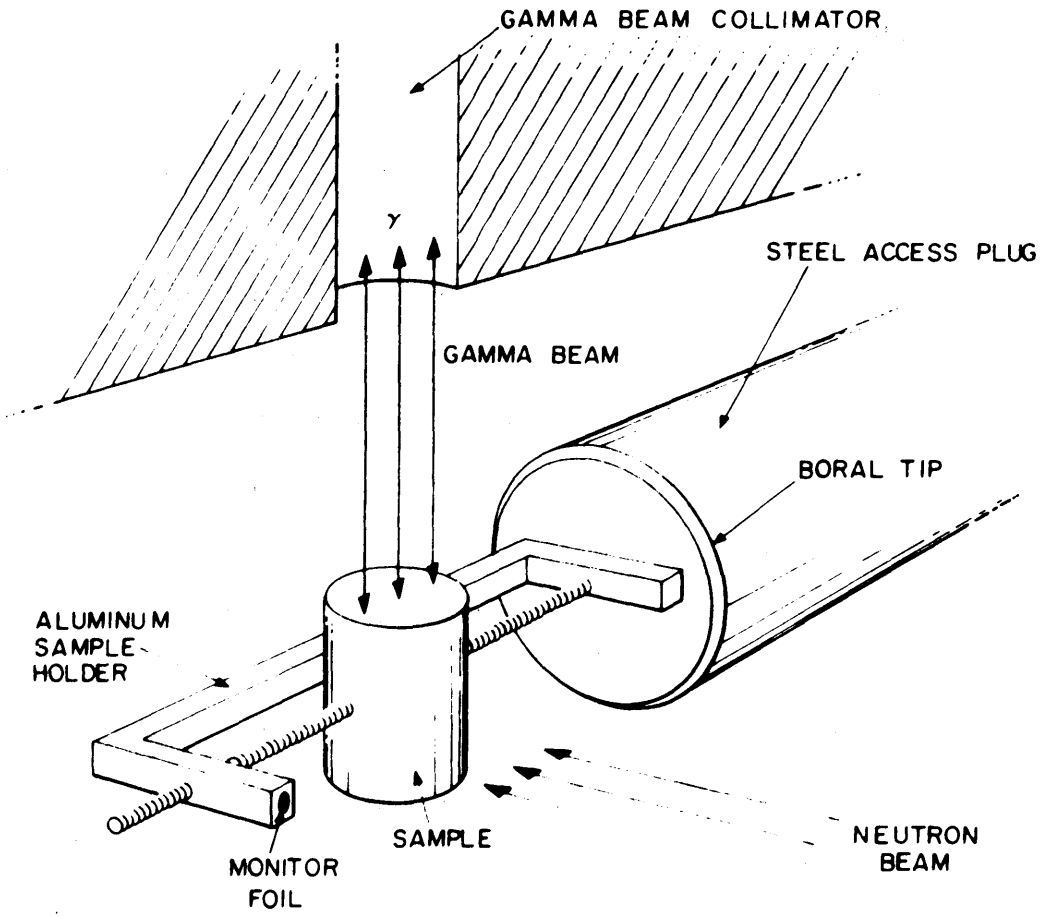

FIG 2 3 (a) GEOMETRIC CONFIGURATION FOR FUEL SAMPLE IRRADIATION AT THE FRONT FACILITY

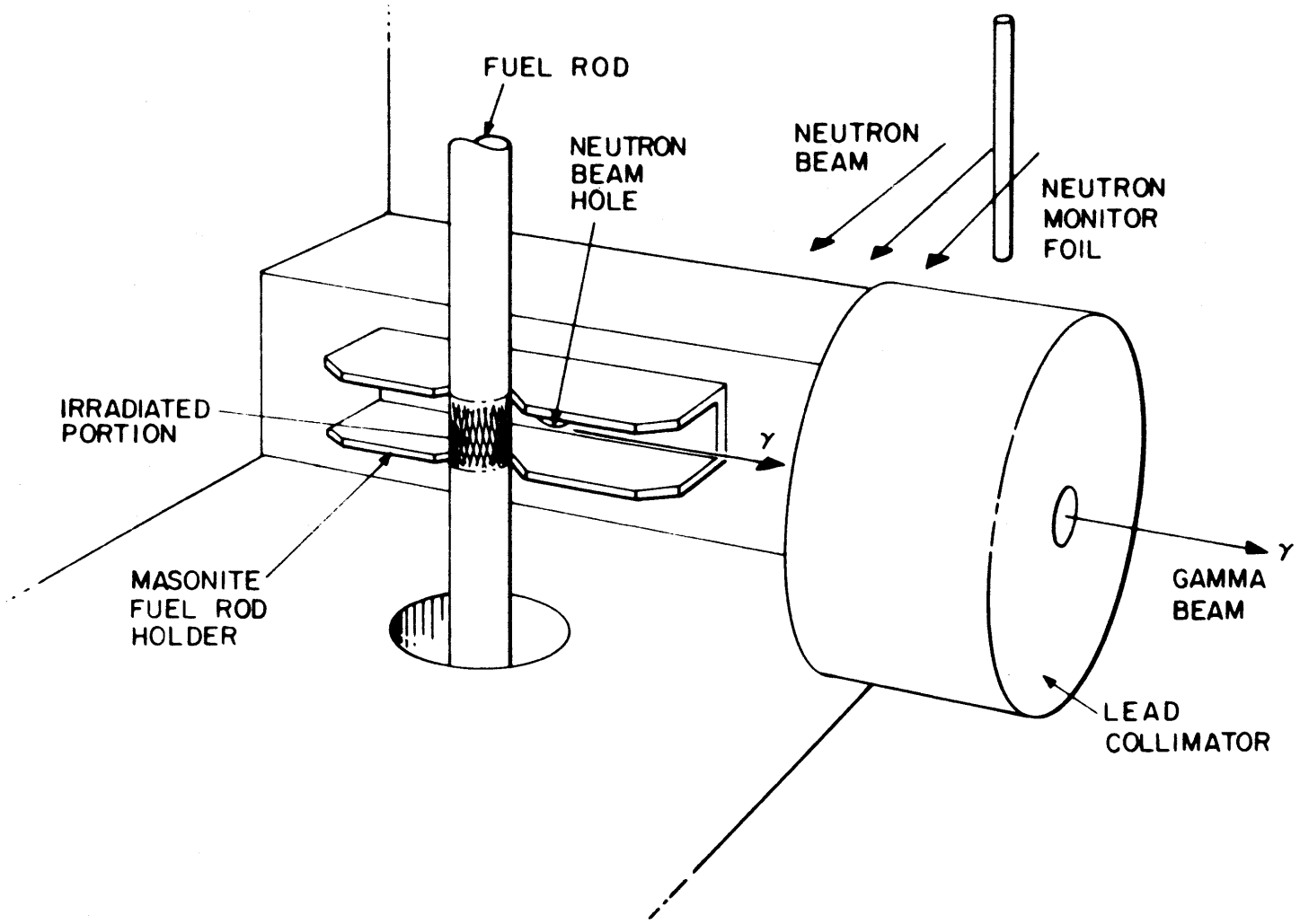

FIG. 2.3 (b) GEOMETRIC CONFIGURATION FOR FUEL ROD IRRADIATION AT THE REAR FACILITY

experiments involving the fission product gammas were performed at the rear facility. In this latter case, the irradiated samples were taken out of the irradiation position after the irradiation was over and placed in a counting arrangement outside the facility in order to avoid the background contribution from the irradiated shielding structure. A detailed account of these delayed gamma experiments is given in Chapter III.

2.2.2 The Cryostats and Detectors

Two gamma detecting systems, both with Ge(Li) detectors, were used in this present work. One of them used a 35-cc coaxial detector with 24 cc of active volume. It was used in all the experiments involving the fission product delayed gammas and in the fission neutron yield determinations. The other, a planar, hexagonal-shaped, 7-cc Ge(Li) detector with 5 cc of active volume, was used in conjunction with the pair spectrometer in all the experiments involving the prompt gammas. The use of two different detectors was dictated by availability, the nature of the experiments and the obvious convenience of having two independent systems operating alternately in conjunction with one multichannel analyzer.

The 35-cc detector was mounted beneath a 2-liter capacity, inner cylindrical vessel containing liquid nitrogen (LN), surrounded by a 5-inch-diameter, 0.030-inch-thick, outer cylinder of stainless steel, and was made by A. D. Little, Inc. A vacuum of less than 10^{-5} Torr was maintained by a 1-liter/sec Varian ion pump. This detector was operated in the free mode in the rear facility. The schematic diagram of the vacuum dewar and electronics is shown in Fig. 2.4.

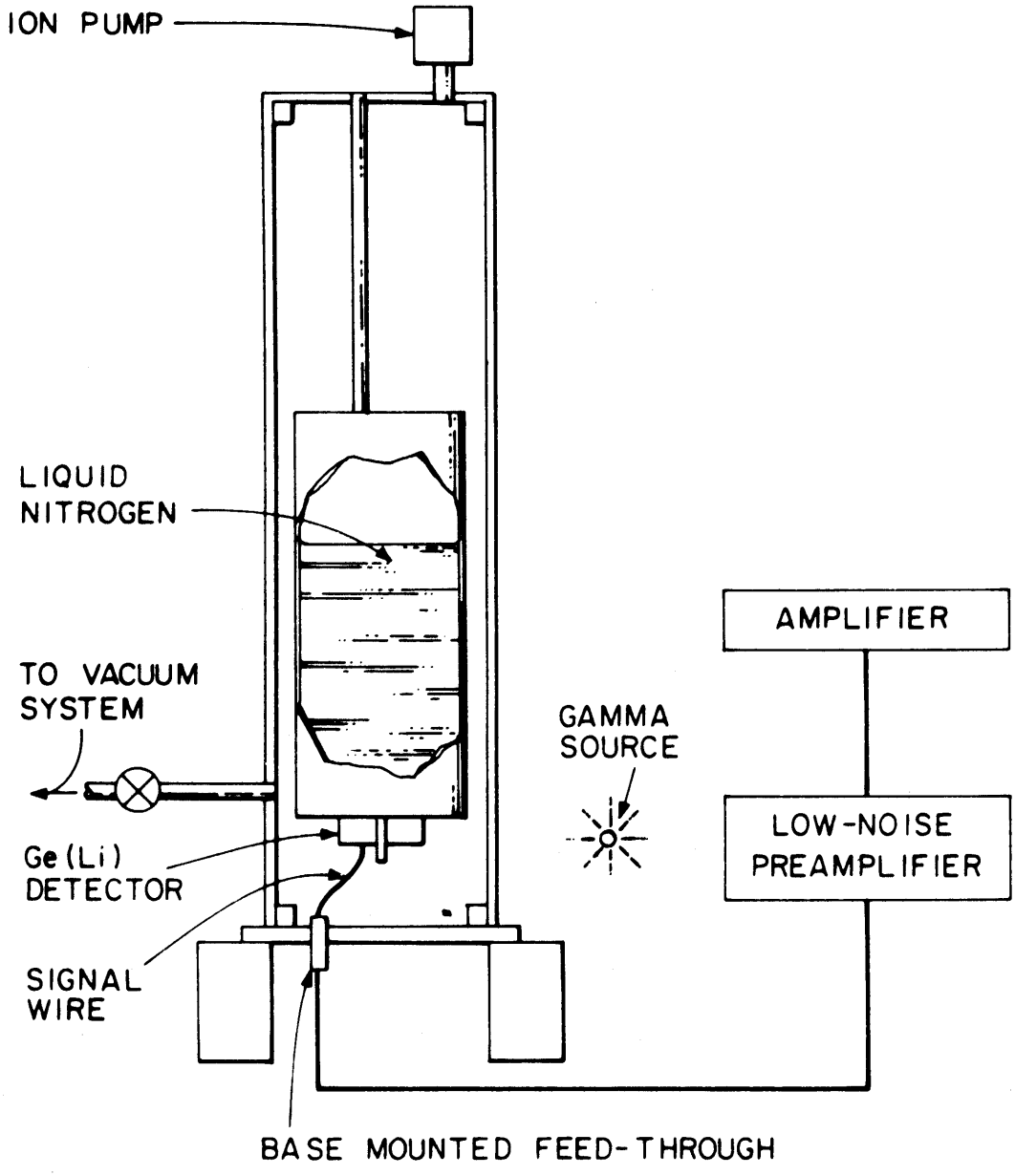

FIG. 2.4 SCHEMATIC DIAGRAM OF VACUUM DEWAR AND ELECTRONICS FOR THE 35 cc GE(Li) DETECTOR

For the front irradiation facility, where the pair spectrometer was installed for detecting gammas in triple coincidence and Compton suppression modes of operation, a more sophisticated cryostat for the 7-cc detector was constructed. The design of this cryostat was based on a similar cryostat constructed by Miner (M3). Figure 2.5 shows a general view of the cryostat and the detector. The LN was supplied to the tip of the LN finger by an MVE (Minnesota Valley Engineering) 16-liter capacity, well-insulated gravity feed reservoir. A "chicken-feeder" method for supplying LN to the cold finger was employed. A desirable characteristic of this cooling method is that the liquid level remains constant within the cryostat and maintains a stable thermal environment. The hollow LN-filled cold finger carries the LN from the reservoir down to the detector-mount assembly. This hollow finger is made of 1/16-inch-thick stainless steel tube of 7/16-inch i.d. and is welded at the upper end to the small end of a stainless steel concentric reducer of 7/8-inch i.d. at its larger end. Except at the ends which are kept thick to facilitate welding, this tube is machined down to a 0.020-inch-thick wall to provide a heat transfer barrier between the LN and the room temperature environment. The vacuum of less than 10^{-5} Torr is maintained in the cryostat by a 1-liter/sec ion pump. A set of two Nupro Swagelok valves, one of 1/4-inch i.d. and the other of 1/8-inch i.d., are arranged in a configuration to permit removal and replacement of the ion pump without affecting the vacuum in the cryostat. Hence, the ion pump can be replaced without warming the detector.

At the lower end of the cold finger, the detector-mount assembly is located. Aluminum was selected for this portion of the cryostat

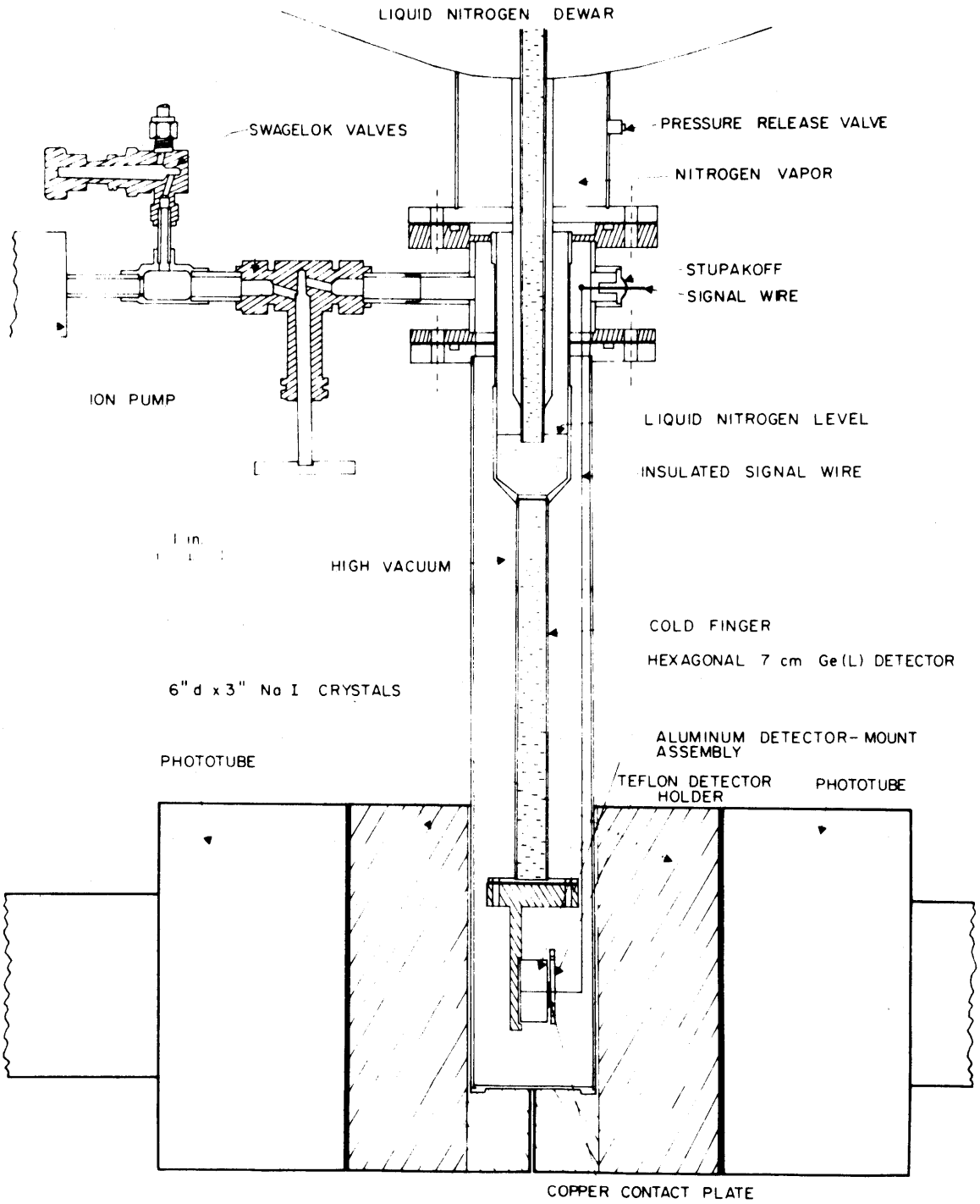

FIG 2.5 PLAN VIEW OF THE CRYOSTAT FOR THE PAIR SPECTROMETER

because it is a good vacuum material, having a low neutron capture cross section and low scattering cross section for gamma rays (see Fig. 2.6).

The signal wire between the detector and the input of the preamplifier was kept as short as possible in order to minimize noise. This signal wire is brought out of the cryostat through a Stupakoff one-wire terminal which was soft-welded to a BNC connector to which the preamplifier input is directly connected.

The Ge(Li) detector for this cryostat was centered inside a 2-inch-diameter, aluminum cover tube. The free surface of one of the faces of the hexagonal detector was oriented toward the gamma-ray beam in order to maximize the detection efficiency and optimize the resolution.

The 2-inch-diameter aluminum cover of the snout of the dewar was placed between two NaI(Tl) crystals of 6-inch diameter and 3-inch thickness inside the Atomium gamma shield. Each of the sodium crystals has a 1-inch radius, semicircular slot cut into its face so that the snout of the dewar containing the germanium detector just fits into the 2-inch-diameter hole formed when both sodium crystals are positioned face to face. The geometrical arrangement is such that the Ge(Li) crystal is located at the central region between the two sodium crystals.

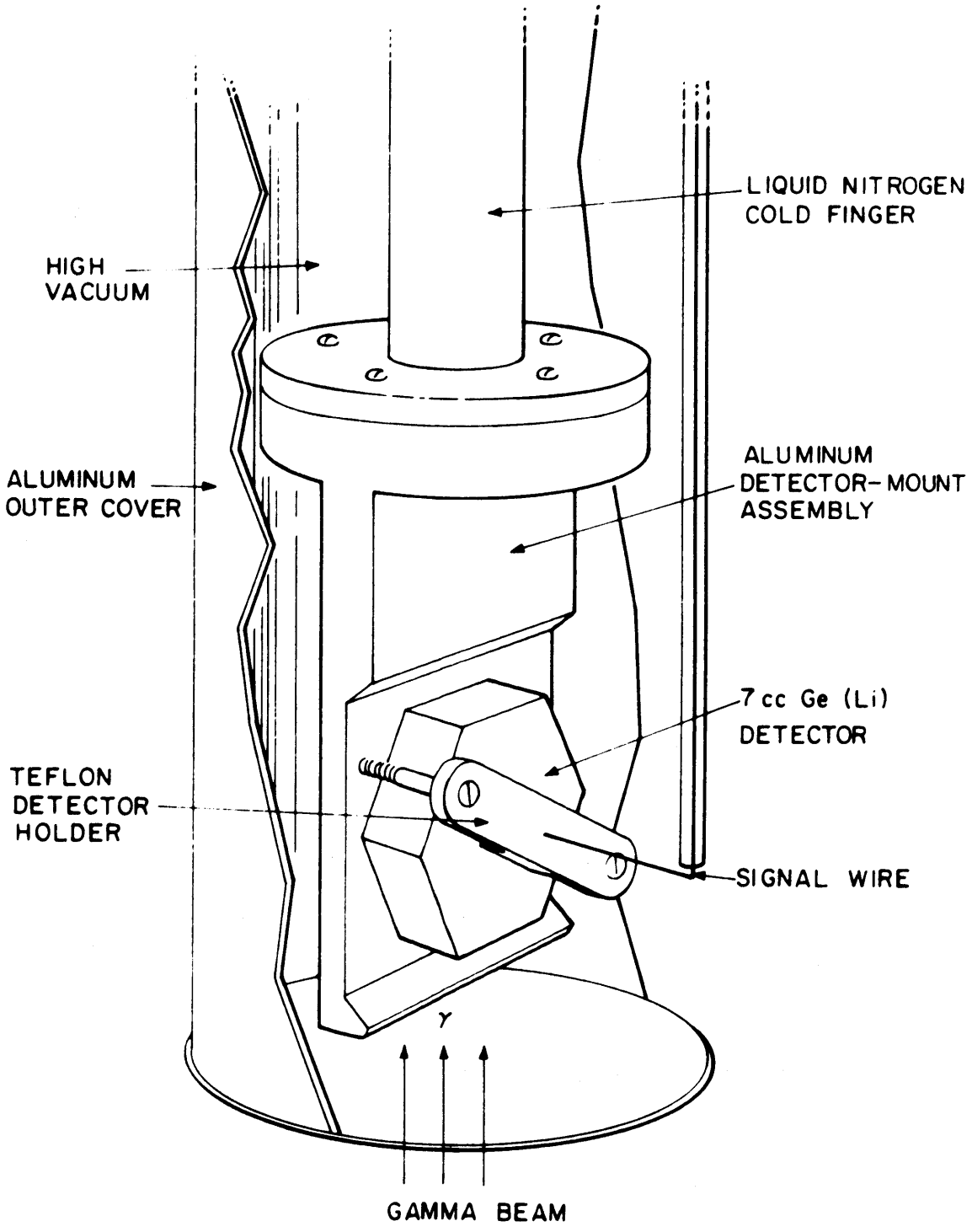

FIG. 2.6 DETECTOR MOUNT ASSEMBLY AND THE ALUMINUM COVER TUBE OF THE CRYOSTAT FOR THE PAIR SPECTROMETER.

2.2.3 Associated Electronics

The electronics associated with the 35-cc detector was the standard arrangement for free mode operation. The signal is amplified by a Cambridge Industries CI-1408C preamplifier and CI-1417 amplifier, and thereafter fed into a Nuclear Data ND-161F 4096 channel analyzer. The free mode operation using the large detector had the advantage of accumulating good counting statistics in a short time, which was essential for the low intensity fission product gamma rays.

Figure 2.7 shows a block diagram of the triple coincidence electronics. Each of the signals from the NaI crystals was amplified and the window of the single channel analyzer set on the annihilation 511-keV peak. A crossover pickoff generates a timing pulse whenever a pulse is within the 511-keV window for each of the sodium crystals, and then it is fed into a Hamner NL-16 triple coincidence unit.

The signal from the Ge(Li) detector is preamplified by a CI-1408C unit and amplified by a CI-1417 unit set in the bipolar output mode, and then it is split into two branches; the delayed output is fed directly into the 4096 channel analyzer, while the prompt output line of the amplifier is fed to a crossover pickoff which generates the third timing pulse into the triple coincidence unit. Each crossover pickoff is equipped with a variable delay line for adjusting the timing of the system.

Whenever the two timing pulses from each of the NaI crystals and the timing pulse from the Ge(Li) detector are in triple coincidence (2τ = 120 nsec), the multichannel analyzer is gated on and therefore the signal from the Ge(Li) detector is accepted and analyzed. This arrangement yields a spectrum in which only double escape peaks appear, full

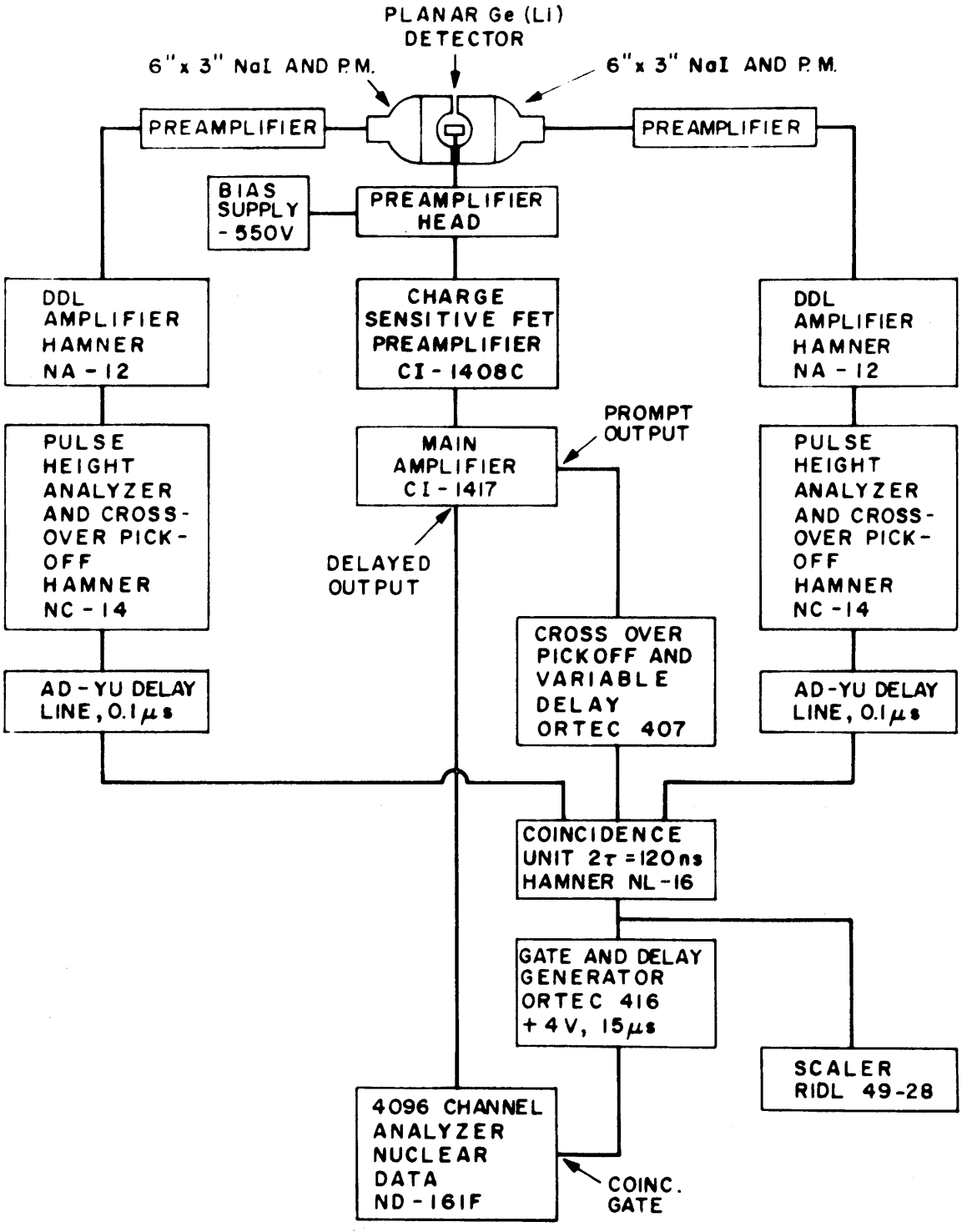

FIG. 2.7 BLOCK DIAGRAM OF ELECTRONICS FOR OPERATION IN THE TRIPLE COINCIDENCE MODE

energy peaks and Compton background being rejected.

The pair spectrometer electronics used in this work differed from that used by Harper in that the CI-1417 amplifier was operated in the bipolar instead of the unipolar mode, which eliminated one component (DDL amplifier ORTEC-410). With this change, however, an AD-YU delay line unit was added to each branch of the NaI crystal circuit between the Hamner NC-14 unit and the coincidence unit, Hamner NL-16.

The block diagram for the Compton suppression mode of operation is shown in Fig. 2.8. The electronic components are the same as for the triple coincidence mode of operation, but in this case the timing pulses from the NaI crystals are joined into one of the input gates of the coincidence unit which was set in anticoincidence mode. Thus, whenever a pulse from either NaI crystal, this time set in the integral mode, was in time coincidence with the pulse coming from the Ge(Li) detector, the multichannel analyzer was gated off and the signal from the Ge(Li) was not accepted. With this arrangement, whenever the Compton scattered gammas from the Ge(Li) crystal interacted in any one of the NaI crystals, the signal from the Ge(Li) was rejected, thereby lowering the Compton contribution to the background of the gamma spectrum.

The optimum operating bias for the 35-cc coaxial detector was 660 volts and the leakage current at this bias was about 4.0×10^{-9} amperes. For the 7-cc planar detector, the optimum bias was 550 volts and the corresponding leakage current about 1.0×10^{-10} amperes. Both detectors were cleaned with a solution of 10 grams per liter of $CaCl_2$ in the final stage of the etching process just before mounting the crystals

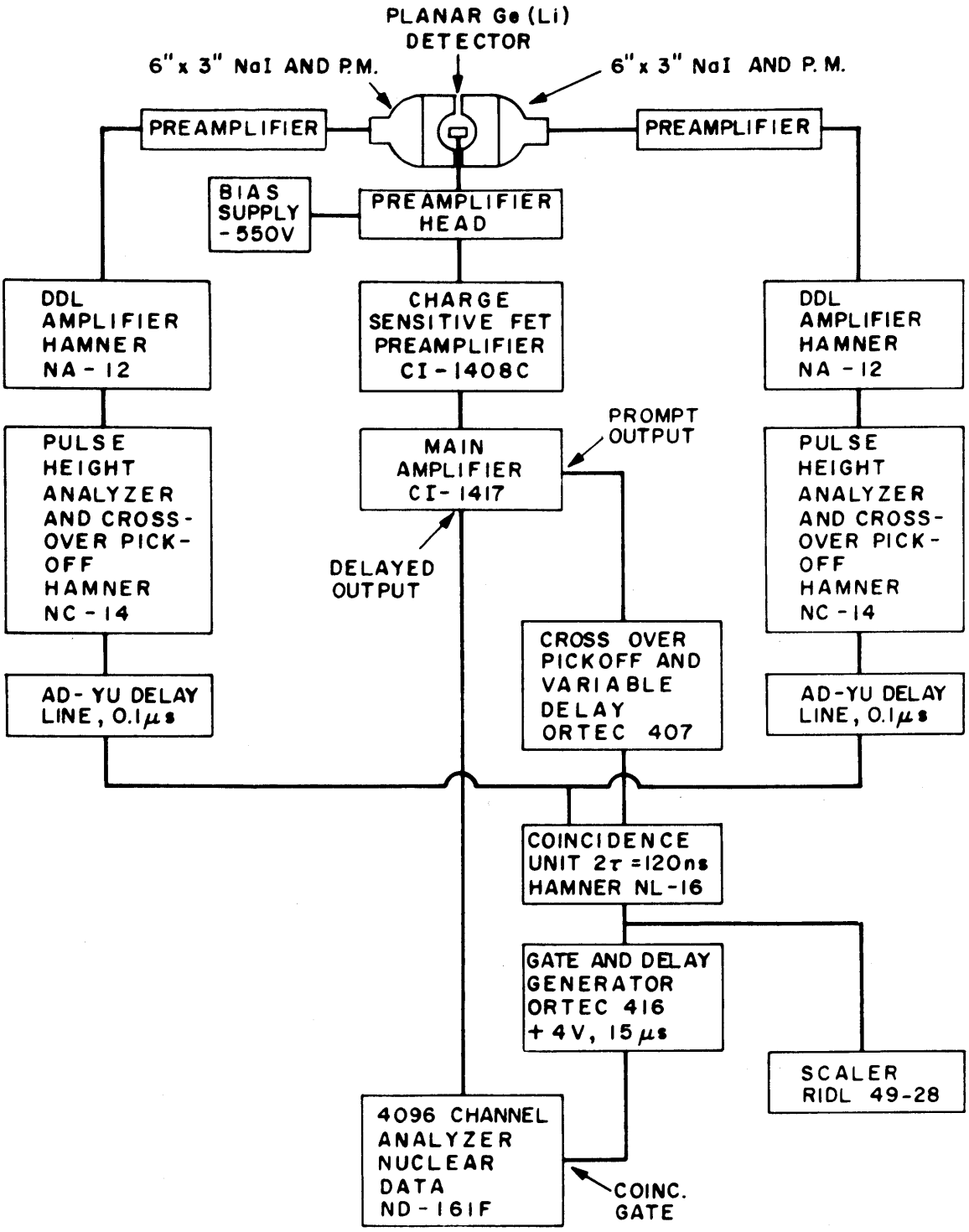

FIG. 2.8 BLOCK DIAGRAM OF ELECTRONICS FOR OPERATION IN THE COMPTON SUPPRESSION MODE

in their respective cryostats.

The energy resolution was 4.5 keV and 2.9 keV for the Co^{60} lines for the 35-cc and 7-cc detectors, respectively. The best pulse shaping was found to be 1 microsecond, and during typical operation the noise level was about 4 mVolts for both the detectors. Some problem was encountered with the pickup of RF signals from many sources inside the reactor building, but it was overcome by using heavy electrical shielding. Although some problem was expected due to the observed boiling of LN in the cryostat dewar, no attributable effects were identifiable during the experiments. Nevertheless, it is believed that even better resolution could be obtained if the boiling could be eliminated.

For typical runs, a count rate of up to 4000 counts per second could be tolerated without loss of resolution. A digital stabilizer, ND-502, was used to prevent gain shift and consequent loss of resolution for runs of up to 30 hours' duration.

2.3 OPERATING CHARACTERISTICS

2.3.1 The Irradiation Facility

During each irradiation, the incident neutron flux was monitored by using thin gold foils of 1/8-inch diameter, weighing a few milligrams. For the rear facility, the monitor foil was held with mylar tape against the end of an aluminum rod 1/8 inch in diameter, which was in turn inserted through a steel tube until the gold foil touched the bottom of the tube located at the edge of the neutron beam collimator but completely exposed to the incident neutrons. The position of the monitor foil is shown in Fig. 2.2.

The neutron monitoring for the front irradiation facility was accomplished by placing the gold foil, again held with mylar tape, at a position two inches from the center of the sample being irradiated, at the end of the aluminum sample holder as shown in Fig. 2.3(a).

The magnitude of the neutron flux from the 4TH1 beam port varied by ±10% when the reactor was running at its normal fixed power level of 4.9 MW. This variation was not observed for short periods of time but it was perceptible for runs of more than 10 hours' duration. The gold foil monitor gave the absolute integral flux averaged over the time of irradiation, once it was calibrated against a standard. This calibration was performed in the following way: first, a factor correlating the flux level at the monitor foil location and the sample position was obtained by irradiating one foil in each position simultaneously. Then a calibration of the monitor foil against a series of similar foils irradiated in a standard flux at the National Bureau of Standards was performed. These foils were irradiated for 212 hours in a flux of 4280 n/cm^2-sec known to an accuracy of ±2% at the laboratories of NBS in Washington, D. C. Thus, the absolute average flux measured in this work was estimated to be accurate to within better than ±3%. A typical value for the flux was 4.0×10^8 n/cm^2-sec at the front facility and 1.5×10^8 n/cm^2-sec for the rear facility. The uniformity of the neutron flux in the region of the sample position at the front facility was checked using gold foil activation. Eight foils, 1/8 inch in diameter and 0.005 inch thick, of pure gold were attached by mylar tape to a thin aluminum plate, 2-1/2 inches long by 3 inches wide, and irradiated at the sample position with the plate positioned normal to the neutron

beam. Figure 2.9 shows the profile of the flux in two dimensions. A variation of about 13 percent was noticed in the vertical direction. This variation was considered tolerable, and no correction due to this non-uniformity was necessary because in the actual measurements of the prompt gammas, both the samples under study and the standard samples used to obtain the efficiency of the system were irradiated with the same geometry.

The cadmium ratio for gold foil at the front irradiation position was measured in two independent experiments and it was found to be 54. In the calculation of the effective cross sections for the samples, Westcott's formulation was used.

The only background line present in all the sample spectra was the 2223.3-keV line of hydrogen coming mainly from the polyethylene vial which encased the sample or from the plastic material covering the LiF used for the fissile material samples, as explained in Chapter IV. The other ubiquitous line that appeared in some of the triple coincidence spectra was that at 1533.0 keV, which is the result of detecting an annihilation photon in the central crystal and at the same time satisfying the triple coincidence condition in the NaI detectors by accidental processes. In all the spectra taken in Compton suppression mode, the annihilation gamma was present together with the 2223.3-keV line of hydrogen and its escape peaks.

In some cases the lines of lead and iron were deliberately brought into the triple coincidence spectra either by placing lead together with the sample during irradiation or by opening the lead collimator to place part of the steel structure in view of the detector. This was done in

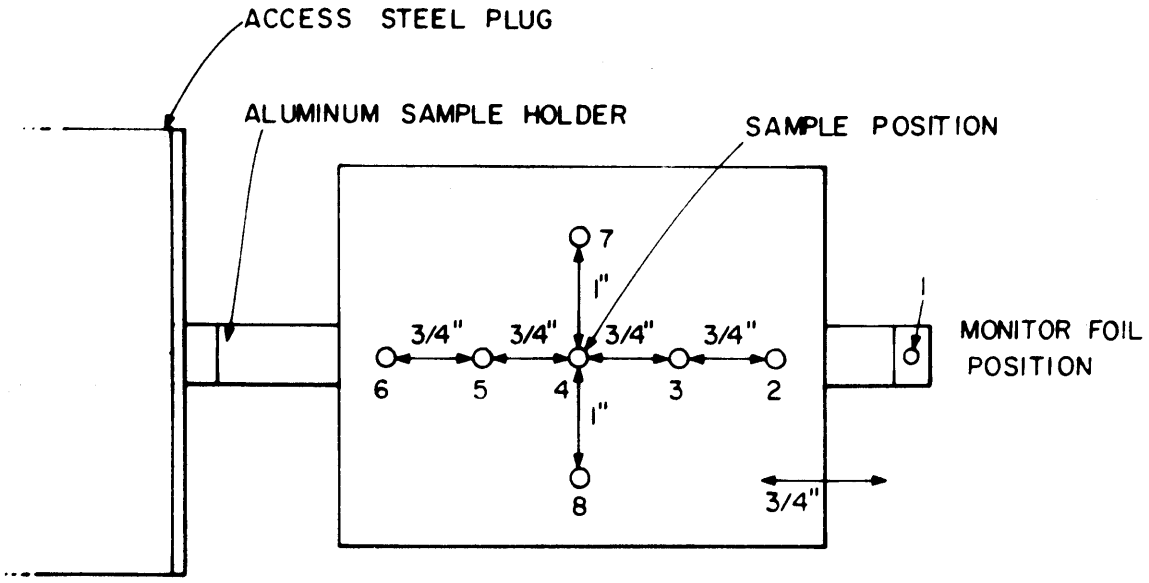

NEUTRON BEAM INCIDENT FRONTALLY, NORMAL TO PAPER

FLUX AT THE MONITOR FOIL POSITION IS TAKEN AS 1.00

POSITION	RELATIVE INTENSITY OF NEUTRON BEAM
1	1.00
2	1.05
3	1.11
4	1.13
5	1.13
6	1.09
7	1.03
8	1.16

FIG. 2.9 GEOMETRIC CONFIGURATION OF MONITOR FOILS FOR THE MEASUREMENT OF THE UNIFORMITY OF NEUTRON FLUX AT THE SAMPLE POSITION.

order to have the second line in addition to the hydrogen line to calibrate the spectrum and check the energy linearity.

2.3.2 The Free Mode Operation

The free mode operation was used in conjunction with the 35-cc detector for the fission product gamma-ray experiments and in the determination of fission neutron yield at the rear irradiation facility.

The 4096 channel analyzer was used with the live time clock set for 80 or 160 minutes, depending on the nature of the measurement, so that the correction for the dead time of the electronics was done automatically by the analyzer.

A typical spectrum of prompt gamma rays from the irradiation of a fuel rod is shown in Fig. 2.10. It contains many peaks from the interaction of fission neutrons with the germanium crystal because in this case, no scattering material was placed in the gamma beam. A detailed explanation of this spectrum is presented in section 5.4. Another typical spectrum is shown in Fig. 2.11. This is a spectrum of the fission product gamma rays from the fission of U^{235} after cooling for a short period of time. A detailed explanation of this spectrum is presented in Chapter III. The resolution of the system operating in the free mode was from about 3.7 keV for 300-keV gammas up to about 5.5 keV for 2.5-MeV gammas.

2.3.3 The Pair Spectrometer

A typical spectrum for natural iron taken in the triple coincidence mode and used in the determination of the absolute total efficiency of the system is shown in Fig. 2.12.

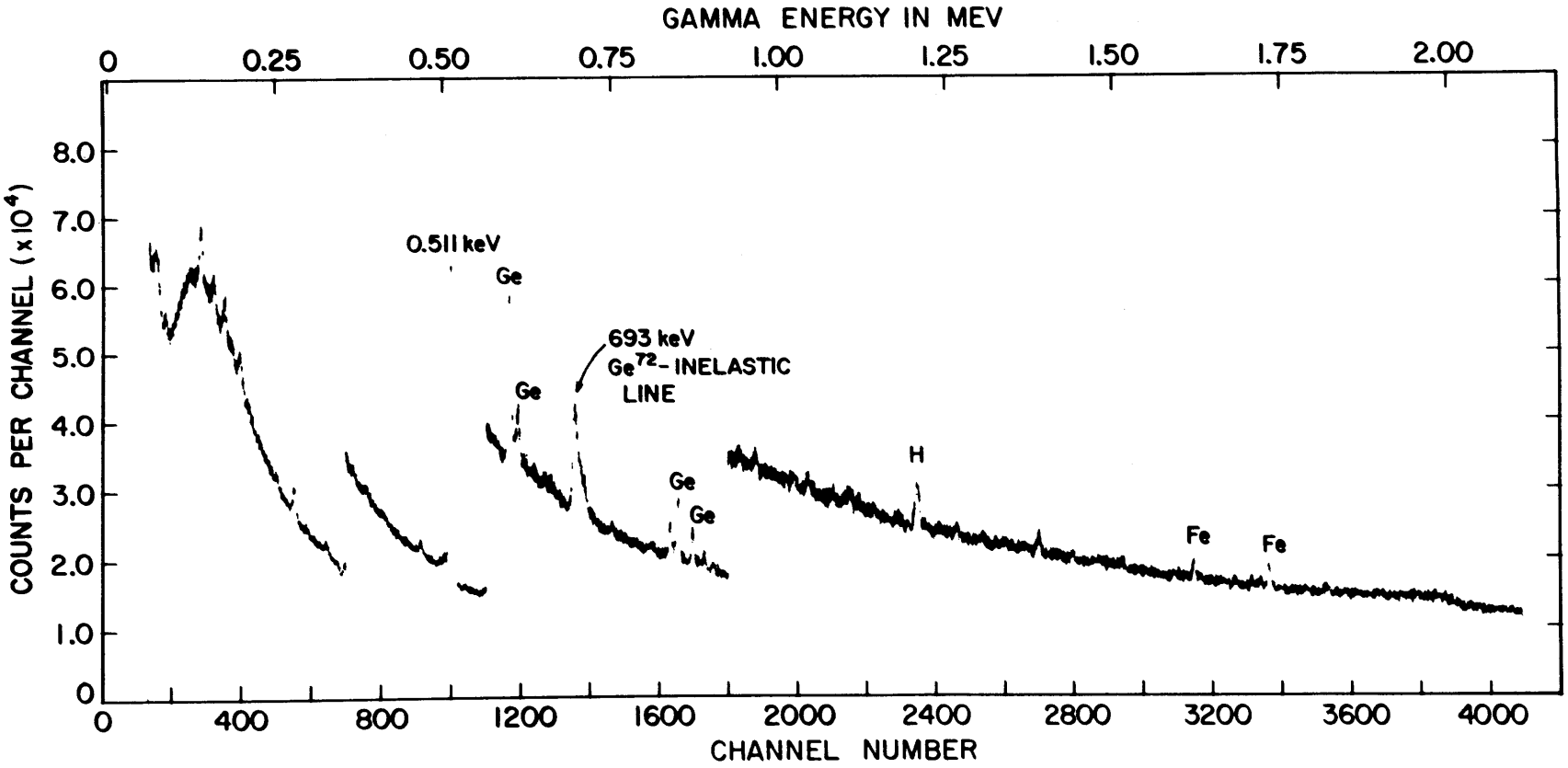

FIG. 2.10 THE PROMPT GAMMA-RAY SPECTRUM FROM 2% ENRICHED UO_2 FUEL ROD WITHOUT NEUTRON SCATTERER IN THE GAMMA BEAM

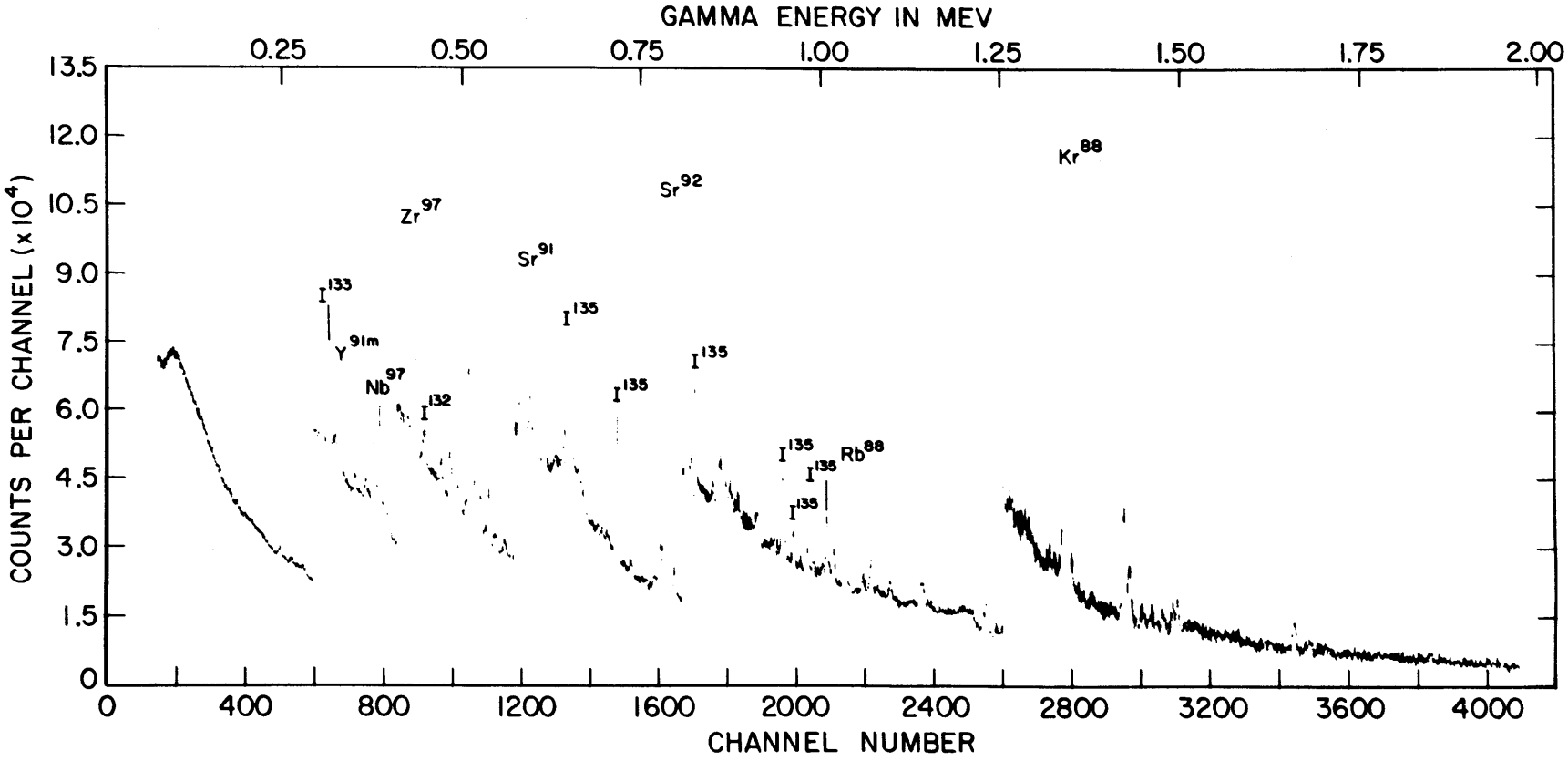

FIG. 2.11 U^{235} FISSION PRODUCT GAMMA-RAYS (4 HOURS IRRADIATION, 2 HOURS COOLING, AND 160 MINUTES COUNTING)

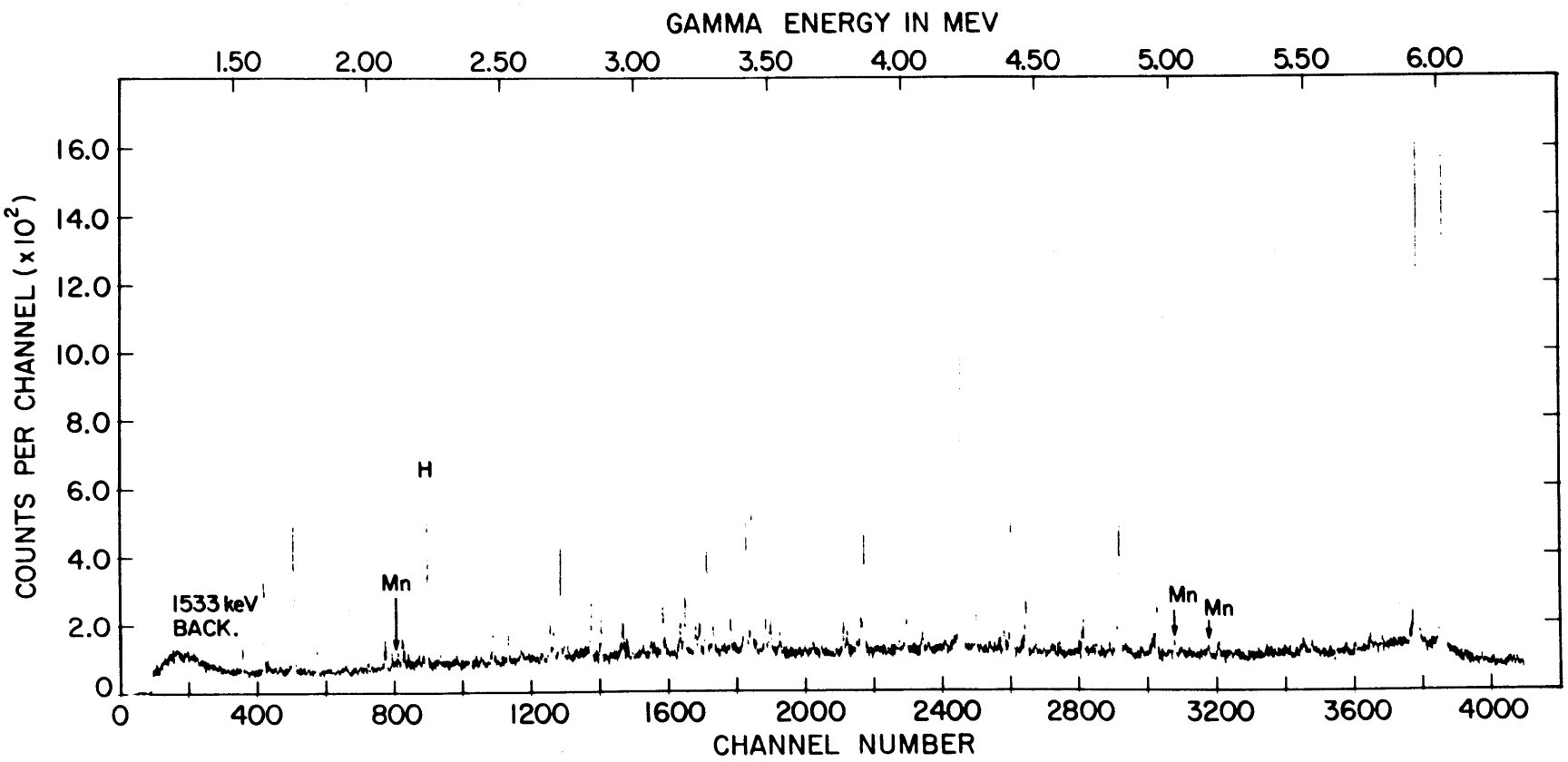

FIG. 2.12 TRIPLE COINCIDENCE SPECTRUM FOR NATURAL IRON USED IN THE DETERMINATION OF TOTAL EFFICIENCY OF THE SYSTEM

The characteristics and performance of the triple coincidence mode of operation compared to the free mode have been extensively studied by Orphan (O2). In this section a comparative study is made of the performance of the present system with the pair spectrometer used by Orphan.

The three principal characteristics of pair spectrometers are: the resolution of the system, the peak-to-background ratio in the gamma spectrum and the overall absolute efficiency for detection of gamma rays of different energies.

It is well known that a planar detector like the one used in the present system offers better resolution, compared to large coaxial detectors like the one used by Orphan, due to several characteristics such as shorter charge collection time, better uniformity of the internal electric field and lower capacitance. Nevertheless, in addition to these intrinsic factors, the resolution of the system depends heavily on extrinsic factors such as the surface leakage current, the noise pickup, and notably on the electronics of signal amplification. The resolution obtained with the present system was at best 2.8 keV for the Co^{60} lines and 6.0 keV for 6-MeV capture gammas, in comparison with 5.0 keV and 6.8 keV for the same lines with Orphan's system. In the present work the main interest was on gammas of less than 6.5 MeV with particular emphasis in the region of 2 to 5 MeV.

The peak-to-background ratio for the spectrum also depends on many factors such as the amount of background coming to the detector from the irradiation of materials other than the sample, the aperture of the window for the annihilation gammas of the single channel

analyzer for the NaI crystals, the overall resolution of the system, and the geometry and material of the detector-mount assembly. The extraneous background obviously adds to the normal background of the spectrum. A larger than necessary window aperture for the annihilation gammas increases the chance for coincidence of spurious signals contributing to an increase in the background and lowering of the peak-to-background ratio. Heavy and thick material in the detector-mount assembly placed in the path of the annihilation gammas from the Ge(Li) into the NaI crystals will decrease the chance of a true signal being accepted due to the attenuation of the 511-keV gammas. In Orphan's cryostat two copper bars, 1/8 inch thick, held the Ge(Li) crystal and served also as the cold finger to cool the detector; whereas in the present system only one such plate, made of aluminum, is placed in with the detector. Orphan found a better peak-to-background ratio for a 3-cc coaxial detector compared to a 5-cc planar detector by a factor of 4. Nevertheless, a comparison between his spectrum for iron taken with the coaxial detector and the same spectrum taken with the present system shows that for the 1725-keV gamma, the peak-to-background ratio of the present system is 7 to 1 compared to 1 to 1 for Orphan, and at 6018 keV the ratio for the present system is 14 to 1 compared to 5.3 to 1.

The efficiency of the pair spectrometer is important in regard to the statistics of counting. With the digital stabilizer working, a triple coincidence run has to be capable of accumulating a significant number of counts per channel within a period of less than 30 hours in order to avoid excessive loss of resolution. The overall efficiency depends on

many factors such as the size of the germanium crystal, the aperture of the window for the annihilation gammas, proper timing of the components of the electronics, and the geometry and material of the detector-mount assembly. The overall absolute efficiency of the present pair spectrometer, including the solid angle, the neutron shielding in the gamma beam, and the percentage of the sample "viewed" by the detector, has a maximum around 4.5 MeV and goes down with increasing energy somewhat faster than a larger coaxial detector due to the higher bremsstrahlung losses. At around 4 MeV the present system has an overall efficiency about 2.5 times lower than that of Orphan's system using the 30-cc coaxial detector. Nevertheless, and fortunately, lower efficiency can be compensated for by using a larger sample, greater flux, larger solid angle, or greater counting time. Thus, low efficiency is not a serious limitation insofar as it can be compensated for by one or a combination of the above factors. In the present work, the faster decrease in efficiency at energies higher than 6 MeV did not constitute a serious hindrance since the interest remained concentrated on gammas of less than 6 MeV.

The absolute efficiency for the present system as a function of the energy of the gammas was determined by using two samples for which the intensities of the lines were well known (within ±10% error) and the energies of the lines well-spread over the range of interest. The samples chosen were of natural metallic iron powder and natural nitrogen in the form of melamine powder. The values of the intensities were taken from references R1 and B2. Both samples were placed in the sample holder in the same geometrical arrangement as for the

samples to be studied. Both samples combined have a total of 40 strong lines distributed uniformly in the energy range from 1.6 MeV to 6.3 MeV.

Once the experimental points for the efficiency curve were obtained, a least square fit was performed by using an adaptation of the computer code POLYFIT written by Hamawi and described in reference H3. It was found that a second order, and also the third order, curve fit the experimental data well.

Two efficiency curves were determined for the pair spectrometer. One, which includes the effect of 1.6 cm of LiF plate in the gamma beam, was used in the analysis of the samples of U^{238} and Th^{232} and is shown in Fig. 2.13. Another, which includes the effect of 4 inches of borated paraffin plus 1.6 cm of LiF and 1/4 inch of lead, was used in the analysis of the data of U^{235} and plutonium and is shown in Fig. 2.14. The reason for placing these different shielding materials in the gamma beam is explained in Chapter IV. The efficiency in Fig. 2.14, corresponding to the geometry having borated paraffin and the lead plate in the gamma beam, is lower than the efficiency shown in Fig. 2.13 only by about 15% – not, as would be expected, due to the larger gamma attenuation but due to the geometrical positioning of the iron sample used to obtain these curves. For the first case, the cylindrical sample of iron was placed horizontally; in the latter case, it was placed vertically to match the geometry of the uranium and plutonium samples studied. In the vertical position, the actual portion of the sample viewed by the detector is larger by about a factor of two.

The linearity of the electronics was checked according to a method described by Heath (H5) and used by Orphan and Harper. An

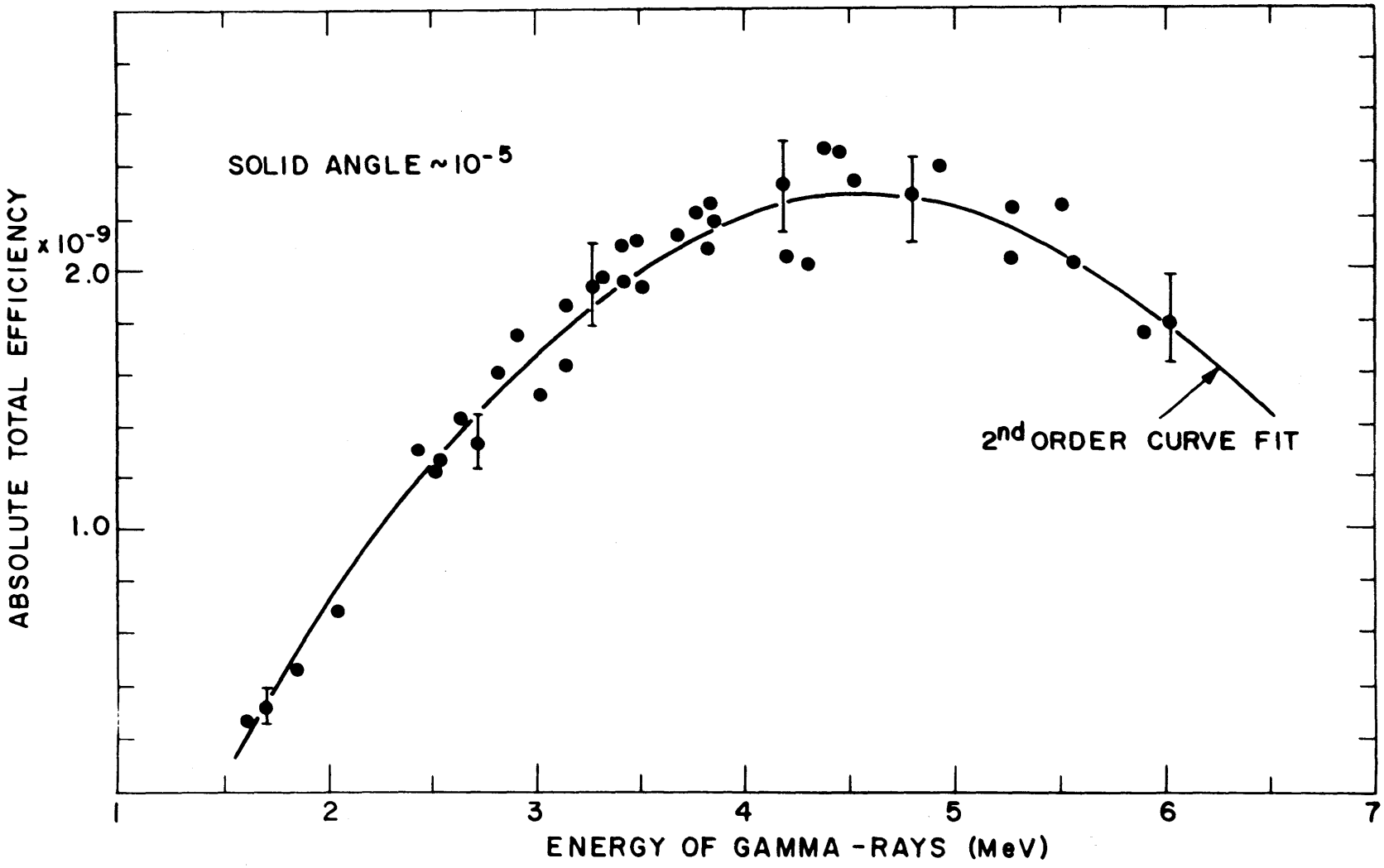

FIG. 2.13 TOTAL EFFICIENCY OF TRIPLE COINCIDENCE MODE WITH LiF PLATE IN THE GAMMA BEAM

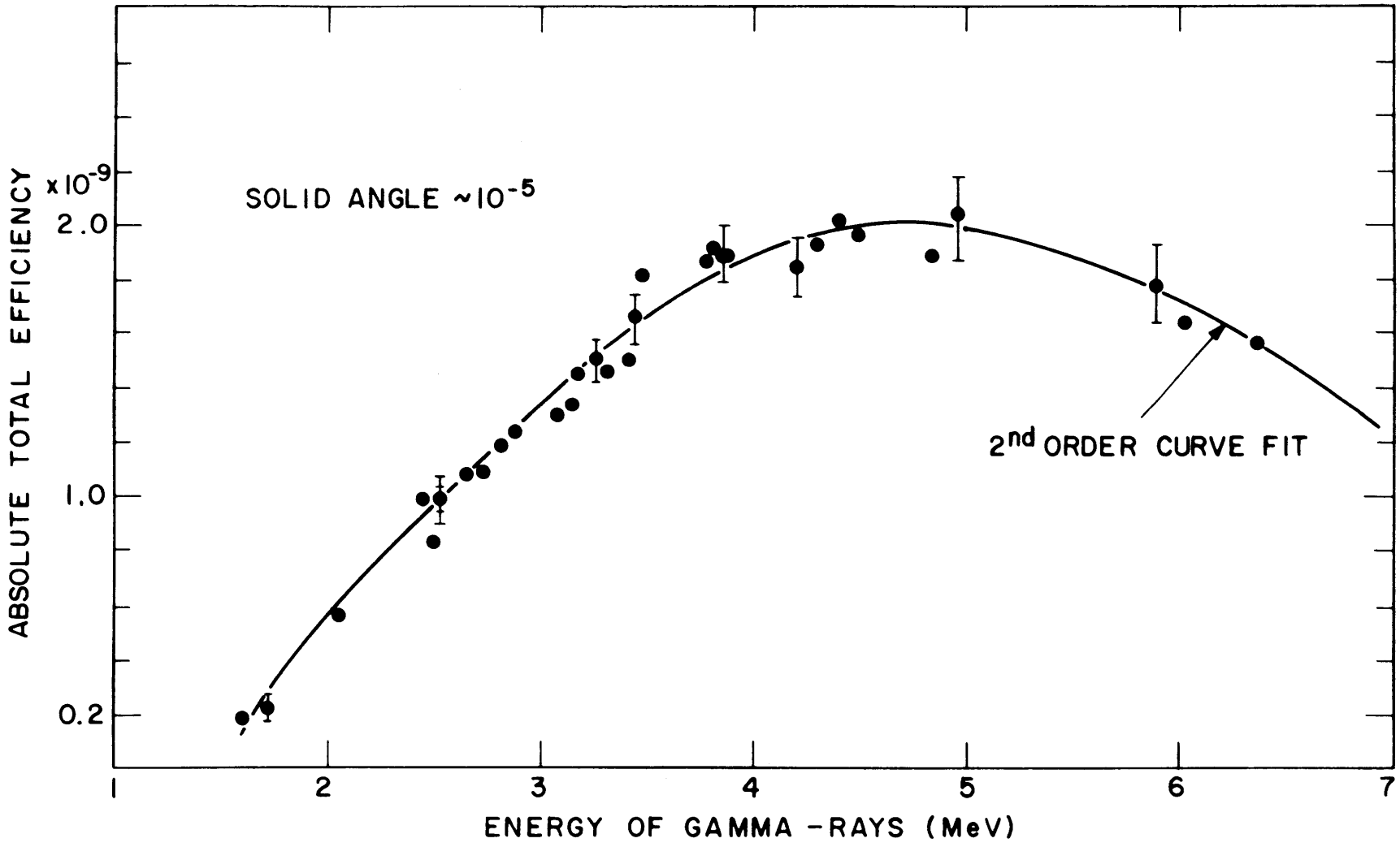

FIG. 2.14 TOTAL EFFICIENCY OF TRIPLE COINCIDENCE MODE WITH LiF, BORATED PARAFFIN AND Pb IN THE GAMMA BEAM

EDC Model MV-100 millivolt standard power supply, accurate to one part in 10^4, was used in conjunction with a mercury relay pulser to perform the linearity check, for which about 130 equally spaced pulser peaks were recorded for the triple coincidence mode and inserted through the preamplifier of the Ge(Li) detector. The peaks so obtained were analyzed for energy separation and compared against what the separation would be if the system were perfectly linear. The difference produced a linearity correction factor in channels, for each peak, that was used to correct the energy of the observed gamma lines in a spectrum, as explained in more detail in section 4.1. The correction factors versus the channel numbers obtained for the data in triple coincidence are shown in Fig. 2.15. The nonlinearity of the spectrum was found to be less than ±0.1% over the energy range of interest.

2.3.4 The Compton Suppression Mode

The peak to Compton edge ratio is higher for larger detectors due to the better photopeak efficiency of larger detectors as compared to smaller ones, although the absorption of Compton gammas is higher for larger detectors. Nevertheless, due to the improvement in the electronics and in the experimental arrangement, a performance similar to that of Orphan using a 30-cc detector was attained by the present system using a 7-cc detector. Compared to a spectrum taken in free mode, the spectrum of Co^{60} taken in the Compton suppression mode presents a reduction of about 1.5 in the Compton edge of the spectrum, while the plateau was reduced by a factor of as much as 2.

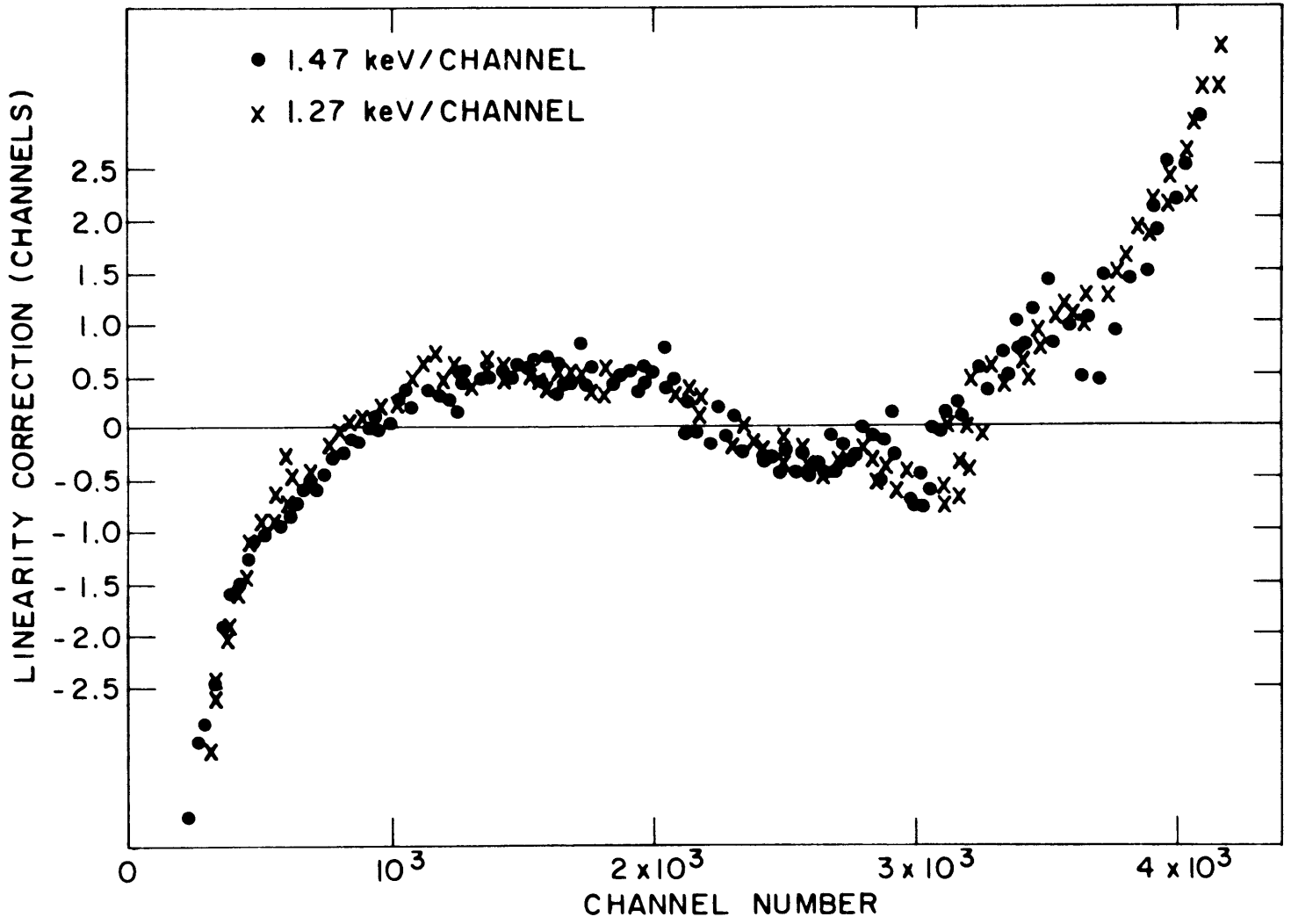

FIG. 2.15 LINEARITY CORRECTION AS A FUNCTION OF CHANNEL NUMBER FOR THE TRIPLE COINCIDENCE MODE OF OPERATION

Figure 2.16 shows a spectrum for the capture gamma rays for natural cobalt taken in the Compton suppression mode. This metal was used in order to determine the absolute efficiency curve, which is shown in Fig. 2.17, and it includes the effect of 1.6 cm of LiF in the gamma beam. Cobalt was chosen because it has about 15 very strong lines well-spread in energy from about 162 keV up to 1.836 MeV, and its intensities are known within ±10% error (B2). The resolution for the Compton suppression spectrum was about 3.0 keV.

The correction for the nonlinearity was done in the same fashion as for the triple coincidence mode of operation. Here, 116 peaks from the pulser covered the entire range of channels of interest.

The equipment discussed in this chapter was used in all the experiments which are described in the following chapters.

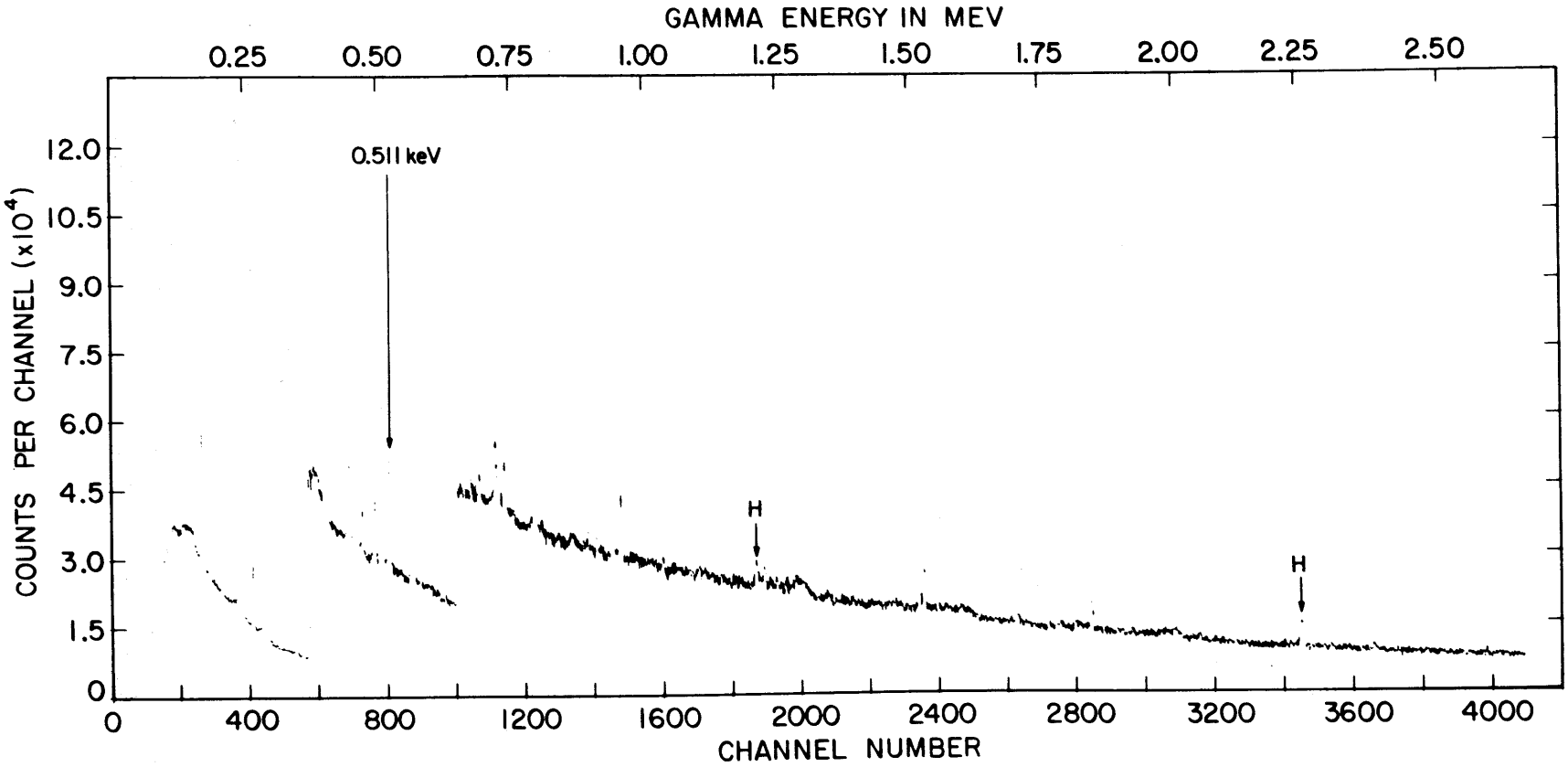

FIG. 2.16 THE LOW ENERGY GAMMA-RAYS FOR COBALT TAKEN IN COMPTON SUPPRESSION MODE

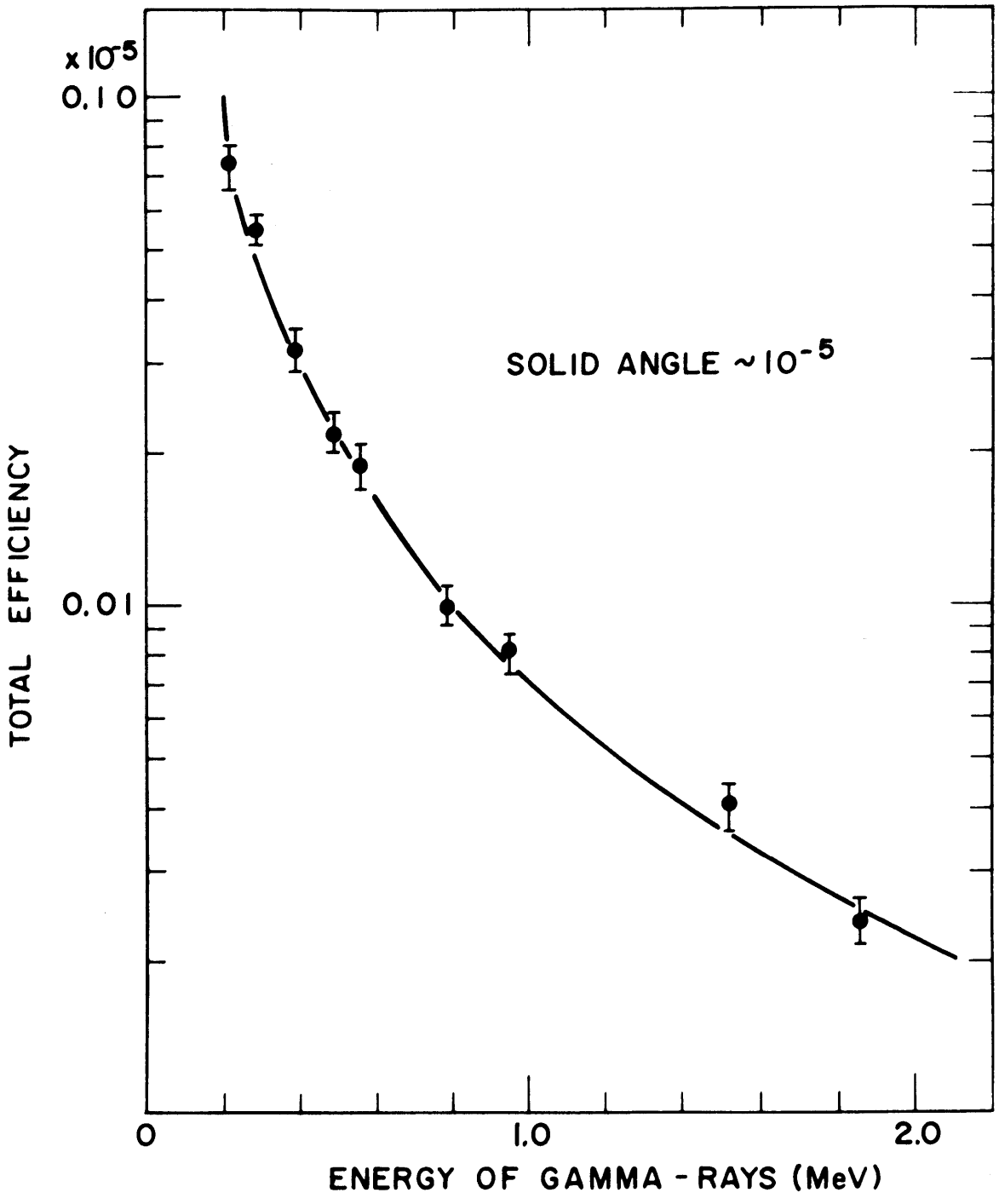

FIG. 2.17 ABSOLUTE TOTAL EFFICIENCY OF COMPTON SUPPRESSION MODE OF OPERATION

Chapter III

NONDESTRUCTIVE ASSAY OF FUEL RODS CONTAINING A MIXTURE OF PLUTONIUM AND URANIUM OXIDE BY USING FISSION PRODUCT GAMMA RAYS

3.1 INTRODUCTION

In recent years considerable attention has been devoted to the problem of nondestructive techniques for assay of nuclear fuel, and this attention certainly will increase with the sharp increase in the number of commercial nuclear power stations and their associated nuclear fuel inventory. These techniques have importance from the economic standpoint as well as from the safeguards standpoint.

An extensive literature has been published recently in this field. A comprehensive review of the situation up to July, 1967 is described in references E1 and M2. Nondestructive nuclear techniques can be classified as passive and active methods. Passive methods refer to those methods which use the spontaneously generated nuclear radiations from an isotope to quantitatively determine its presence. In contrast, the active methods use an external radiation source to excite the nuclei of the sample, and the radiations thus produced are used for analyzing the sample. Delayed fission product decay gammas have been the primary radiation used in passive methods (H1, R2, T1), although delayed neutrons are also being investigated for the same purpose (K1). For the active methods, the prompt neutrons have been used as the response radiation for assay of uranium samples (J2), but

no technique using prompt gamma-ray spectra has been reported previously.

For the assay of irradiated fuel, in safeguards applications, the aim is to develop rapid nondestructive techniques having an accuracy comparable to that of radiochemical and mass spectrometric methods of analysis, but this objective is still unrealized.

For unirradiated fuel, several methods using either neutrons (J1) or delayed gammas (T1) have been developed which give precision comparable with the destructive techniques. However, most of these methods were tested with samples containing uranium only, that is, free of plutonium.

Depisch et al. (D1) have developed a neutron transmission method for analysis of plutonium samples of different isotopic content by using a chopper to select neutrons of energies corresponding to large resonances for the different isotopes. He claims an accuracy of ±5%.

In the present work, we consider three independent techniques for the analysis of fresh fuel rods containing a mixture of plutonium and uranium. The first, a passive method, uses the difference in the yield of certain fission products of U^{235} and Pu^{239}; the second uses the prompt gammas of these two nuclei under thermal neutron bombardment (section 5.3); and the third uses the fission neutron yield (section 5.4). The latter two methods are active methods. An extension of these methods for burned fuel analysis is also considered.

In this chapter, the method using fission product decay gammas is described.

Forsyth and Ronquist (F1) have studied the possibility of using the activities of Ru^{103} and Ru^{106} as a measure of the relative fission rate in U^{235} and Pu^{239} by the simultaneous study of the spectra of two irradiated mixtures of plutonium and uranium, plus two irradiated samples, one containing only plutonium and the other containing only uranium. This study suggested the possibility of using short-lived fission product gamma rays for assaying fuel rods containing uranium and plutonium. This method avoids the measurement of any variable which is intrinsically difficult to measure without being accompanied by a high uncertainty (>2%). Thus, variables such as the efficiency of the detector, the yield of fission products, and cross sections are treated in a way such that they can be cancelled out in ratio form. On the other hand, it is preferred that one retain variables such as the weight of fissile foils, which can be measured with great accuracy, so that the number of sources of error is reduced to a minimum, essentially that of the statistics of counting gamma rays.

3.2 THEORY

3.2.1 Equations Governing the Decay of Fission Products

A typical mass chain of short-lived fission products (T2) that is visible in the gamma spectrum of an irradiated fissile material is presented by the mass chain 92 that leads to the stable Zr^{92}.

$$3.0 \text{ sec } Kr^{92} \rightarrow 5.3 \text{ sec } Rb^{92} \rightarrow 2.7 \text{ hr } Sr^{92} \rightarrow 3.6 \text{ hr } Y^{92} \rightarrow \text{Stable } Zr^{92}$$

Each of the components, besides being genetically related, is directly produced by fission.

The equations necessary for the determination of the activity of Sr^{92} as a function of time after the irradiation is over are:

During the irradiation,

$$\frac{dK}{dt} = Y_K N\sigma\phi - \lambda_K K$$

$$\frac{dR}{dt} = Y_R N\sigma\phi + \lambda_K K - \lambda_R R \qquad (3.1)$$

$$\frac{dS}{dt} = Y_S N\sigma\phi + \lambda_R R - \lambda_S S$$

In the above equations, the absorption term was neglected compared to the remaining terms because of the very low neutron flux involved (1×10^8 n/cm^2-sec).

After the irradiation, during the decay period,

$$\frac{dK}{dt} = -\lambda_K K$$

$$\frac{dR}{dt} = \lambda_K K - \lambda_R R \qquad (3.2)$$

$$\frac{dS}{dt} = \lambda_R R - \lambda_S S$$

where

N = number of atoms of fissile element under irradiation

K = number of atoms of element Kr^{92}

R = number of atoms of element Rb^{92}

S = number of atoms of element Sr^{92}

Y = fission yield

σ = fission cross section

ϕ = neutron flux

λ = decay constant

The variables σ, Y and λ are to be subscripted relative to one of the specific elements Kr^{92}, Rb^{92} and Sr^{92}. For example, Y_K = fission yield of the element Kr^{92}, etc.

The solution for the Sr^{92} is straightforward but rather tedious. The decay of the activity A_S of Sr^{92} as a function of decay time t is given by the following expression:

$$A_S = N\sigma\phi F(\lambda_K, \lambda_R, \lambda_S, Y_K, Y_R, Y_S, t_i, t) \tag{3.3}$$

where F is a function of all the variables contained in the parentheses; t_i is the irradiation time, and t is the decay time after the start of cooling. The function F is given explicitly by the following equation:

$$F = S_o\lambda_S e^{-\lambda_S t} + K_o \frac{\lambda_S\lambda_R\lambda_K}{(\lambda_K-\lambda_R)(\lambda_S-\lambda_K)}\left(e^{-\lambda_S t} - e^{-\lambda_K t}\right) +$$

$$+ \frac{(R_o+K_o)\lambda_S\lambda_R\lambda_K - R_o\lambda_S\lambda_R^2}{(\lambda_R-\lambda_K)(\lambda_S-\lambda_R)}\left(e^{-\lambda_S t} - e^{-\lambda_R t}\right) \tag{3.4}$$

where the constants S_o, K_o and R_o are given by the expressions below:

$$K_o = \frac{Y_K}{\lambda_K}\left(1 - e^{-\lambda_K t_i}\right) \tag{3.5}$$

$$R_o = \frac{Y_R + Y_K}{\lambda_R}\left(1 - e^{-\lambda_R t_i}\right) - \frac{Y_K}{\lambda_R - \lambda_K}\left(e^{-\lambda_K t_i} - e^{-\lambda_R t_i}\right) \tag{3.6}$$

$$S_o = \frac{Y_R + Y_K + Y_S}{\lambda_S}\left(1 - e^{-\lambda_S t_i}\right) - \frac{Y_R\lambda_R - Y_R\lambda_K - Y_K\lambda_K}{(\lambda_R-\lambda_K)(\lambda_S-\lambda_R)}\left(e^{-\lambda_R t_i} - e^{-\lambda_S t_i}\right) -$$

$$- \frac{Y_K\lambda_R}{(\lambda_R-\lambda_K)(\lambda_S-\lambda_K)}\left(e^{-\lambda_K t_i} - e^{-\lambda_S t_i}\right) \tag{3.7}$$

The fundamental equation is Eq. 3.3. It can be shown that the activity of any fission product can be put in basically the same form as Eq. 3.3: that is, a product of $N\sigma\phi$ and a function F dependent on the decay constants and fission yields of that fission product and all its precursors, and the irradiation and decay times.

In the specific case of mass chain 92, by observing that λ_K and λ_R are of the order of 10^3 larger than λ_S, a drastic simplification of the equations can be made for irradiation and decay times greater than a few minutes. By expanding the proper exponentials, Eq. 3.3 becomes

$$A_S = N\sigma\phi(Y_K+Y_R+Y_S)(1 - e^{-\lambda_S t_i}) e^{-\lambda_S t} \qquad (3.8)$$

That is, because of the relatively very short lifetime of Kr and Rb, the activity of Sr^{92} is the same as if all Kr and Rb atoms were produced directly as Sr atoms through the fission process and decayed as such.

3.2.2 The Method of Two Fission Products of Distinct Yields

Suppose two fuel rods have been irradiated for the same period of time with the same geometry of irradiation and then, after equal cooling times, counted over the same period of time with the identical geometrical arrangement of fuel rods, collimators and detector. Suppose one of the fuel rods contains uranium oxide enriched in U^{235} as its only fissile element in a well-known quantity, and it can therefore serve as the standard or calibrating rod. Another fuel rod contains a mixture of uranium and plutonium oxide with total enrichment not very different from the calibrating rod but of unknown composition

of U^{235} and Pu^{239}. Assume, for simplicity, that both rods are made up of pellets of the same diameter.

Suppose two prominent peaks can be selected from the spectrum of the fission product gamma rays coming from two distinct short-lived fission products (numbers 1 and 2) present in the spectrum of both fuel rods.

The activity of one of the fission products, as given by one of the gamma lines from the calibrating rod, is expressed in the form of Eq. 3.3 by the relation:

$$A^{1s} = N_5^s \sigma_5 \phi^s F_5^1 \epsilon^1 \tag{3.9}$$

where the superscript 1 stands for fission product number 1, s stands for standard, and the subscript 5 stands for U^{235}. The detector efficiency for the energy of peak number 1 is given by ϵ.

The activity of the same fission product in the unknown rod using the same gamma rays is expressed by the equation,

$$A^{1x} = N_5^x \sigma_5 \phi^x F_5^1 \epsilon^1 + N_9^x \sigma_9 \phi^x F_9^1 \epsilon^1 \tag{3.10}$$

where the superscript x stands for the unknown rod containing U^{235} and Pu^{239}, and the subscript 9 stands for Pu^{239}. The function F_9 differs from F_5 because, although the decay constants and the irradiation and decay times are the same for both U^{235} and Pu^{239} composing the same fuel rod, the yields of the fission product under consideration and of its precursors are different.

Dividing Eq. 3.10 by Eq. 3.9 and noticing that both rods were irradiated and cooled for the same period of time, the result is

$$\frac{A^{1x}}{A^{1s}} = \frac{N_5^x}{N_5^s}\cdot\frac{\phi^x}{\phi^s} + \frac{N_9^x}{N_5^s}\cdot\frac{\phi^x}{\phi^s}\cdot\frac{\sigma_9 F_9^1}{\sigma_5 F_5^1} \tag{3.11}$$

For the fission product number 2, we have a similar relation:

$$\frac{A^{2x}}{A^{2s}} = \frac{N_5^x}{N_5^s}\cdot\frac{\phi^x}{\phi^s} + \frac{N_9^x}{N_5^s}\cdot\frac{\phi^x}{\phi^s}\cdot\frac{\sigma_9 F_9^2}{\sigma_5 F_5^2} \tag{3.12}$$

Now, from the experiment, the ratios A^x/A^s are given by the ratio of areas under the peaks for the calibrating and unknown rod spectra. The ratio of the neutron flux, ϕ^x/ϕ^s, is given by the flux monitor foils. Thus, Eqs. 3.11 and 3.12 are two equations with four unknowns, for which two of the unknowns are the ratios, $\sigma_9 F_9^1/\sigma_5 F_5^1$ and $\sigma_9 F_9^2/\sigma_5 F_5^2$, which can be obtained by an independent experiment, as described below.

Suppose two different fissile foils of the same geometry are irradiated, cooled and counted in the same fashion as for the rods. One of the foils contains a well-known quantity of U^{235} as the only fissile element, and the other contains only Pu^{239}.

For fission product number 1, the activity will be given by the expression,

$$A^{1F} = N_5^F \sigma_5 \phi_5^F F_5^1 \epsilon^1 \tag{3.13}$$

for the uranium foil, and

$$A_9^{1F} = N_9^F \sigma_9 \phi_9^F F_9^1 \epsilon^1 \tag{3.14}$$

for the plutonium foil, where N_5^F and N_9^F are the number of atoms of U^{235} and Pu^{239}, respectively, in each foil. By putting N_5^F and N_9^F in

terms of the weights and the atomic mass of the elements in the foils and dividing Eq. 3.14 by Eq. 3.13, the result is

$$\frac{\sigma_9 F_9^1}{\sigma_5 F_5^1} = \frac{A_9^{1F}}{A_5^{1F}} \frac{\phi_5^F}{\phi_9^F} \frac{M_9}{M_5} \frac{W_5^F}{W_9^F} \tag{3.15}$$

where M_9/M_5 is the ratio of the atomic mass of Pu^{239} to U^{235}, and W_5^F/W_9^F is the ratio of the weight (area density) of the foils. Here also, the atomic mass ratio is known with great accuracy and the neutron flux can be determined accurately from the monitor foil activities. The weight of the foils can also be measured accurately and is considered in section 3.3.1; the activity ratio is obtained by the gamma counting.

Thus, the ratio given by Eq. 3.15 can be measured, and the result will be denoted R_1. A similar treatment is applied for fission product number 2. Thus, there results the following expressions:

$$R_1 = \frac{\sigma_9 F_9^1}{\sigma_5 F_5^1} = \frac{A_9^{1F}}{A_5^{1F}} \frac{\phi_5^F}{\phi_9^F} \frac{M_9}{M_5} \frac{W_5^F}{W_9^F} \tag{3.16}$$

$$R_2 = \frac{\sigma_9 F_9^2}{\sigma_5 F_5^2} = \frac{A_9^{2F}}{A_5^{2F}} \frac{\phi_5^F}{\phi_9^F} \frac{M_9}{M_5} \frac{W_5^F}{W_9^F} \tag{3.17}$$

Substituting Eq. 3.16 and Eq. 3.17 into Eq. 3.11 and Eq. 3.12, the result is:

$$\frac{A^{1x}}{A^{1s}} = \frac{N_5^x}{N_5^s} \frac{\phi^x}{\phi^s} + \frac{N_9^x}{N_5^s} \frac{\phi^x}{\phi^s} R_1 \tag{3.18}$$

$$\frac{A^{2x}}{A^{2s}} = \frac{N_5^x}{N_5^s}\,\frac{\phi^x}{\phi^s} + \frac{N_9^x}{N_5^s}\,\frac{\phi^x}{\phi^s}\,R_2 \tag{3.19}$$

which then is a set of two equations with two unknowns, namely, N_5^x/N_5^s and N_9^x/N_5^s, which are found by solving the above set of equations. The results are:

$$\frac{N_9}{N_5^s} = \frac{\phi^s}{\phi^x}\,\frac{\dfrac{A^{1x}}{A^{1s}} - \dfrac{A^{2x}}{A^{2s}}}{R_1 - R_2} \tag{3.20}$$

and

$$\frac{N_5^x}{N_5^s} = \frac{\phi^s}{\phi^x}\,\frac{R_1\,\dfrac{A^{2x}}{A^{2s}} - R_2\,\dfrac{A^{1x}}{A^{1s}}}{R_1 - R_2} \tag{3.21}$$

The right-hand members of these equations involve only measurable quantities and the final results can be calculated with greater accuracy as the terms in the differences are widely different.

The enrichment can be obtained, once the ratios given by Eqs. 3.20 and 3.21 are known. The enrichment E of plutonium and uranium of the unknown rod will be given, respectively, by

$$E_9^x = E_5^s\,\frac{N_9^x}{N_5^s}\,\frac{M_9}{M_5}\,\frac{D^s}{D^x} \tag{3.22}$$

$$E_5^x = E_5^s\,\frac{N_5^x}{N_5^s}\,\frac{D^s}{D^x} \tag{3.23}$$

where E_5^s is the enrichment of the calibrating rod and D^s/D^x is the ratio of the density of oxide pellets between the calibrating rod and the unknown rod. It is supposed that the densities are known.

3.2.3 Extension of the Method by Using Several Gamma-Ray Lines

As shown in section 3.3.6, for each fission product of interest, there are often several prominent peaks. Thus, the opportunity of using several gamma-ray lines from one fission product, instead of only one line, introduces the possibility of increasing the accuracy by decreasing the statistical error of counting which is, in fact, the greatest source of uncertainty.

Thus, by indicating by $\sum_i$ the summation for i = 1 up to the number of peaks for a fission product observable in the spectrum, Eqs. 3.9 and 3.10 become, respectively,

$$\sum_i A_i^{1s} = N_5^s \sigma_5 \phi^s F_5^1 \sum_i \epsilon_i^1 I_i \tag{3.24}$$

$$\sum_i A_i^{1x} = N_5^x \sigma_5 \phi^x F_5^1 \sum_i \epsilon_i^1 I_i + N_9^x \sigma_9 \phi^x F_9^1 \sum_i \epsilon_i^1 I_i \tag{3.25}$$

where I_i is the partial yield of gamma rays for the considered energy level of the particular fission product.

Equation 3.16 becomes

$$R_1 = \frac{\sigma_9 F_9^1}{\sigma_5 F_5^1} = \frac{\sum_i A_{9i}^{1F}}{\sum_i A_{5i}^{1F}} \frac{\phi_5^F}{\phi_9^F} \frac{M_9}{M_5} \frac{W_5^F}{W_9^F} \tag{3.26}$$

which, together with similar equations for fission product number 2 with summation index j, will give the results,

$$\frac{N_9^x}{N_5^s} = \frac{\phi^s}{\phi^x} \frac{\dfrac{\sum_i A_i^{1x}}{\sum_i A_i^{1s}} - \dfrac{\sum_j A_j^{2x}}{\sum_j A_j^{2s}}}{R_1 - R_2} \tag{3.27}$$

and

$$\frac{N_5^x}{N_5^s} = \frac{\phi^s}{\phi^x} \frac{R_1 \dfrac{\sum_j A_j^{2x}}{\sum_j A_j^{2s}} - R_2 \dfrac{\sum_i A_i^{1x}}{\sum_i A_i^{1s}}}{R_1 - R_2} \tag{3.28}$$

where R_1 is given by Eq. 3.26 and R_2 is given by

$$R_2 = \frac{\sum_j A_{9j}^{2F}}{\sum_j \sum_{5j}^{2F}} \frac{\phi_5^F}{\phi_9^F} \frac{M_9}{M_5} \frac{W_5^F}{W_9^F} \tag{3.29}$$

By using the ratios given in Eqs. 3.27 and 3.28, the enrichments of the unknown rods are given by the relations (3.22) and (3.23).

3.3 EXPERIMENTAL PROCEDURE AND RESULTS

3.3.1 The Uranium and Plutonium Foils

The uranium foil used was in metallic form, 1 inch in diameter and 0.0052 inch thick, with a surface density equal to 0.2425 g/cm^2 and an enrichment of 93.17 weight percent. Thus, the surface density for U^{235} was 0.2259 g/cm^2. To avoid escape of any recoil or gaseous fission products, the foil was encased in a 3-inch-diameter, aluminum leakproof cladding, 0.015 inch thick.

The plutonium foil was a neutron flux filter commonly used in neutron diffraction experiments and fabricated by Numec of Apollo, Pennsylvania. The specifications given by the fabricator were:

Composition: 91% Pu^{239}, 8% Pu^{240}, and 1% Pu^{241}.
Plutonium-aluminum alloy (1% Al)

Total weight of Pu isotopes: 7.45 g

Total isotope weight of fissile Pu: 6.93 g

Total surface density: 0.300 g of Pu/cm^2

Fissile surface density: 0.276 g/cm^2

Homogeneity: ±2%

Cladding: 0.020-inch-thick Al foil, 3 inches in diameter

Total foil thickness: 0.046 inch

Pu foil thickness: 0.006 inch

These data were checked by dividing the total weight (6.93 g) of the two fissile Pu isotopes by the total area of the foil obtained from a radiographic print of the radioactive foil on a Polaroid film. The area of a 2-inch-square profile with rounded corners was measured and the value obtained for the surface density was 0.272 g/cm^2. The average value assumed and used to calculate R_1 and R_2 was 0.274 g/cm^2. From this foil, only a circle of 1-inch diameter was actually irradiated, as explained in the next section.

To have an extra assurance of the value of the average surface density of both foils and to assure also that no significant nonuniformity of the distribution of the fissile material in the foils was present, a check was done by a transmission experiment.

In this transmission experiment, a monochromatic neutron beam from one of the diffraction spectrometers at the MIT Research Reactor was used. A plan view of the experimental arrangement is shown in Fig. 3.1. The neutron beam from the reactor is diffracted by a

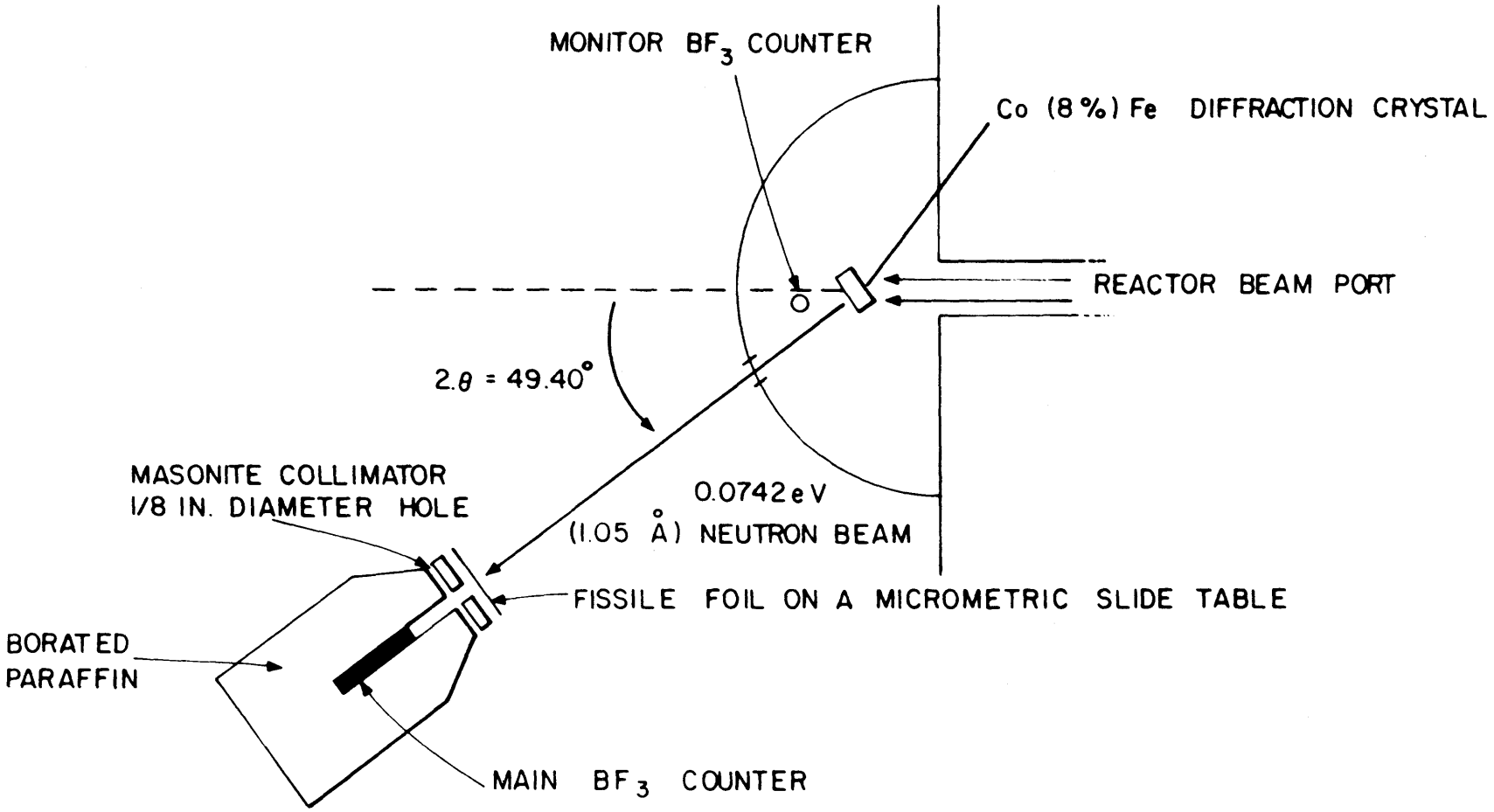

FIG. 3.1 MONOCHROMATIC NEUTRON TRANSMISSION EXPERIMENT

Co(8%)Fe single diffraction crystal to an angle $2\theta = 49.4°$, making a monochromatic beam of 0.0742 eV contaminated by one percent of its harmonic 0.297 eV. The monochromatic beam is attenuated by the fissile foil being checked, and then the transmitted beam passes through a 1/8-inch-diameter masonite collimator, before being detected by a BF_3 counter of 90 percent efficiency surrounded by a cylindrically shaped borated paraffin shield. A neutron beam monitor, a low pressure BF_3 counter, is located immediately after the diffraction crystal and is used to trigger off the main counter whenever the accumulated counts of the incident monochromatic neutrons reach a fixed value of 80,000 counts. The fissile foil was placed one inch from the masonite collimator, fixed on a slide table controlled by a micrometer, and it was scanned in two perpendicular directions and the attenuation factor calculated. The statistics of counting gave an error of less than ±0.3%.

The experimental values of the attenuation factor for both foils along the two perpendicular directions are shown in Fig. 3.2. These data show that the uniformity is within ±1%.

The average values of the attenuation factor for both foils obtained from the experiment are compared with the calculated values for the surface density: 0.2259 g/cm^2 for U^{235} in the uranium foil and 0.274 g/cm^2 for fissile plutonium isotopes in the plutonium foil. The results are given in Table 3.1.

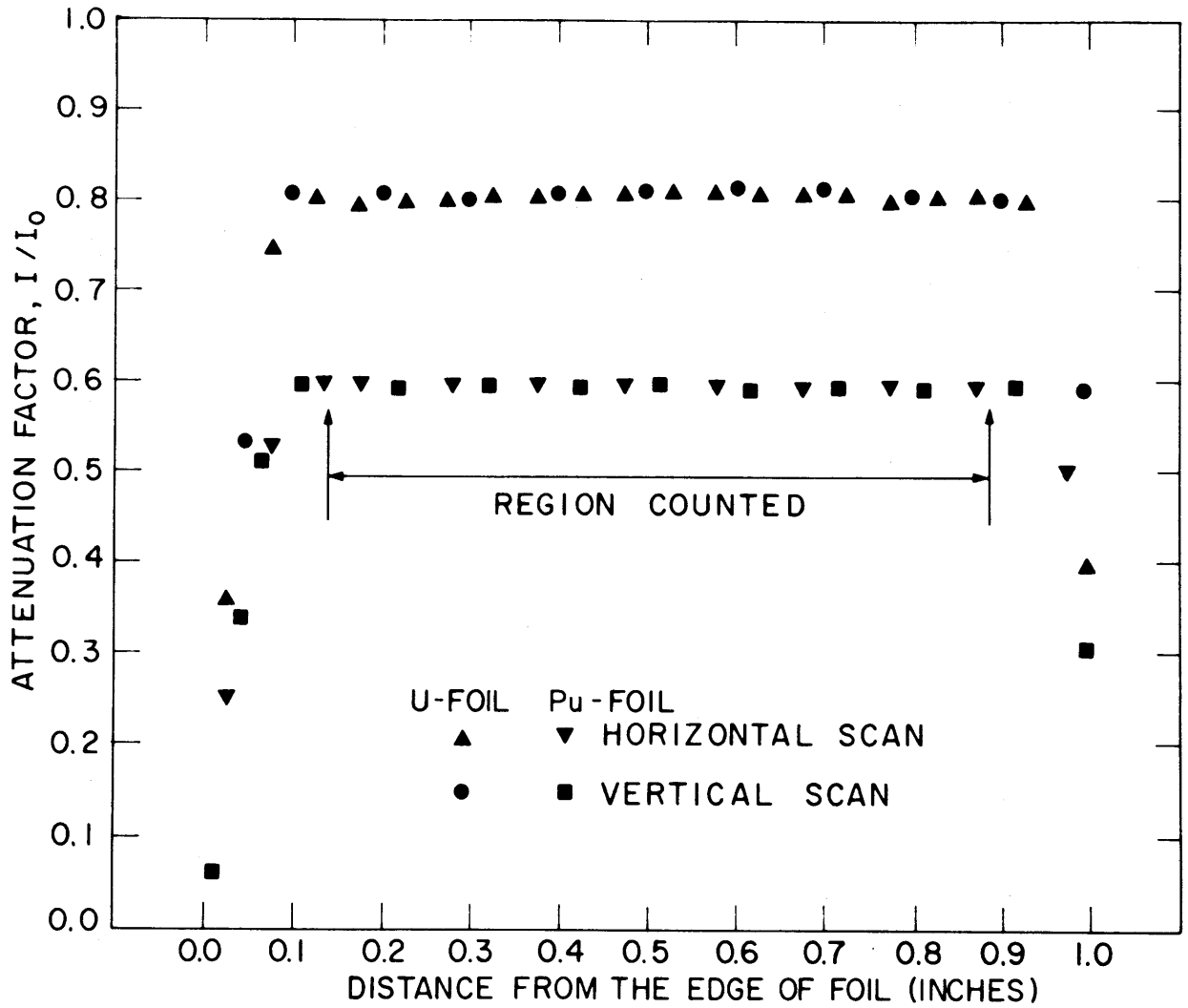

FIG. 3.2 THE ATTENUATION FACTOR I/I_0 OF A MONOCHROMATIC NEUTRON BEAM (0.0742 eV) BY FOILS OF URANIUM AND PLUTONIUM

TABLE 3.1

The Monochromatic Neutron (0.0742 eV) Attenuation Factor for Uranium and Plutonium Standard Foils

Foils	Attenuation Factor, I/I_o	
	Experimental	Calculated
Uranium	0.8075	0.8074
Plutonium	0.5908	0.5917

Thus, there is a striking agreement between the experimental value for the attenuation factor and the calculated value, which indicates that the estimated values for the surface density for both foils are correct within an accuracy of less than ±1%.

3.3.2 Geometry for the Irradiation of the Foils

An important part of the experimental procedure is to assure the same geometrical configuration for irradiation of both foils. Due to the difference in their sizes, both foils were compressed between two 3-inch by 5-inch cadmium sheets, 0.020 inch thick, with a circular 1-inch-diameter hole at the center. Each uranium foil was checked to be sure that it was located exactly inside that hole.

Figure 3.3(a) shows the geometry for irradiation of the foils. The irradiations were done at the central chamber of the rear facility described in section 2.2.1. Both foils were irradiated for the same period of time which was 15 hours.

Due to the difference in absorption cross sections and the thickness of the two foils, the incident neutron flux is attenuated differently

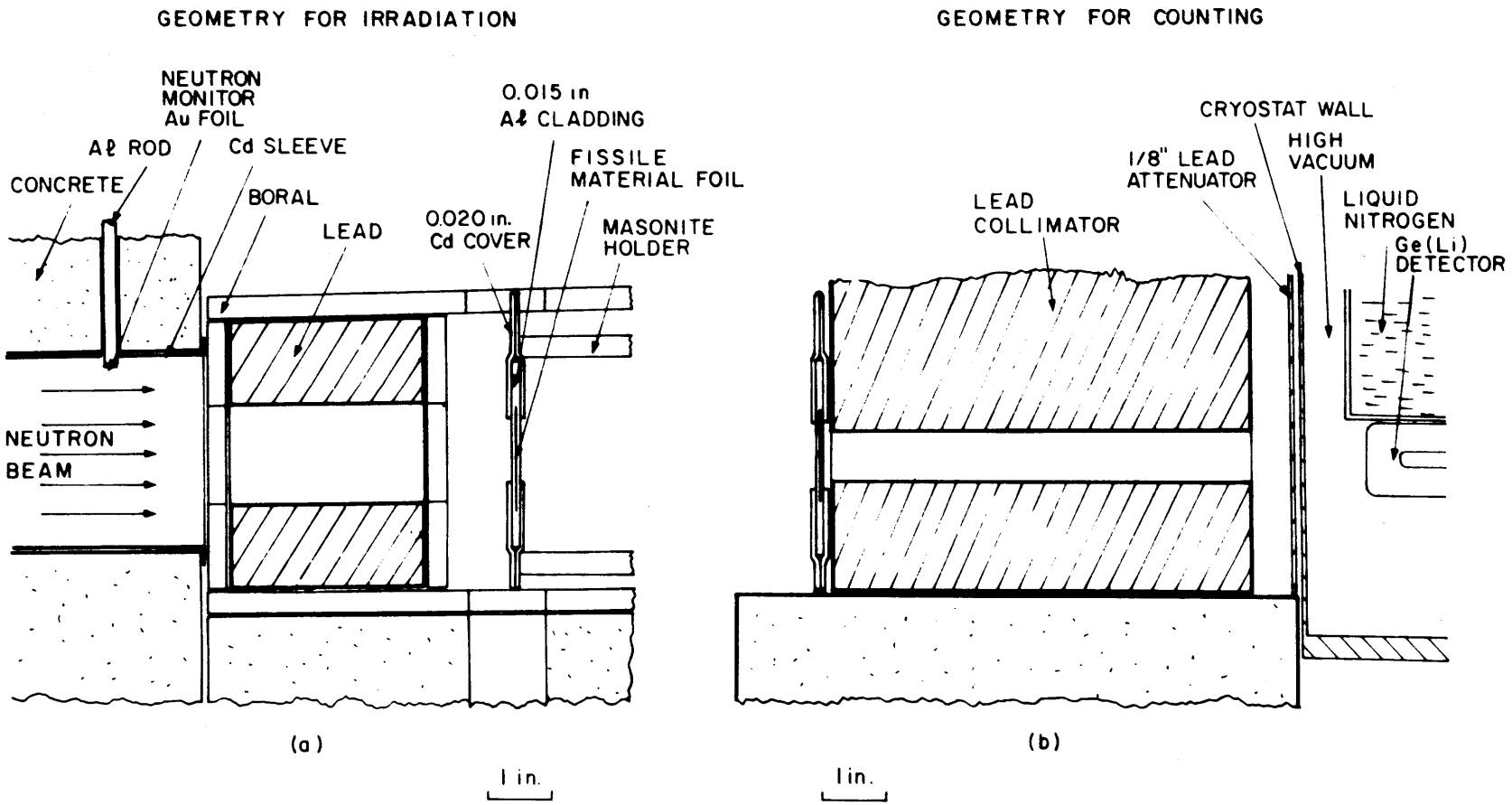

FIG. 3.3 GEOMETRY FOR IRRADIATION AND COUNTING OF FISSILE FOILS

for the foils, and so the effective incident neutron flux will be somewhat different from the actual incident flux. A correction due to this attenuation was made to obtain the ratios R_1 and R_2 given by Eqs. 3.26 and 3.29.

The correction factor C_A for the ratios R_1 and R_2 due to this attenuation is given by

$$C_A = \frac{\Sigma_5}{\Sigma_9} \frac{1 - e^{-\Sigma_9 x_9}}{1 - e^{-\Sigma_5 x_5}} \tag{3.30}$$

where Σ is the macroscopic absorption cross section, and x is the thickness of the foil. The numbers 5 and 9 stand for U^{235} and Pu^{239} as before.

3.3.3 Gamma-Ray Counting of the Irradiated Foils

After the irradiation, each foil was set in place for counting and left to cool for a fixed amount of time: 160 minutes. The geometry for counting is shown in Fig. 3.3(b).

The lead collimator had a 3/4-inch-diameter hole and was 6-1/2 inches long. The foil was attached by mylar tape to the collimator and set to have the center of the 1-inch irradiated circle aligned with the center line of the collimating hole. The 3/4-inch-diameter hole for the collimator was chosen to be less than the 1-inch irradiated circular portion in order to avoid any edge effect in the counting. The geometry was exactly the same for both foils.

The detector used was the 35-cc Ge(Li) crystal, described in section 2.2.2, which was aligned with the collimator having its closed end oriented toward the source. The electronics was set for operation

in the free mode of counting as described in section 2.3.2.

One problem that arose in counting the fission product gamma rays was the difference in the electronic dead time for any two pairs of sources from which the ratio of the areas under certain peaks was to be obtained because one of them was inevitably more active than the other. In this particular case, at the beginning of the counting the plutonium foil was about 17 percent more active than the uranium foil, and consequently the dead time for the counting of the plutonium foil was about 17 percent higher. This dead time also varied with time, decreasing in value as the time of counting increased. Because of this effect, for the multichannel analyzer set for 80 minutes of live time, for example, the total actual time in which the analyzer was on differed for the two foils by 18 minutes, being longer for the plutonium foil. Thus, by considering a specific fission product, Sr^{92} for instance, which decays with a half life of 2.7 hours, for the plutonium foil — which took a longer actual counting time than for the uranium foil — Sr^{92} had decayed to a relatively weaker activity by the end of the counting.

This effect is illustrated in Fig. 3.4. Thus, the value for the ratios of activities in Eqs. 3.16 and 3.17 will be not exactly the ratio between the areas under the peaks for both foils but rather it will be given by the ratio of the true count rate for the fission product in both foils at the beginning of counting.

This ratio of true count rate for the foils was obtained as described below. Considering the case of Sr^{92} as an example, let

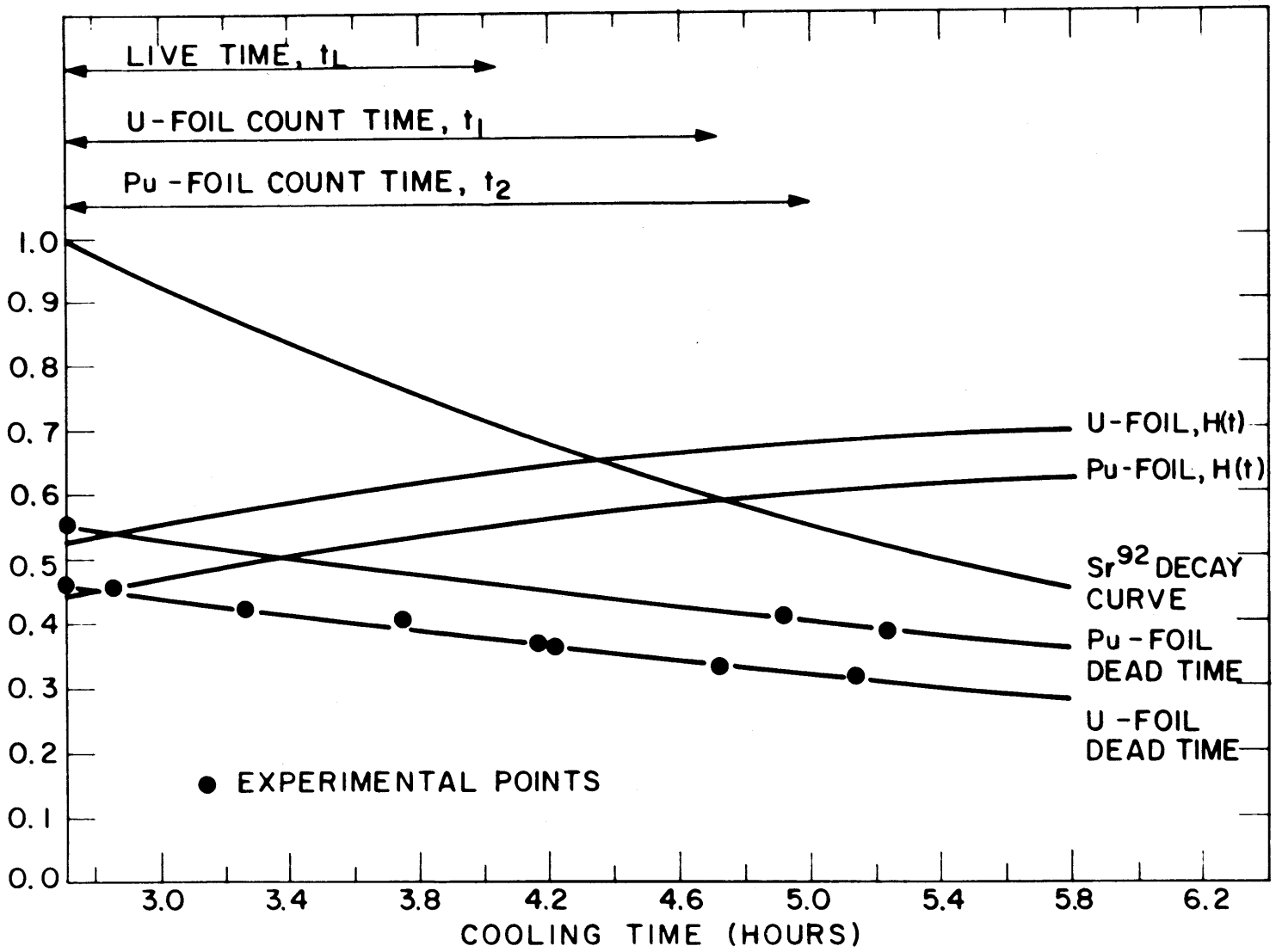

FIG. 3.4 ELECTRONIC DEAD TIME VARIATION CURVE AND Sr^{92} DECAY CURVE

C = true count rate for a Sr^{92} gamma line at the start of counting,

T = total number of counts for the Sr^{92} line recorded in the analyzer during the entire actual counting period,

H(t) = electronic live-time efficiency,

t_1 = actual counting time period for uranium foil,

t_2 = actual counting time period for plutonium foil.

The function H(t) of the decay time t is the fraction of the time when the electronics is free to detect a signal; i.e., it is the ratio between the live time and the actual counting time. Each of the above parameters is accompanied by a subscript, where 5 stands for the uranium foil and 9 for the plutonium foil.

In the case of fission products for which the activity at the time of counting decreases exponentially, such as I^{135} and Sr^{92} for the present work, the following expressions are established:

$$T_5 = \int_0^{t_1} C_5 e^{-\lambda t} H_5(t)\, dt \tag{3.31}$$

$$T_9 = \int_0^{t_2} C_9 e^{-\lambda t} H_9(t)\, dt \tag{3.32}$$

where λ is the decay constant of the fission product under consideration. From these two equations, the expression below results:

$$\frac{C_5}{C_9} = \frac{T_5}{T_9} \cdot \frac{\int_0^{t_2} e^{-\lambda t} H_9(t)\, dt}{\int_0^{t_1} e^{-\lambda t} H_5(t)\, dt} \tag{3.33}$$

which is the value of the ratio of the true activities at the start of

counting required for Eqs. 3.16 and 3.17. That is,

$$\frac{A_5^F}{A_9^F} = \frac{T_5}{T_9} \frac{\int_0^{t_2} e^{-\lambda t} H_9(t)\, dt}{\int_0^{t_1} e^{-\lambda t} H_5(t)\, dt} \tag{3.34}$$

where T_5/T_9 is the ratio between the areas under the peaks for the foils. The ratio between the integrals can be calculated if $H_9(t)$ and $H_5(t)$, the electronic live-time efficiency functions, are known. These functions are obtained empirically.

As shown in Fig. 3.4, the dead time DT decreases with time because of the decay of the foils' total activity. The live-time efficiency is given by

$$H(t) = 1 - DT(t) \tag{3.35}$$

This function is obtained empirically by fitting a parabolic curve to the experimentally obtained H(t) of Fig. 3.4, and its value is

$$H(t) = -0.022t^2 + 0.113t + K \tag{3.36}$$

The constant K is the initial value of the live-time efficiency curve and is obtained accurately from the relation

$$\text{live-time} = t_L = \int_0^t H(t)\, dt \tag{3.37}$$

where the actual counting time t is equal to t_1 for the uranium foil and t_2 for plutonium, and the live-time t_L is chosen in the multichannel analyzer. Explicitly, Eq. 3.37 gives

$$K = \frac{t_L}{t} + 0.022\,\frac{t^2}{3} - 0.113\,\frac{t}{2} \tag{3.38}$$

In order to establish its final form, the function H(t) was extensively studied numerically by using a PDP-8/L digital computer of Digital Equipment Corporation and the computer program C-FOCAL. H(t) is weakly dependent on the values of the coefficients 0.113 and -0.022 and is strongly dependent on the value of K. Fortunately, this latter constant can be calculated accurately by Eq. 3.38.

Thus, the ratio of the activities A_5^F/A_9^F is given by the product between the ratio of observed total counts T_5/T_9 and a correction factor C_{DT} given by

$$C_{DT} = \frac{\int_0^{t_2} e^{-\lambda t} H_9(t)\, dt}{\int_0^{t_1} e^{-\lambda t} H_5(t)\, dt} \tag{3.39}$$

which can be calculated with the function H(t) given by Eq. 3.36. This correction is executed by the computer code FUEL ASSAY described in Appendix B.

The expression for C_{DT} given by Eq. 3.39 can also be used for two fuel rods of different activities, such as the case for the standard and the unknown rods. It is also observed that because of the linearity of the expressions (3.31) and (3.32), the same correction factor is applicable when the method is extended to several gamma lines from one fission product, that is, specifically to the ratios of activities in Eqs. 3.26 and 3.29.

3.3.4 Fuel Rods

The fuel rod used as the standard to which the unknown rod is compared and analyzed was made up of 1.30% enriched uranium oxide cylindrical pellets of 0.500 inch in both diameter and height. Its density was obtained by weighing five typical pellets, and calculated as 10.11 g/cm^3. The fuel is clad in a 9/16-inch-o.d., aluminum tube 0.030 inch thick and has 48 inches of active length. For the irradiation of the fuel rod, the pellets were pressed together to assure that there was no gap open between the pellets within the irradiation region's 2-inch length.

The rod which is treated as "unknown" throughout this work was a simulated burned fuel from the USAEC-AECL Cooperative Program (B3). In fact, two rods of different composition were used. Both were composed of coprecipitated oxide pellets of average density 10.41 g/cm^3 and of the same dimensions as those of the standard rod, i.e., 0.500 inch in both diameter and length. Their compositions are given in Table 3.2 below.

TABLE 3.2

Isotopic Composition of the Pu-Containing Fuel Rods

Fuel Type	Isotopic Weight Percent of Total Uranium and Plutonium				
	U-235	Pu-239	Pu-240	Pu-241	Pu-242
A-Red*	0.30	0.24	0.062	0.009	0.001
B-Gold*	0.30	0.25	0.016	0.002	0.001

*The colors, red and gold, refer to the paint on top of each rod for identification purposes.

Both of the mixed fuel rods were clad in aluminum tubing 0.020 inch thick and 54 inches long. The geometry for irradiation and gamma-ray counting of the fuel rods used in this work is shown in Fig. 3.5. The geometrical arrangements for all the rods were reproduced exactly. They were irradiated, cooled, and counted for the same period of time as the two standard foils described in the preceding section. The correction due to the electronic dead time was done in the same fashion as for the foils. The incident neutron attenuation correction factor, because of the difference in enrichment, was given by the expression:

$$C_{AR} = \frac{\frac{2R}{\Sigma_x} - \frac{2}{\Sigma_x}\int_0^R e^{-2\Sigma_x\sqrt{R^2-y^2}}\,dy}{\frac{2R}{\Sigma_s} - \frac{2}{\Sigma_s}\int_0^R e^{-2\Sigma_s\sqrt{R^2-y^2}}\,dy} \tag{3.40}$$

where R is the radius of the fuel rods which was the same for both the unknown and standard rods; Σ is the macroscopic absorption cross section where the subscript x stands for the unknown rod and the subscript s stands for the standard rod. The quantity C_{AR} is also to be multiplied by the ratio ϕ_x/ϕ_s.

Expression (3.40) was obtained by considering the ratio of the volume within the cylindrical surface of the rod, and the exponential attenuation curve of the incident neutron beam, for both the unknown and calibrating rods. Ultimately, C_{AR} is calculated by a numerical integration in the computer code FUEL ASSAY, written for this work and explained in Appendix B.

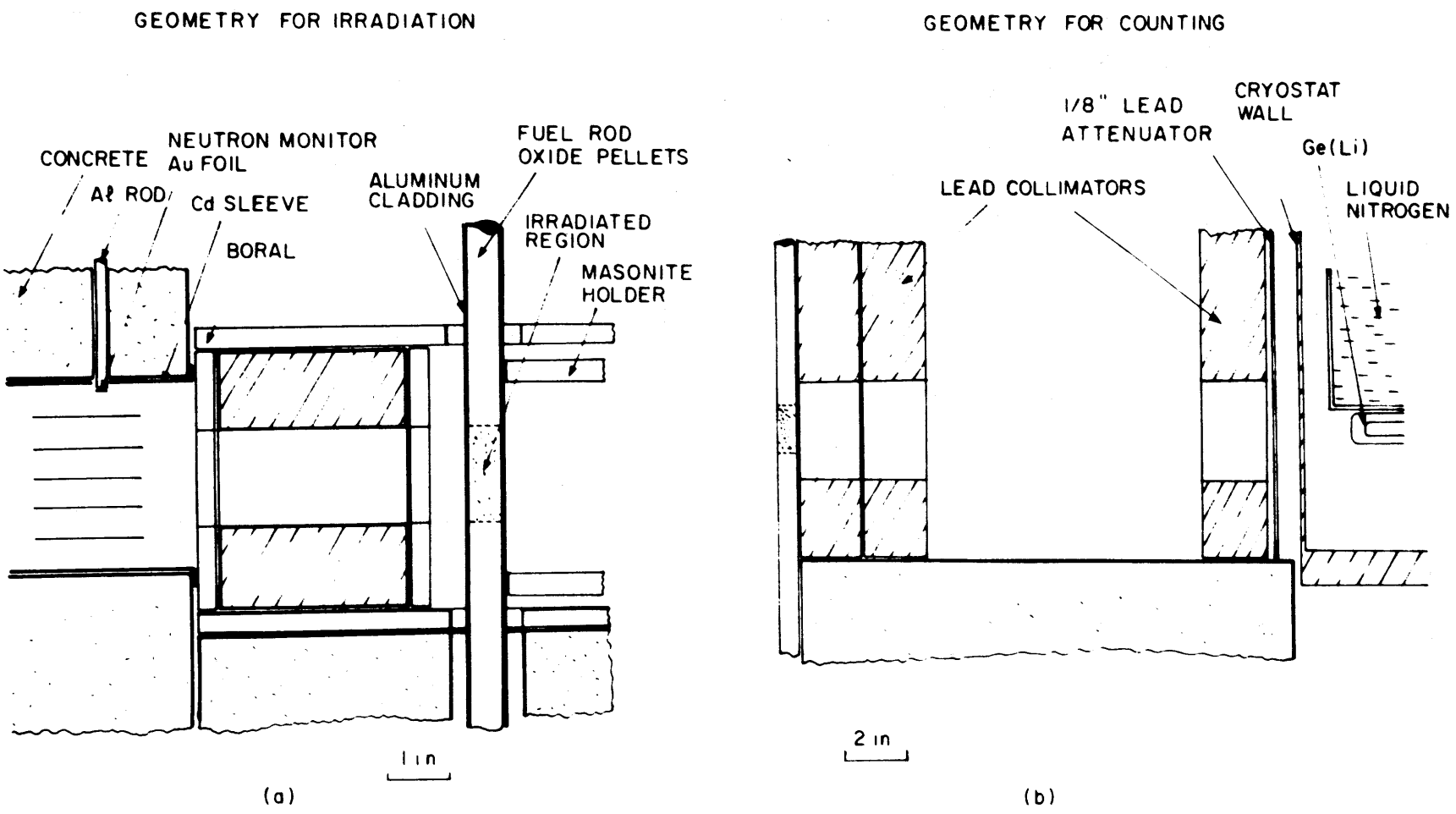

FIG. 3.5 GEOMETRY FOR IRRADIATION AND COUNTING OF FUEL RODS

3.3.5 The Observable Short-Lived Fission Product Gamma Rays

The primary interest was focused on short-lived fission products. It was intended to investigate the possibility of analyzing a fresh fuel rod containing plutonium and uranium in a matter of hours or a day. Too short-lived fission products, on the other hand, would raise the problem of accumulating enough counts to yield a meaningful result.

A series of spectra were taken from irradiated uranium metal foil with irradiation time varying from 4 hours to 24 hours and cooling time ranging from 10 minutes to 60 days. Figure 3.6 is a good example of short-lived fission product gammas. For this spectrum, a uranium foil enriched to 93.1% in weight of U^{235} was irradiated during 24 hours, cooled for 3 hours and then counted for the next 9 hours. In order to calibrate the energies of the peaks, a Na^{22} gamma source was placed within the view of the detector during the counting process so that both its peaks at 0.5110 keV and 1.2745 MeV could be seen superposed in the spectrum as shown in Fig. 3.6. The computer code GAMANL was used to debug the data (see section 4.1 for a summary description of GAMANL). The identification of the peaks was performed based on the data of Heath (H1) and Gordon (G1). Table 3.3 gives the energies and the corresponding fission products for the principal lines shown in Fig. 3.6.

Figures 3.7 and 3.8 are the spectra of the uranium and plutonium foils, respectively, that were described in section 3.3.1 and used for the calculations in this work. Both foils were irradiated at a flux level of 10^8 n/cm^2 sec for 15.00 hours with the same geometry for irradiation as described in section 3.3.2, and thereafter cooled for

TABLE 3.3

Some Short-Lived Fission Products and Their Gamma Rays

Line Number*	Energy (keV)	Fission Product
1	141.8	Tc^{99}
6	229.3	Te^{132}
7	250.7	Xe^{135m}**
8	267.2	Y^{93}
9	294.1	Ce^{143}
10	306.9	Ru^{105}
11	320.5	Rh^{105}
12	329.6	La^{140}
13	339.8	Ce^{143}
14	364.8	I^{131}
18	487.7	La^{140}
19	497.7	Ru^{103}
21	524.4	I^{132}
22	530.2	I^{133}
25	556.0	Y^{91m}
28	641.1	La^{142}
30	658.4	Nb^{97}
31	667.9	I^{132}
32	706.4	I^{134}

* The line numbers correspond to the numbers identifying the peaks in the spectrum shown in Fig. 3.6. The accuracy in energy determination was ±1 keV.

**The superscript m refers to isomeric states.

TABLE 3.3 (concluded)

Line Number	Energy (keV)	Fission Product
33	723.9	I^{132}
34	743.5	Zr^{97}
35	750.2	Sr^{91}
37	772.9	I^{132}
38	815.0	$I^{132} + La^{140}$
39	836.5	I^{135}
40	846.2	I^{134}
43	884.6	I^{134}
46	934.8	Y^{92}
48	954.2	I^{132}
50	1024.3	Sr^{91}
51	1038.4	I^{135}
54	1115.1	I^{134}
56	1131.3	I^{135}
60	1260.1	I^{135}
64	1383.1	Sr^{92}
68	1456.8	I^{135}
74	1595.6	La^{140}
76	1677.2	I^{135}
77	1705.9	I^{135}
81	1790.5	I^{135} (?)
83	1835.2	Rb^{88}

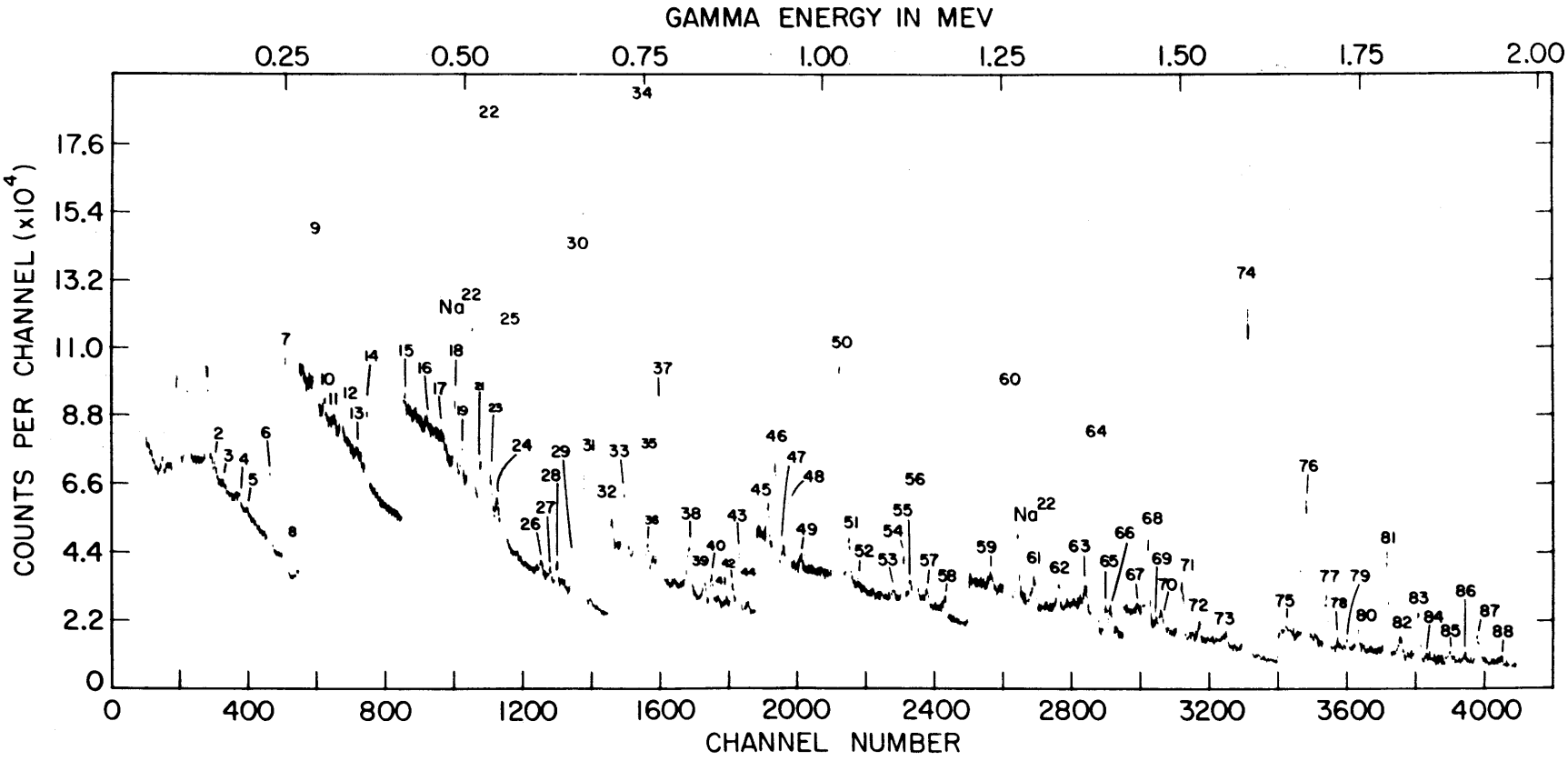

FIG. 3.6 U^{235} FISSION PRODUCT DECAY GAMMAS (24 HOURS IRRADIATION, 3 HOUR COOLING, AND 9 HOURS COUNTING)

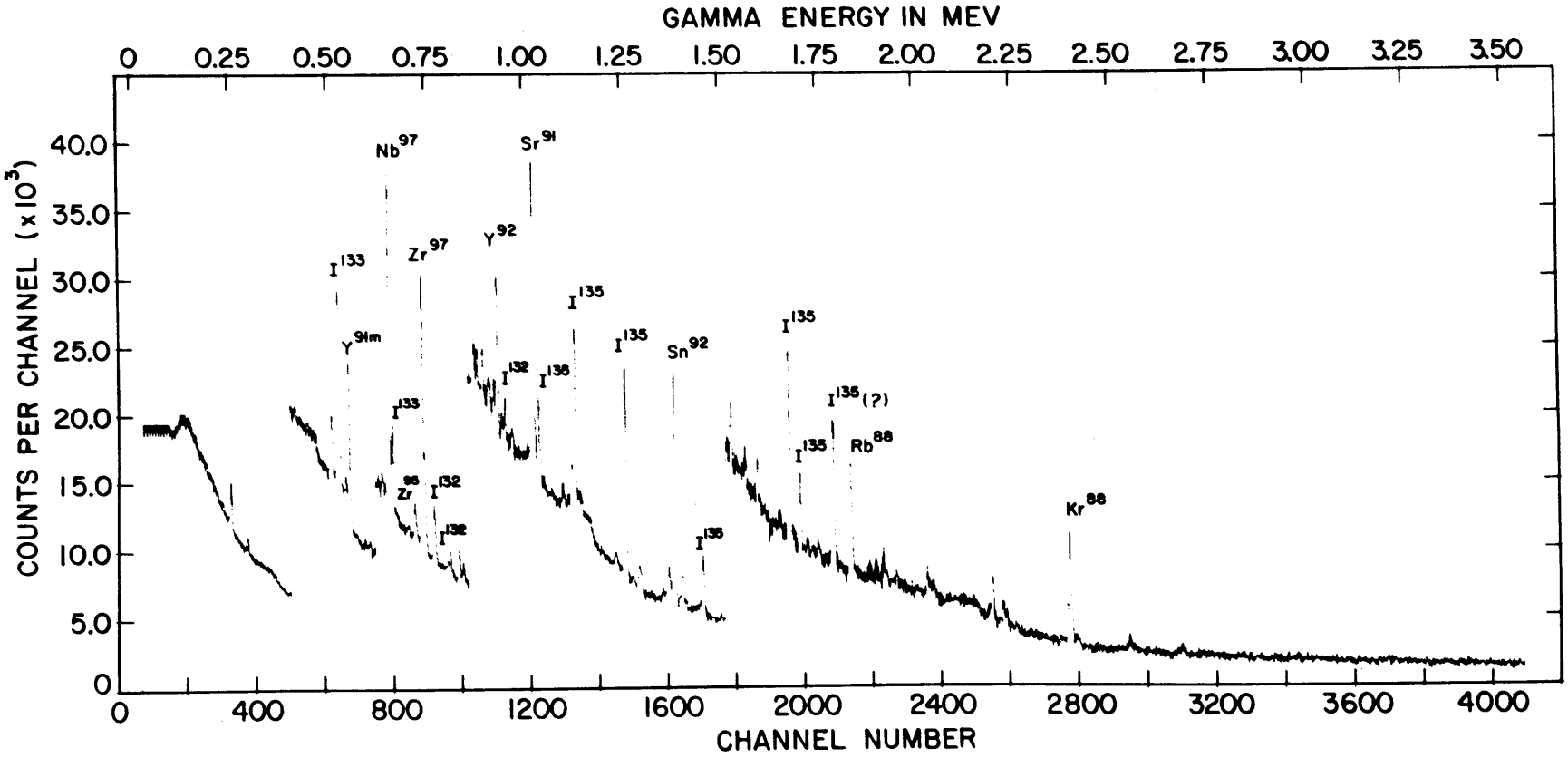

FIG. 3.7 SHORT-LIVED FISSION PRODUCT GAMMA-RAYS FOR U^{235}

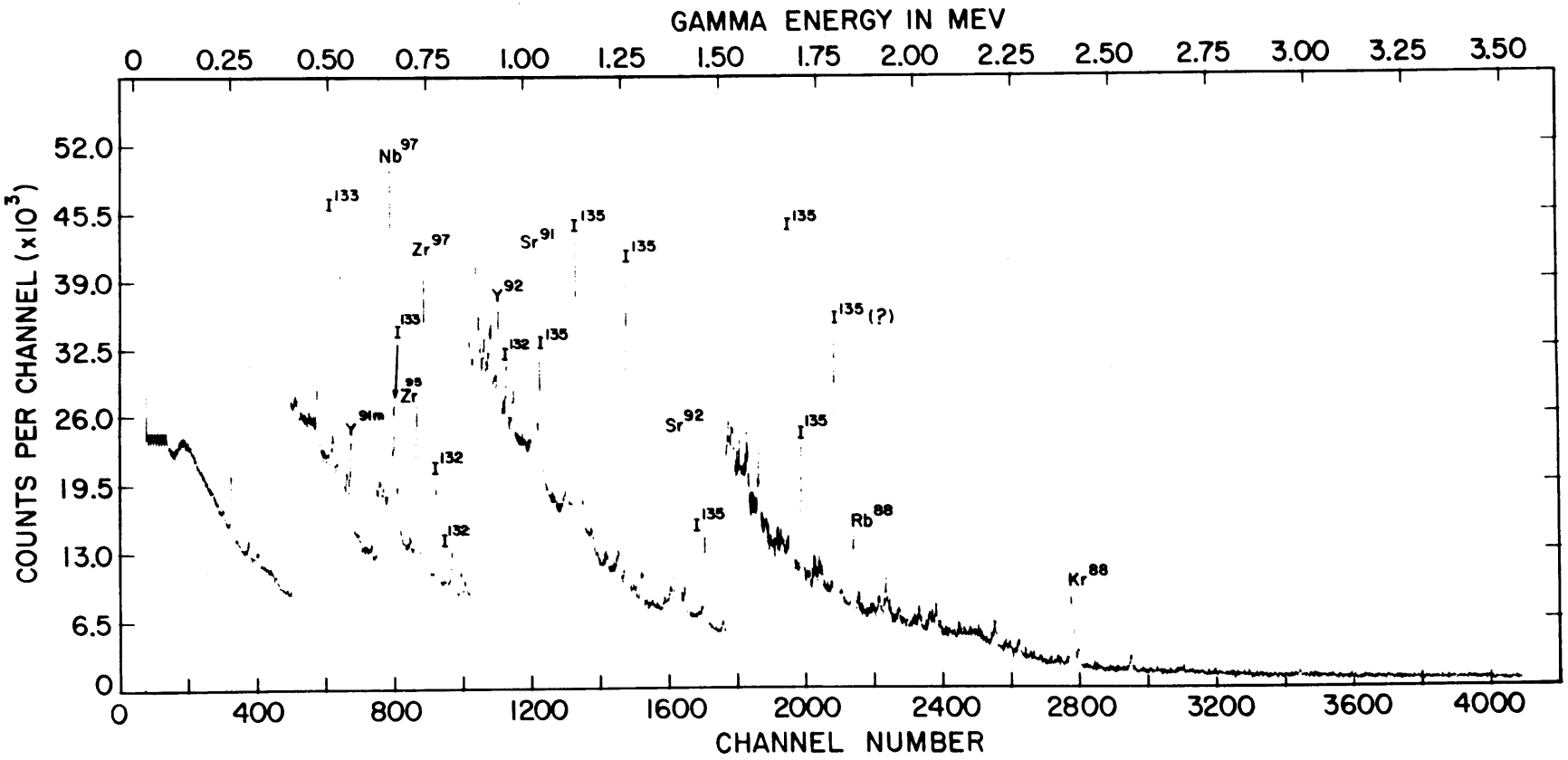

FIG. 3.8 SHORT-LIVED FISSION PRODUCT GAMMA-RAYS FOR Pu^{239}

130 minutes and counted for 160 live minutes with the geometrical arrangement described in section 3.3.3. Figure 3.7 is the spectrum for the fission products of U^{235}, and Fig. 3.8 is that for Pu^{239} (with 1% contamination of Pu^{241}). Table 3.4 shows the principal lines of these fission products and their corresponding nuclei. This combination of irradiation, cooling and counting hours appeared to be optimum since the spectrum contains well-spaced peaks and a combination of four pairs of fission products for which the observed yields are different for U^{235} compared to Pu^{239}.

3.3.6 The Choice of Fission Products

The choice of a pair of fission products is not as obvious as it seems to be. They are not chosen solely on the basis of the relative difference in their percent yield from fission nor of the product of the yield and the fission cross section. But rather there are other parameters to be considered also, such as the yield of all the radioactive parents that decay to the fission product considered (each one is produced in different amounts for U^{235} and Pu^{239} fissions), their decay constants, and also the intensity of the transition gammas which are different for each energy level.

The choice still cannot be made based on the data for each of the parameters mentioned above due to the fact that the detailed knowledge of the percent yield for the components of many decay chains for the fission products of Pu^{239} is still lacking and knowledge of the intensities of the transition gammas in the decay scheme of each fission product is incomplete. Thus, the choice is an empirical task and,

TABLE 3.4

The Principal Fission Product Gammas of Figures 3.7 and 3.8

Fission Product	Energy (keV)
I^{133}	529.9
Y^{91m*}	555.5
Nb^{97}	657.2
I^{132}	666.2
Zr^{95}	723.3
Zr^{97}	743.2
I^{132}	771.5
I^{132}	811.8
Y^{92}	933.8
I^{132}	953.2
Sr^{91}	1024.4
I^{135}	1038.0
I^{135}	1133.2
I^{135}	1260.4
Sr^{92}	1384.3
I^{135}	1458.9
I^{135}	1678.3
I^{135}	1705.9
I^{135} (?)	1794.5
Rb^{88}	1837.0
Kr^{88}	2395.8

*The superscript m refers to isomeric states.

ultimately, it depends solely on the relative difference of the observed areas under the peaks of a pair of fission products in the spectrum for U^{235} compared with Pu^{239}.

By comparing the spectrum for U^{235} shown in Fig. 3.7 with the same spectrum for Pu^{239} shown in Fig. 3.8, the following conclusions can be drawn:

(a) By taking the areas under the peaks of I^{135} in both spectra as a reference, the observed yields of the gammas from I^{132}, I^{133}, Zr^{97} and Nb^{97} are about the same in both spectra.

(b) With the same reference, the observed yields of the gammas from Y^{92} and Sr^{92}, Y^{91m} and Sr^{91}, and Rb^{88} and Kr^{88} are about a factor of two smaller for Pu^{239} than for U^{235}.

(c) The number of gammas from Zr^{95} in the spectrum of Pu^{239} is much higher than that for U^{235}, but this is due to the background activity of Zr^{95} from the previous irradiation of the Pu foil which has been used many times in neutron diffraction experiments at much lower flux (10^5 n/cm^2-sec) but for a long time. The nuclide Zr^{95} has a half life of 65 days which is much longer than that of the other fission products shown in both spectra.

Thus, any pair formed by one fission product mentioned in item (a) and another in item (b) could satisfy the basic requirement that the observed yields are different between them and between the two fissile elements.

Nevertheless, in dealing with gamma rays, it is wiser to concentrate on the use of high energy gammas due to self-absorption effects inside the fuel rods which are much stronger for low energy gamma

rays. In the present case, although much of this effect is cancelled out by using the ratios of the areas under the peaks of one fuel rod to another, some influence is expected due to the different spatial distribution of the fission product gamma source strength inside the fuel rods, since the incident neutron flux is attenuated differently due to the dissimilar enrichment of the fuel rods.

Thus, in order to minimize this effect, the use of the gamma rays was restricted to those with energy higher than 1 MeV. Therefore, the choice is narrowed to a pair formed by I^{135} and one of the nuclei Sr^{91}, Sr^{92}, Rb^{88} and Kr^{88}. The last two nuclei were disqualified due to their lower gamma intensity. In Table 3.5 are shown the decay chains for these three remaining nuclei.

3.4 FINAL RESULTS AND COMMENTS

Theoretically, a pair of lines – one formed by the sum of all I^{135} peaks for which the observed yield is in fact about 63% higher for Pu^{239} than for U^{235}, and another formed by the sum of all the peaks of Sr^{91}, Sr^{92}, Rb^{88} and Kr^{88} for which the observed yield is lower for Pu^{239} than for U^{235} – could be used to obtain the ratios of activities in Eqs. 3.27 and 3.28 and hence yield the desired results. Nevertheless, the correction factor due to the dead time, in the way it was formulated and expressed by Eq. 3.39, is no longer applicable because it assumed a simple exponential decay for the activities of only one fission product for numerator and denominator corresponding, respectively, to two distinct foils or rods. A rather cumbersome correction factor is expected for the generalization suggested above, and this was not

TABLE 3.5

Fission Product Decay Chains of Interest to the Present Work

Decay of Mass Chain - 91

$$10\ \text{sec}\ Kr^{91} \rightarrow 72\ \text{sec}\ Rb^{91} \rightarrow 9.7\ \text{hr}\ Sr^{91} \begin{cases} \xrightarrow{0.60} 50\ \text{min}\ Y^{91m} \downarrow \\ \xrightarrow{0.40} 58\ \text{day}\ Y^{91} \end{cases} \rightarrow \text{Stable}\ Zr^{91}$$

Decay of Mass Chain - 92

$$3.0\ \text{sec}\ Kr^{92} \rightarrow 5.3\ \text{sec}\ Rb^{92} \rightarrow 2.7\ \text{hr}\ Sr^{92} \rightarrow 3.6\ \text{hr}\ Y^{92}\ \ \text{Stable}\ Zr^{92}$$

Decay of Mass Chain - 135

$$6.0\ \text{sec}\ Sb^{135} \rightarrow 1.4\ \text{min}\ Te^{135} \rightarrow 6.7\ \text{hr}\ I^{135} \begin{cases} \xrightarrow{0.30} 15.3\ \text{min}\ Xe^{135m} \downarrow \\ \xrightarrow{0.70} 9.2\ \text{hr}\ Xe^{135} \end{cases} \rightarrow 2.0\times10^{6}\ \text{yr}\ Cs^{135} \rightarrow \text{Stable}\ Ba^{135}$$

considered in this work. The pair chosen for the present analysis was made up of I^{135} and Sr^{92}. From the data of Table 3.5, both nuclei are expected to decay with a simple exponential rate during the counting, as predicted in Eq. 3.8 for the case of Sr^{92}, due to the fact that their precursors have half lives of the order of seconds compared to their own half lives of the order of hours.

The analysis of the mixed rod type B-Gold is described in some detail below in order to illustrate the statistics involved and the corresponding errors. For the mixed rod A-Red, the numbers are very similar because its composition does not differ significantly from the B-Gold type.

Figure 3.9 shows a detail of the spectra presented in Figs. 3.7 and 3.8, together with the same segment of spectrum for the rod containing a mixture of plutonium and uranium, to illustrate the difference in the observed yield of the Sr^{91} and Sr^{92} gammas relative to the I^{135} peaks.

In Table 3.6 is shown the breakdown of the number of counts for the peaks of I^{135} and Sr^{92} used for the analysis of the fuel rod B-Gold. Table 3.7 gives the correction factors involved in the calculation of the ratios of activities for the same rod, and Table 3.8 gives the final results of the analysis of the mixed rods types B-Gold and A-Red.

It is concluded that, with the present method, it is possible to determine the U^{235} and Pu^{239} content in a mixed rod with an accuracy ranging from ±5% to ±10%. The main source of error is the statistical error from the counting of Sr^{92}. It is believed that with a counting time of about 10 hours instead of 160 minutes, the count accumulation could be high enough to increase the accuracy to less than ±5%.

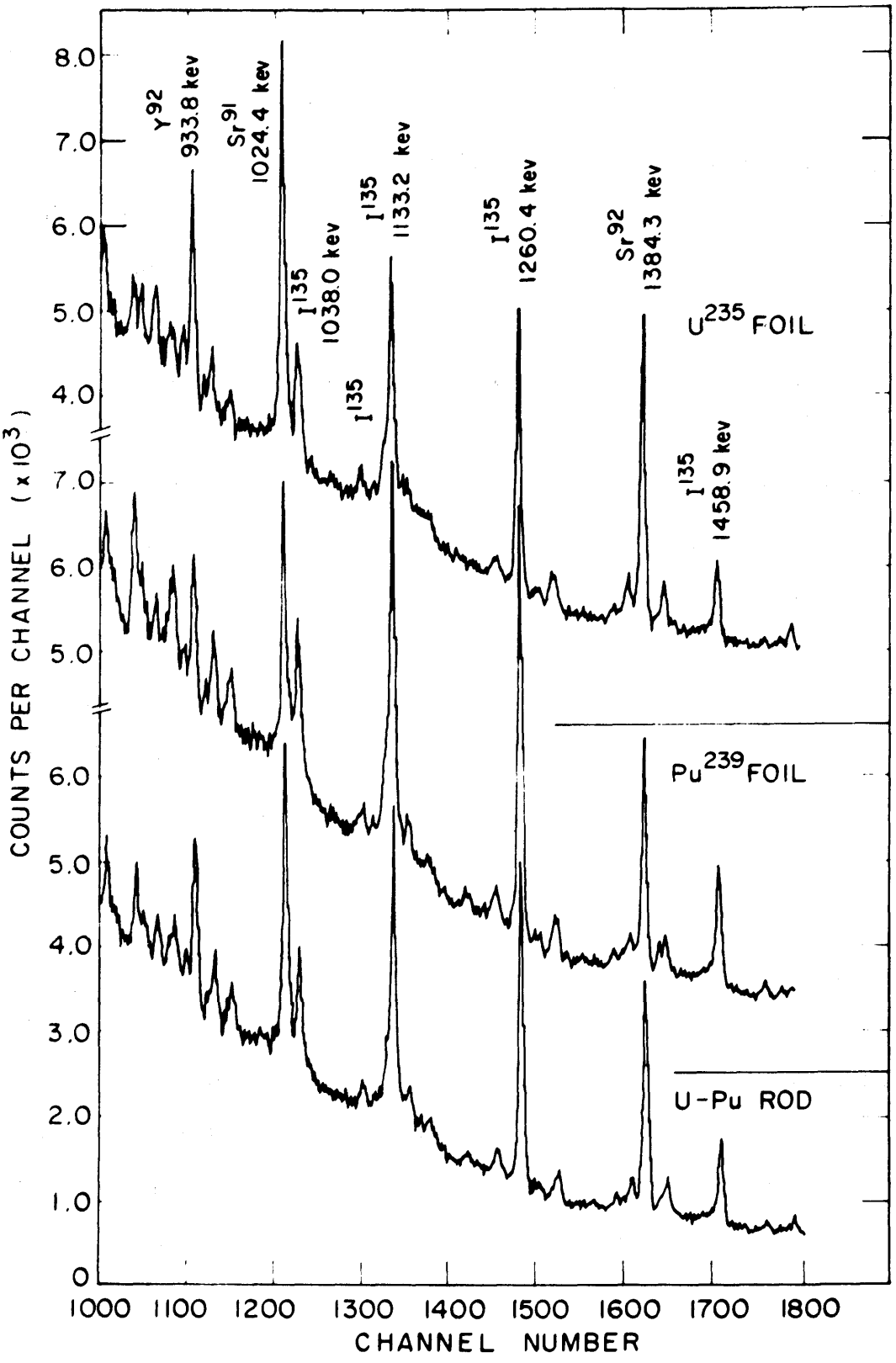

FIG. 3.9 DETAIL OF THE SPECTRA OF FISSION PRODUCTS FOR THE U-FOIL, Pu-FOIL AND MIXED ROD B-GOLD

TABLE 3.6

Count Accumulation for the Analysis of Pu-U Rod, Type B-Gold

Fission Product Number 1, I^{235} Energy (keV)	Number of Counts Under the Peak			
	U-Foil	Pu-Foil	Pu + U Rod	U-Standard Rod
1133.2	16341 ± 457	30156 ± 603	25084 ± 602	45132 ± 903
1260.4	16166 ± 388	27231 ± 571	20959 ± 482	37440 ± 711
1459.3	4449 ± 195	8187 ± 327	6477 ± 259	10312 ± 350
1678.3	4488 ± 197	7178 ± 359	5548 ± 277	11030 ± 397
1706.1	1360 ± 114	3178 ± 206	2292 ± 169	4369 ± 240
Total =	42810 ± 670	75930 ± 983	60360 ± 876	108283 ± 1287

Fission Product Number 2, Sr^{92} Energy (keV)	Number of Counts Under the Peak			
	U-Foil	Pu-Foil	Pu + U Rod	U-Standard Rod
1384.1	33094 ± 695	24820 ± 645	27891 ± 669	69317 ± 1317

TABLE 3.7

Correction Factors for the Analysis of Pu + U Rod, Type B-Gold

Correction Factor	For Determining R_1 and R_2
Flux monitor, $\frac{\phi_U}{\phi_{Pu}}$ =	1.0350
Flux attenuation, $\frac{\text{Pu-Foil}}{\text{U-Foil}}$ =	1.0450
Dead time, $\frac{\text{Pu-Foil}}{\text{U-Foil}}$ =	for I^{135} 1.0134
	for Sr^{92} 1.0346

Correction Factor	For Determining A^x/A^s
Flux monitor, $\frac{\phi^s}{\phi^x}$ =	1.080
Flux attenuation, $\frac{\text{U-Rod}}{\text{mixed rod}}$ =	1.0255
Dead time, $\frac{\text{U-Rod}}{\text{mixed rod}}$ =	for I^{135} 1.0344
	for Sr^{92} 1.0895

TABLE 3.8

Final Results for the Analysis of Mixed Rods

Measured Values	B-Gold Fuel	A-Red Fuel
N_9^x/N_5^{s*}	0.193 ± 0.015	0.178 ± 0.017
N_5^x/N_5^s	0.254 ± 0.016	0.270 ± 0.027
E_9^{x**}	0.249 ± 0.019	0.230 ± 0.022
E_5^x	0.322 ± 0.016	0.343 ± 0.034

Fabricator Data	B-Gold Fuel	A-Red Fuel
E_9^{x***}	0.252	0.249
E_5^x	0.30	0.30

* Ratio of the number of atoms between the unknown and the standard rods.

** Lu weight percent enrichment.

*** Weight percent enrichment of $Pu^{239} + Pu^{241}$.

It is observed that the contribution of fissions by U^{238} and Pu^{240}, which are present in both foils, to the total number of fissions in the foils is negligible because of the low percentage of both nuclei in their respective foils (6.9% of U^{238} in the uranium foil and 8% of Pu^{240} in the plutonium foil).

However, the large amount of U^{238} in both the standard and the test rods cannot be overlooked. According to the work of Price et al. (S4), the ratio of the number of fissions of U^{238} nuclei to the number of fissions of U^{235} nuclei in a 1.30% enriched uranium oxide rod can be estimated as 2.3%. These fissions are caused by the fast (fission) neutrons produced within the rod itself as they pass through the rod on their way out. An analysis of the influence of these fast fissions on the final results of the present fuel assay was made. It was concluded that the fissions of the U^{238} nuclei would cause an overestimation of the content of both U^{235} and Pu^{239} in the mixed rods, but this overestimation is less than 1% of the enrichment determined for both U^{235} and Pu^{239}.

On the other hand, both the plutonium foil and the mixed rods contain some Pu^{241} which is fissionable by thermal neutrons. The plutonium foil and the mixed rod B-Gold both contain about 1% Pu^{241} in terms of the total plutonium content, and therefore the results presented above for this rod should give a correct amount of Pu^{239} plus Pu^{241} in the rod, for both the foil and the rod have the same percentage of Pu^{241}. The mixed rod type A-Red contains about 4% Pu^{241} relative to the total amount of plutonium in the rod, according to the fabricator. Thus, in this latter case, an additional uncertainty comes

from the unknown detailed characteristics of Pu^{241} fission products such as percent yield from the fission. This uncertainty could add up to about ±3% in the value obtained for fissile plutonium content.

The spectrum shown in Fig. 2.11 in Chapter II resulted from the irradiation of an uranium foil for 4 hours, subsequent cooling of 2 hours and counting for 160 minutes. With this arrangement, it was estimated that the same results as obtained for 15 hours' irradiation and 130 minutes' cooling could be accomplished with little loss in accuracy. Thus, this method can analyze a mixed rod with an accuracy of less than ±10% in about one day of work.

A natural improvement in the method is the use of certain fission products which have a more dramatic difference in the observed yield for U^{235} compared to Pu^{239}, such as Ru^{103} and Rh^{106} instead of Sr^{92}. A larger difference in the observed yield will help greatly to obtain the differences in the numerator of Eqs. 3.27 and 3.28 with smaller error. For the present scheme of using I^{135} and Sr^{92}, for example, each of the terms in the numerator of Eqs. 3.27 and 3.28 is obtained with an accuracy of about ±3%; but by performing the difference, due to the small magnitude of the resulting number, the relative error more than doubles, leaving the final result with about 7% accuracy. The only practical hindrance in using Ru^{103} or Rh^{106} comes from their relatively much longer half lives (39.7 days for Ru^{103}; and Rh^{106} has as a parent Ru^{106} which has a half life of 1 year); thus, a wait of at least several days after the irradiation would be necessary to have them observable in the spectrum. The irradiation time obviously has also to be longer than for the case of Sr^{92} in order to induce enough activity of these nuclei.

3.5 APPLICATION FOR THE ANALYSIS OF BURNED FUEL RODS

Theoretically, this present method can be used for the analysis of the fissile material remaining in a burned fuel rod by using a standard plutonium foil of appropriate composition. One practical difficulty, however, is the availability of a high intensity neutron flux so that the activity of the short-lived fission product from the fissile elements in the burned fuel could show up clearly on top of the background gamma activity. In order to consider the practicality of such an application, it is necessary to estimate the magnitude of such a neutron flux. To find the order of magnitude of the needed flux, the following reasoning is pursued.

It is well known that the gamma-ray line of Cs^{137} at 661 keV is prominent in the spectrum of typical burned fuel rods. Thus, it is assumed that if the activity of, for example, the Sr^{92}, induced by reirradiating the burned fuel at a flux level given by ϕ_{Sr}, has the same magnitude as the activity of Cs^{137}, this method could be used, since the necessary Sr^{92} and hence I^{135} would be present in the new spectrum.

An estimate of the activity of Cs^{137} can be found in the following fictitious but typical example: Suppose a fuel rod containing a certain amount of U^{235} has been irradiated continuously for one year inside a reactor core at a flux level of 5×10^{13} n/cm^2-sec and then cooled for a few months. The activity of Cs^{137} due to the fissions of U^{235} (not taking into account the plutonium buildup) is given by:

$$A_{Cs} = N^{o}\sigma_f\phi_{Cs}Y_{Cs}\lambda_{Cs}\frac{e^{-\sigma_a\phi_{Cs}t_i} - e^{-\lambda_{Cs}t_i}}{\lambda_{Cs} - \sigma_a\phi_{Cs}}e^{-\lambda_{Cs}t} \qquad (3.41)$$

where

N^o = initial number of U^{235} atoms per cm^3

σ_f = fission cross section

ϕ_{Cs} = neutron flux, 5×10^{13} n/cm^2-sec

Y_{Cs} = yield for Cs^{137}, 6%

λ_{Cs} = decay constant for Cs^{137}, 7.32×10^{-10} sec^{-1}

σ_a = absorption cross section for U^{235}

t_i = irradiation time, 1 year

t = decay time, a few months

The absorption of neutrons by Cs^{137} was not taken into account because its contribution is negligible, according to Sovka (S3).

On the other hand, the saturation activity of Sr^{92} at a flux level ϕ_{Sr} is given by:

$$A_{Sr} = N^t \sigma_f \phi_{Sr} Y_{Sr} \tag{3.42}$$

where N^t = number of U^{235} per cm^3 remaining in the burned fuel at the time of reirradiation, which is given by:

$$N^t = N^o e^{-\sigma_a \phi_{Cs} t_i} \tag{3.43}$$

The fission yield for Sr^{92} is the same as for Cs^{137}, i.e., 6% (T2).

By substituting the values into Eqs. 3.41 and 3.42, dividing the activity of Sr by the activity of Cs, and setting this ratio as 1, the value of ϕ_{Sr} is finally given by:

$$\phi_{Sr} \sim 4 \times 10^{-2} \phi_{Cs} \simeq 2 \times 10^9 \text{ n/cm}^2 \text{ sec} \tag{3.44}$$

Thus, in order to apply the present method for the analysis of a typical fuel rod, a flux level of the order of 10^9 n/cm^2-sec would be

necessary. Presently at M.I.T., V. Agarwala is studying, as part of his Master's thesis research, the gamma spectroscopy of a burned fuel rod (burnup = 20,000 MWD/ton) irradiated at the Dresden Power Reactor and cooled for more than 2 years. After reirradiating this fuel rod at a flux of about 4×10^8 n/cm^2-sec for 15 hours, he has observed in the gamma decay spectra the main peaks shown in Fig. 3.8, although they were very weak. The four peaks between 1 and 1.4 MeV, shown in Fig. 3.9 and used in the present analysis, could be identified on top of the background continuum. These results confirm the prediction given by Eq. 3.44. However, the results of Agarwala have shown that, in order to have significant statistics in the counting for I^{135} and Sr^{92} peaks, a flux level of 5×10^9 n/cm^2-sec would be desired. This flux level could be obtained at the present MITR either internally in one of the beam ports or inside the thermal column.

In conclusion, the assay of mixed fuel rods by using the difference in the observable yield of the decay gammas of short-lived fission products of U^{235} and Pu^{239} has proven possible. An accuracy of the order of ±5% is possible, using the gammas from I^{135} and Sr^{92}.

In the following chapters, the prompt gammas emitted by the products of the interaction of thermal neutrons with fuel elements will be investigated, and some applications of these gammas for assay purposes and for the measurement of some reactor physics parameters will be described.

Chapter IV

STUDY OF PROMPT GAMMA RAYS FROM THERMAL NEUTRON ABSORPTION BY FUEL ELEMENTS

4.1 DATA ANALYSIS

In this section is described the method of analysis used to handle the experimental data recorded in the 4095 channels of the multichannel analyzer.

The analysis of gamma spectra was a subject of an extensive study carried out by Hamawi and Harper who developed the initial ideas of Inouye and Rasmussen. This work is described in detail in references H2, H3 and H6. Here, a summary description of the relevant and important aspects is presented.

From the data of the neutron binding energy for the nuclei of interest to the present work, shown in Table 4.1, it was assumed that a gamma spectrum extending up to 7.0 MeV was enough to cover the energy range of all capture gamma rays under consideration. Two spectra were taken for each sample to cover this range. The Compton suppression mode covered the gamma energies from 130 keV to 2.5 MeV, and the triple coincidence mode covered those from 1.3 MeV to 7.1 MeV. For each spectrum obtained, there was also made a neutron flux measurement, a run time measurement and a linearity check measurement.

TABLE 4.1

The Neutron Binding Energy of the Fuel Rod Constituents

Nuclei	Neutron Binding Energy (keV)	Reference
U^{239}	4784 ± 14	M5
	4802 ± 17	M4
	4801.7 ± 3.0	S1
Th^{233}	4956 ± 24	M5
	4783 ± 16	M4
U^{236}	6467 ± 18	M5
	6540 ± 15	M4
Pu^{240}	6455 ± 18	M5
Pu^{241}	5412 ± 29	M5
Pu^{242}	6219 ± 31	M5

The ultimate information desired from each spectrum was the knowledge of the number of photons emitted for each energy level of the product nuclei per one hundred thermal neutrons absorbed by the target nuclei. The immediate information desired was the energies and intensities of the peaks that appeared in a spectrum. This was done by using the computer program GAMANL described in reference H6. The following steps describe the logical operations performed by GAMANL to obtain the required information from a typical spectrum:

(a) First, the spectral data are smoothed to facilitate the analysis and filter out the nonrelevant noise fluctuations.

To accomplish this, a Fourier transform is performed on the 4095 discrete data points of the spectrum. The transformed function is multiplied by a filter function which cuts its high frequency component, and then an inverse Fourier transform is performed on the filtered data. The result is the desired smoothed data.

(b) The geometrical center of each peak in channel number is obtained by fitting a parabola to the three channels which have the highest counts per channel. The point of zero slope on the parabola is determined and recorded as the peak center. Orphan (O2) has found that the value of the peak center obtained in this fashion is accurate to ±0.2 channels. For triple coincidence runs, for which the channel width was about 1.5 keV, this corresponds to 0.3 keV which, combined with the accuracy of energy calibration standards and the nonlinearity correction factor, results in an estimated standard deviation in the energy value of 1.0 keV.

The correction for the nonlinearity of the electronics is done by using the data shown in Fig. 2.15. The correction value is determined from a second order interpolation curve using the three values of the linearity correction curve that are nearest to the channel number that is to be corrected. After this correction is accomplished, the energy of the gamma peak is determined by using two calibration gamma peaks for which the energies are well known. The corrected peak centers for the calibration peaks are determined and a linear fit is used to convert from channel number to energy for the peak under consideration.

The primary calibration lines used in the present work were the following gamma rays:

For Compton suppression spectra:

Annihilation gamma: (511.006 ± 0.002) keV (Ref. M8)

Hydrogen: (2223.29 ± 0.07) keV (Ref. M8)

For triple coincidence spectra:

Hydrogen: (2223.29 ± 0.07) keV (Ref. M8)

Lead: (7367.7 ± 1.0) keV (Ref. O2)

Iron: (5920.5 ± 1.0) keV (Ref. R1)
(6018.5 ± 1.0) keV (Ref. R1)

(c) A linear background is fit under the peaks using one- to five-point averaging at the minima on each side of the peak, with special criteria being applied for the partially resolved multiplets. For doublets, two Gaussian curves are fitted to the data, and the area within the doublet is divided according to the ratio of the two corrected peak height values in the doublet. Triplets are treated similarly. For multiplets of greater than third order, a warning mention is recorded.

(d) After the background is subtracted from the smoothed data, the area of the peak and the accompanying standard deviation are calculated by two methods. One involves a direct integration of the background subtracted peak. The other method assumes that the peak is a Gaussian curve in shape situated on a linear background and its area, AREA, is given by the following expression:

$$\text{AREA} = \text{PKHT} \times \text{VARIANCE} \times \text{F} \times \sqrt{2\pi} \qquad (4.1)$$

where PKHT is the peak height of the peak in counts per channel above

the background level, VARIANCE is the variance of the Gaussian curve that fits the peak in channels and F is a factor that corrects for any slight non-Gaussian shape of the peak.

(e) Once the area under a peak at a certain energy, E, is determined as the total number of counts, the parameter intensity is defined as the total number of photons of that energy emitted by the target nuclei per one hundred thermal neutrons absorbed in the sample. The intensity, I, is given by the following relation:

$$I = \frac{100 \cdot AREA}{E_t \cdot S \cdot F \cdot N \cdot \sigma \cdot \phi \cdot t} \tag{4.2}$$

where

AREA = peak area in counts

N = total number of atoms in the sample

ϕ = average incident neutron flux (n/cm^2-sec)

σ = absorption cross section, either capture or fission as specified (cm^2)

t = total run time in seconds

E = in-sample neutron flux attenuation factor

S = in-sample gamma-ray self-absorption factor

E_t = energy-dependent total efficiency of the system

The total efficiency of the system is given by the following expression:

$$E_t = E_i A_t A_n S_v \tag{4.3}$$

where

E_i = intrinsic efficiency of the detecting system for gamma rays of energy E at the surface of the Ge(Li) detector, in counts per number of gammas.

A_t = gamma-ray attenuation factor, due to any barrier put in the gamma beam between the sample and the detector.

A_n = geometric solid angle which depends on the collimation and distance between sample and detector.

Sv = correction factor due to the difference between the actual size of the sample and the portion actually viewed by the detector.

In all the experiments performed in the present work, the geometry for irradiation and counting was the same for the standard sample used to measure the energy-dependent total efficiency of the system E_t as well as for the samples under study. Thus, each of the component factors of E_t need not be measured separately. Instead, the overall efficiency, E_t, was obtained for the system, and is given in section 2.3.3 for the triple coincidence mode and in section 2.3.4 for the Compton suppression mode. It was estimated that a standard deviation of ±10% applies to the values on these curves.

The in-sample neutron flux attenuation factor was calculated in the same way as outlined in section 3.3.2 whenever the sample shape was that of a metal sheet, and as outlined in section 3.3.4 whenever it was a massive cylinder. This correction for the samples under study relative to the same correction factor for the standard samples was less than ±10% for all cases.

The gamma self-absorption correction was also less than ±10% for all cases. It was calculated by taking a representative average energy for the spectrum and calculating the exponential attenuation from the center of the sample to the surface toward the detector.

4.2 THE THERMAL NEUTRON CAPTURE GAMMA RAYS FOR Th^{232} AND U^{238}

4.2.1 Introduction

For reactor engineers, the knowledge of the intensity of the radiative capture gamma rays is important for dose level and shielding calculations. For activation analysts, the capture gamma rays can be used in prompt activation analysis. For nuclear physicists, they are especially important for the study of the energy levels of the product nuclei. For both Th^{233} and U^{239}, there are no known parent radioactivities which populate its energy states, so decay-scheme studies are not possible. The complementary ways mostly used are either through capture gamma rays or through (d, p) reactions, or both combined.

For U^{238} samples, during the pre-germanium era of gamma spectroscopy, it is worth mentioning the works of Slaughter et al., Fiebiger et al. and Campion et al. cited in reference G5. More recently, Sheline et al. (S1) have used a 3-cc Ge(Li) detector operated in pair spectrometer and Compton suppression modes to study the capture gamma rays for U^{238} and have obtained 27 high-energy transitions between 3150 and 4850 keV and 27 low-energy transitions between 490 and 900 keV. Previously, Maier (M1) with the bent crystal spectrometer at Risø had established 38 certain and an additional 23 uncertain lines in the low energy portion of the radiative capture gammas for U^{238} up to 780 keV of energy. In this work, 32 certain lines have been found between 130 keV and 4.7 Mev. Several unreported lines were found in the energy region not covered by Sheline.

For Th^{232}, Groshev (G2) used a magnetic Compton spectrometer of about 1% resolution and reported 6 lines from 3.45 MeV to 4.92 MeV. Burgov et al. (G5) also have reported 6 lines in the upper energy portion with 50 keV resolution. In this present work, 64 certain lines were found covering the energy region between 260 keV and 4.75 MeV.

4.2.2 Geometry for Irradiation and Counting

For U^{238} the sample consisted of small metal sheet scraps of depleted uranium with 170 ppm of U^{235} contamination. The sample weighed 45.237 grams and it was tightly sealed in a cylindrical polyethylene vial, 2 inches long and 1 inch in diameter. To insure that no contribution from fission gammas was present in the spectra, an additional sample of 19 grams of depleted uranium having only 18 ppm of U^{235} was also irradiated and the spectral results were compared. No significant differences were noticed.

For Th^{232} the sample consisted of thorium oxide powder of 99.8 percent purity, weighing 115.36 grams and contained in a polyethylene vial similar to that for U^{238}.

The standard samples used to measure the total efficiency of the detecting system, which is shown in Fig. 2.12, consisted of iron metal powder 99.5 percent pure with 0.5 percent contamination of manganese and weighing 93.49 grams, and of melamine powder with 22.19 grams of nitrogen. Both samples were sealed in polyethylene vials of the same dimensions as the samples under study.

All the samples were irradiated in the sample holder in exactly the same position. The plan view of the geometry for irradiation and counting is shown in Fig. 4.1. The counting time for each sample was

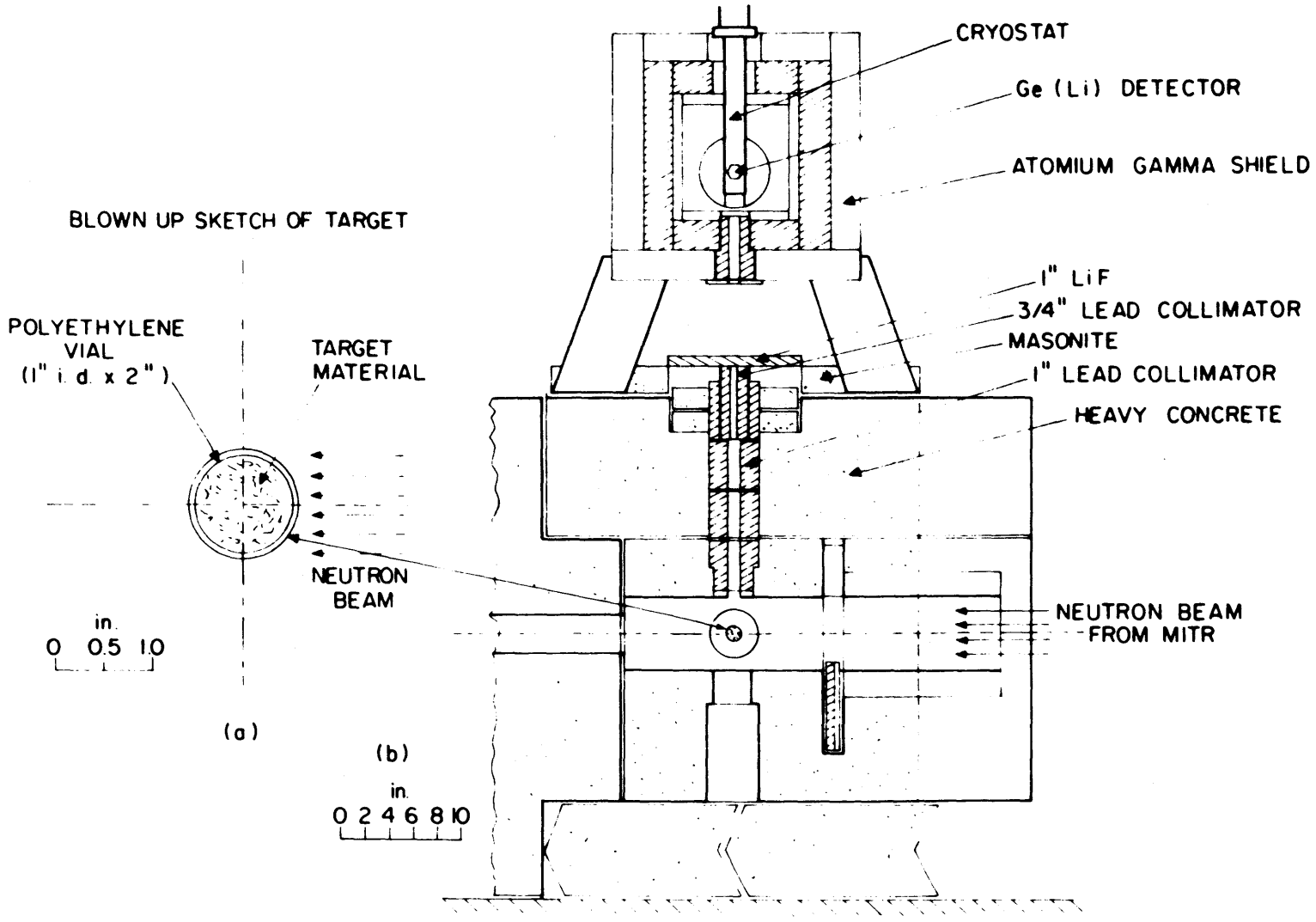

FIG. 41 GEOMETRY FOR IRRADIATION AND COUNTING SAMPLES OF U^{238} AND Th^{232}

between 20 and 25 hours. A sheet of LiF, 1.6 cm thick, was placed in the gamma beam to prevent scattered thermal neutrons from reaching the detector and increasing the background.

For the triple coincidence mode, both samples were irradiated twice. First, with a small piece of pure lead attached to the sample in order to have in the spectrum of the triple coincidence mode the lead line of 7367.7 keV. This was used for calibration together with the 2223.3-keV line of hydrogen. In these runs, graphite was placed in the gamma beam collimation hole to obtain the lines of carbon to check further the energy calibration against the carbon's 3683.9-keV and 4945.5-keV lines. Once the energies of the lines were determined correctly, the samples were again irradiated without the lead and graphite, and cleaner spectra were obtained with only the 1533.0-keV line of annihilation and the 2223.3-keV line of hydrogen in the background. These latter spectra were used primarily for the determination of the intensities of the transitions, and are shown in Figs. 4.3 and 4.5. For the Compton suppression mode, the primary calibration lines were the 511-keV annihilation line and the 2223.3-keV hydrogen line; the double escape peak was used for checking the linearity.

4.2.3 Results and Comments

Figures 4.2 through 4.5 show the spectra taken in the Compton suppression mode and the triple coincidence mode for the samples of U^{238} and Th^{232}.

Tables 4.2 and 4.3 show the results of the data analysis. The energies of the transitions are given in keV and the intensities in number of photons per 100 captures of thermal neutrons.

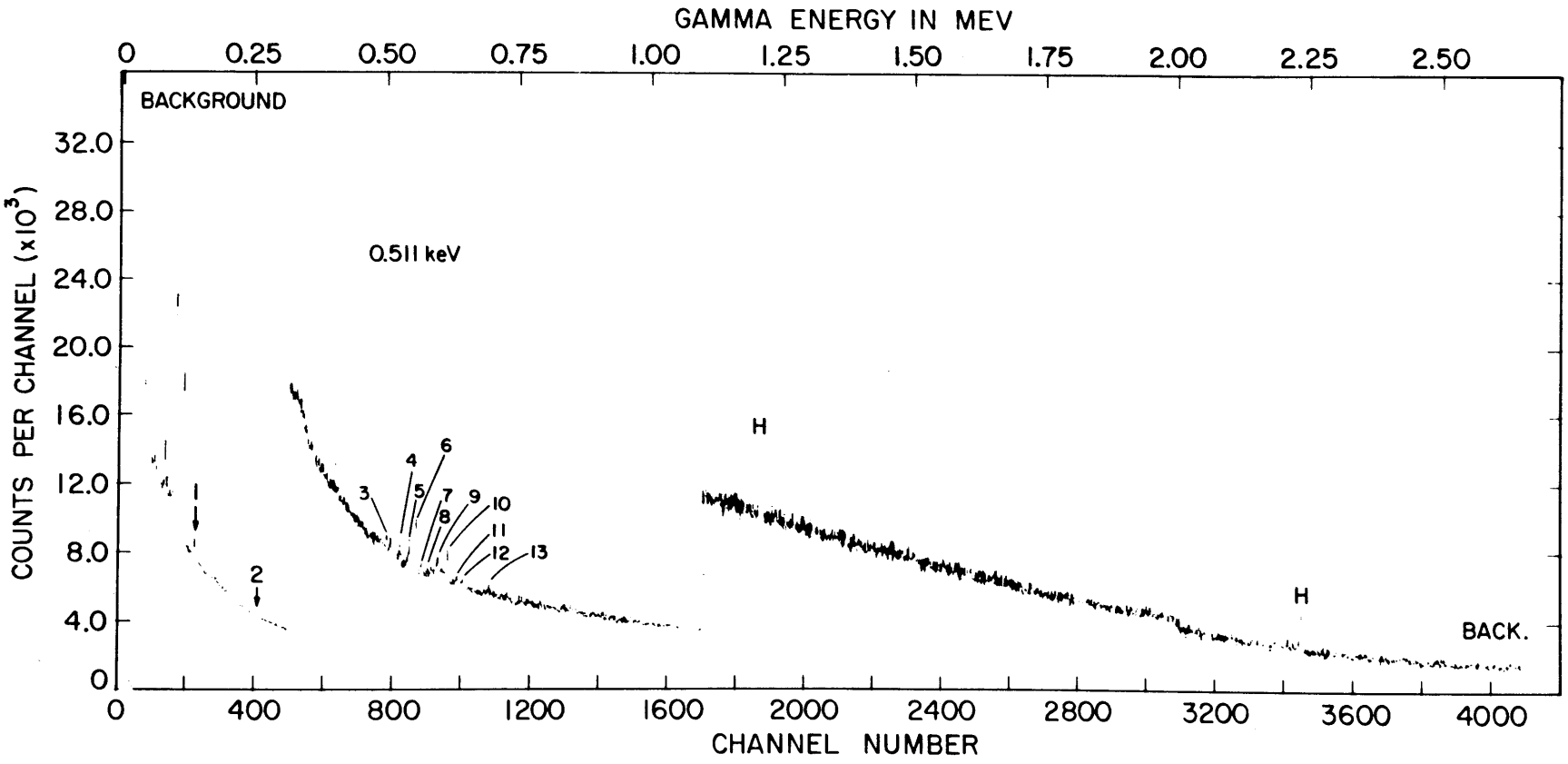

FIG. 4.2 THE LOW ENERGY CAPTURE GAMMA-RAYS FOR U^{238} TAKEN IN COMPTON SUPPRESSION MODE

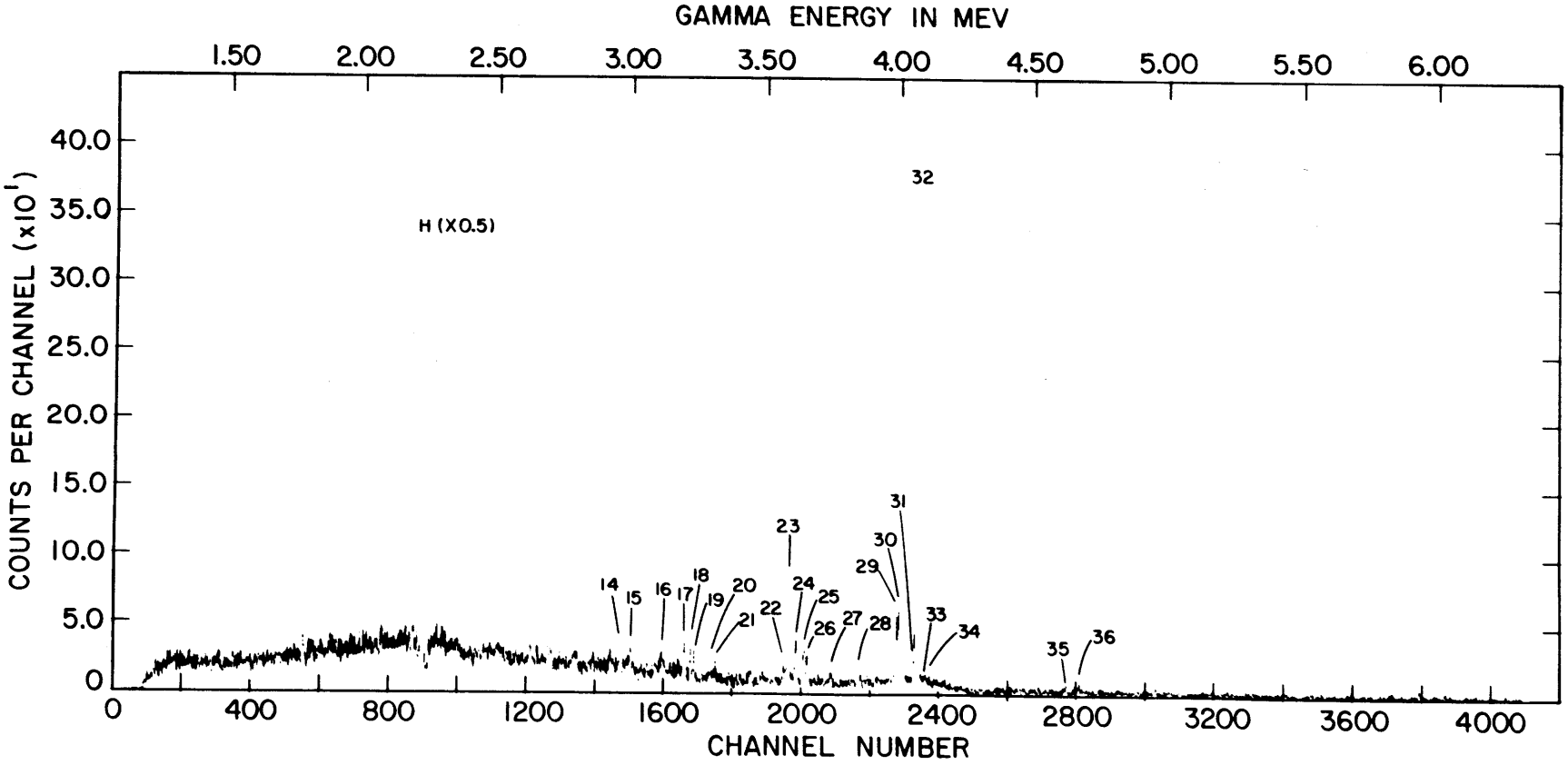

FIG. 4.3 THE HIGH ENERGY CAPTURE GAMMA-RAYS FOR U^{238} TAKEN IN TRIPLE COINCIDENCE MODE

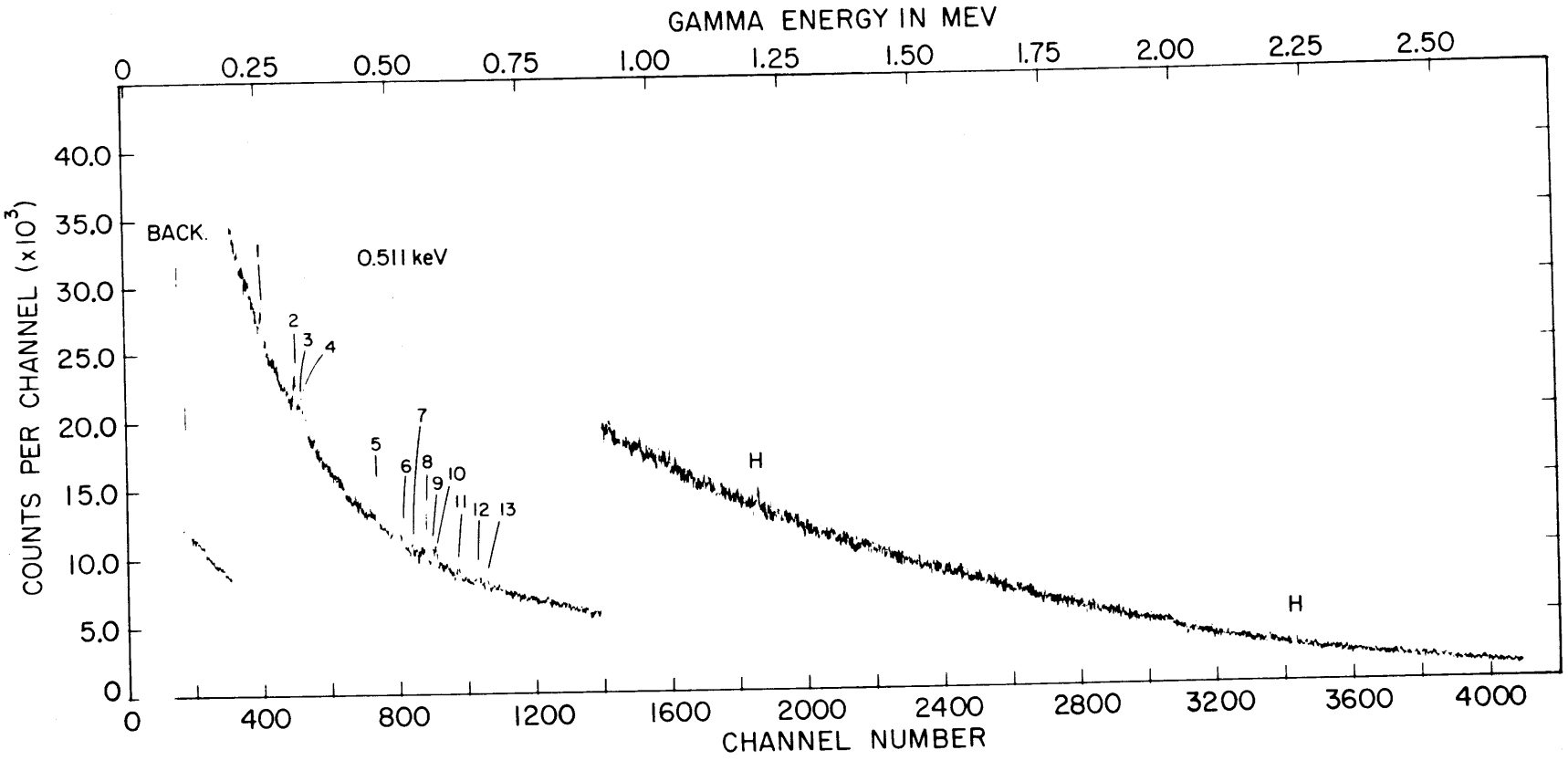

FIG. 4.4 THE LOW ENERGY CAPTURE GAMMA-RAYS FOR Th^{232} TAKEN IN COMPTON SUPPRESSION MODE

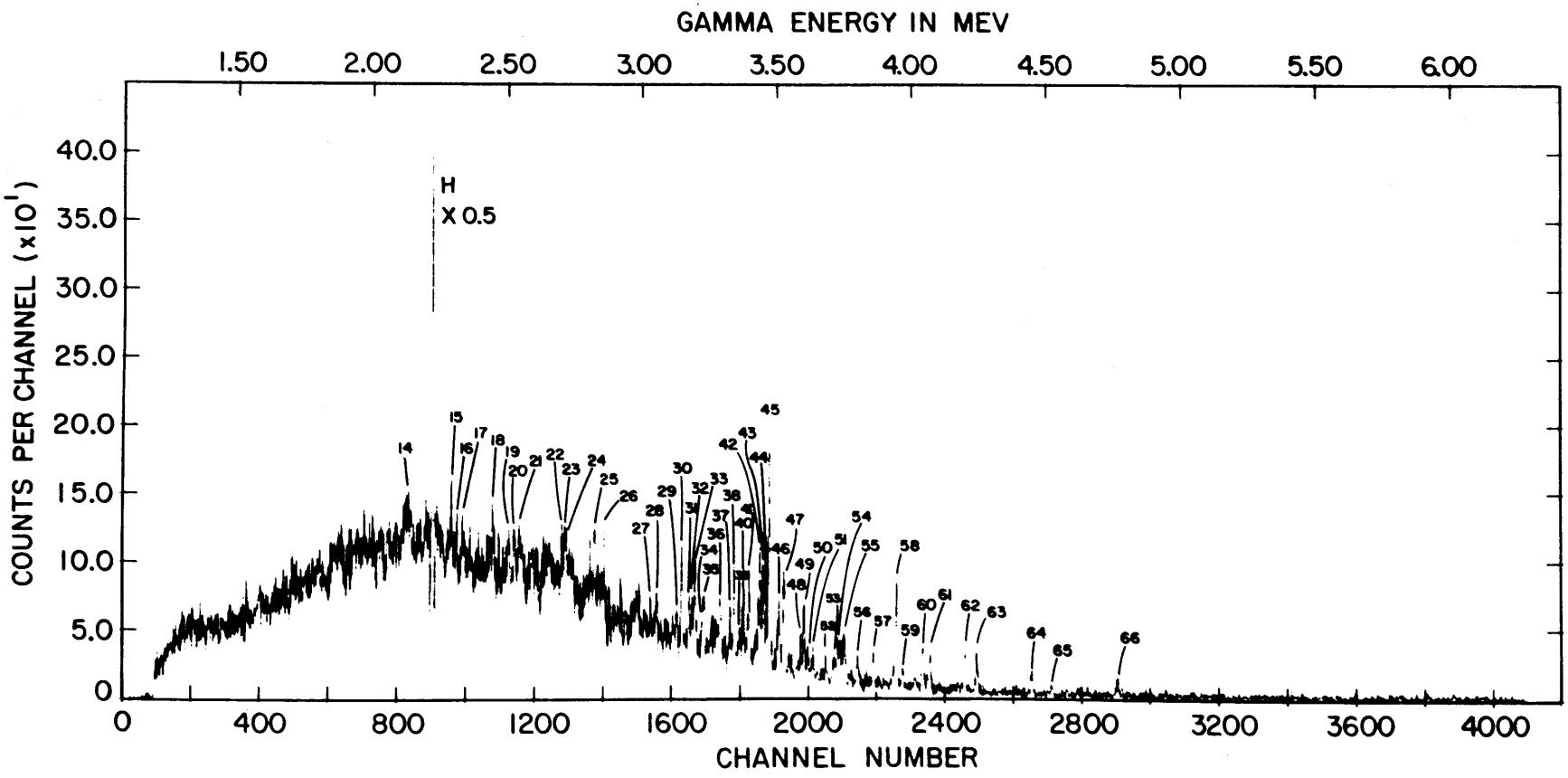

FIG. 4.5 THE HIGH ENERGY CAPTURE GAMMA-RAYS FOR Th^{232} TAKEN IN TRIPLE COINCIDENCE MODE

TABLE 4.2

The Energy and Intensity of the Capture Gamma Rays for U^{238}

Line No.	This Work		Maier (M1)		Sheline et al. (S1)	
	Energy* (keV)	Intensity** (No./100 captures)	Energy (keV)	Intensity (No./100 captures)	Energy (keV)	Intensity (No./100 captures)
1	133.6		133.799	2.3		
2	251	3.2	250.08	2.8		
			341.65	2.6		
3	497.6	0.6			498	0.7
4	521.6	1.67	522.00	2.6	522	2.8
			536.2	1.8	537	4.3
5	539.3	2.31	540.7	3.5	542	1.9
6	552.5	6.54	552.8	6.5	552	10.5
7	562.4	1.10	562.8	0.5	561	1.3
8	580.7	1.40	581.3	1.4	580	2.4
9	592.9	1.82	592.9	2.0	592.4	4.8
			603.9	2.2	601	2.0
					609	1.2
10	611.6	2.73	612.0	3.0	612	8.0
11	628.7	0.5	629.7	1.6	629	2.3
12	637.6	0.4			638	1.8
					658	0.6
			669.7	1.5		
13	683.7	1.19			683	1.1
			687.5	1.5	690	2.4
					698	0.9
					713	0.7
					722	0.7
					750	0.7
					770	0.6
			780	1.5		
					788	0.8
					797	0.7

* The standard deviation for energy determination is ±1 keV.
**The accuracy for the intensity was estimated as ±15% for the lines for which the intensity is higher than 1.00 photons/100 captures and better than ±30% for the others.

TABLE 4.2 (continued)

Line No.	This Work		Sheline et al. (S1)	
	Energy* (keV)	Intensity** (No./100 captures)	Energy (keV)	Intensity (No./100 captures)
14	2959.7	0.85		
15	3000.4	0.90		
16	3114.6	0.95		
			3186	0.24
17	3197.4	0.98	3201	0.22
			3208	0.65
18	3220.1	0.98		
			3229	0.63
19	3233.4	0.45		
			3242	0.38
20	3295.6	0.35	3293	0.20
			3304	0.48
21	3311.5	0.35		
			3318	0.45
			3406	0.20
			3446	0.41
			3532	0.14
			3540	0.23
22	3565.2	0.32	3567	0.22
23	3583.0	3.04	3584	2.5
24	3612.6	1.20	3612	0.84
25	3641.1	0.93	3639	0.68
			3653	0.63
26	3729.0	0.85		
27	3739.6	0.30	3739	0.23
			3818	0.12
28	3844.6	0.50	3843	0.56
			3873	0.13

TABLE 4.2 (concluded)

Line No.	This Work		Sheline et al. (S1)	
	Energy (keV)	Intensity (No./100 captures)	Energy (keV)	Intensity (No./100 captures)
29	3982.3	1.87	3982	1.5
30	3991.0	1.81	3991	1.5
			4052	0.5
31	4059.7	12.1	4059.4	11.0
32	4090.2	0.15	4090	0.22
33	4105.2	0.20	4117	0.08
34	4610.2	0.25	4610	0.21
35	4659.8	0.37	4659	0.22

TABLE 4.3

The Energy and Intensity of the Capture Gamma Rays for Th^{232}

Line No.	This Work		Burgov et al. (G5)	
	Energy* (keV)	Intensity** (No./100 captures)	Energy (MeV)	Intensity (No./100 captures)
1	264.2	0.11		
2	319.2	0.21		
3	326.0	0.12		
4	336.6	0.25		
5	472.5	0.72		
6	522.6	0.39		
7	540.0	0.32		
8	566.6	0.99		
9	577.9	0.33 (semiresolved doublet)		
10	584.7			
11	626.6	0.18		
12	665.3	0.26		
13	681.3	0.22		
14	2127.8	(unresolved triplet)		
15	2294.9	0.38		
16	2314.9	0.26		
17	2334.9	0.25		
18	2447.0	0.33		
19	2503.9	0.13		
20	2525.6	0.24		
21	2544.8	0.29 (semi-resolved doublet)	2.60(5)	5.6
22	2702.8	0.23		
23	2712.9	0.21		

* The standard deviation for energy determination is ±1 keV.

** The accuracy for the intensity was estimated as ±20% for the lines for which the intensity is higher than 0.50 photons/100 captures and better than ±35% for the others.

TABLE 4.3 (continued)

Line No.	This Work		Groshev et al. (G2)		Burgov et al. (G5)	
	Energy (keV)	Intensity (No./100 captures)	Energy (MeV)	Intensity (No./100 captures)	Energy (MeV)	Intensity (No./100 captures)
24	2719.1	0.21			2.76(5)	4.2
25	2823.3	0.25				
26	2861.0	0.36				
27	3005.0	0.12				
28	3027.9	0.15				
29	3129.8	0.12				
30	3147.4	0.33			3.15(5)	1.6
31	3175.4	0.17				
32	3186.3	0.18				
33	3197.0	0.33				
34	3227.4	0.13				
35	3230.9	0.15				
36	3288.5	0.19				
37	3326.3	0.15				
38	3342.0	0.27				
39	3372.1	0.08				
40	3376.8	0.17				
41	3396.5	0.26				
42	3436.2	0.29				
43	3447.7	0.23	3.45(3)	0.6		
44	3461.5	0.07				
45	3473.5	0.71				
46	3508.7	0.22				
47	3527.3	0.31	3.53(2)	1.1	3.55(5)	3.4
48	3590.3	0.08				
49	3603.0	0.17				
50	3615.7	0.05				

TABLE 4.3 (concluded)

Line No.	This Work		Groshev et al. (G2)		Burgov et al. (G5)	
	Energy (keV)	Intensity (No./100 captures)	Energy (MeV)	Intensity (No./100 captures)	Energy (MeV)	Intensity (No./100 captures)
51	3633.6	0.08				
52	3682.5	0.09				
53	3725.1	0.11			3.71(5)	0.4
54	3740.2	0.12				
55	3752.9	0.12	3.75(3)	0.4		
56	3801.8	0.09				
57	3860.6	0.10				
58	3946.3	0.33	3.94(3)	0.5		
59	3959.0	0.05				
60	4004.5	0.14				
61	4072.6	0.12				
62	4201.5	0.14				
63	4244.7	0.13	4.25(3)	0.3		
64	4448.0	0.06				
65	4486.2	0.03				
66	4749.3	0.05				
			4.92(3)	0.3		
					5.11	0.2

For U^{238}, several unreported lines in the region of 3 MeV were found. The higher energy lines agree with the data of Sheline both in intensity and energy. Excellent agreement in energy is noticed for gamma lines with energy higher than 3.5 MeV. However, in the region between 3.2 MeV and 3.5 MeV conflicting energies occur, with Sheline observing about 9 lines more than the present work, all of weak intensities. In the low energy portion in some of the lines, the intensities given by Sheline are much higher than those of Maier and the present work, and there is a general agreement between the data of Maier and of this work.

For Th^{232}, not much comparative data can be found. Nevertheless, there is an agreement of the intensities given by Groshev (G2) with the present work if, due to the superior resolution of the Ge(Li) detector, a sum of several line intensities is performed in the same energy region of the data presented by Groshev. No lines above 4749.3 keV were found, contradicting the data of Groshev who has a line at 4.92 MeV, and Burgov who reports one at 5.11 MeV. In both cases, these lines are of weak intensity.

It is believed that the present results would be especially valuable for the study of the structure of the energy levels of Th^{233} combined with (d, p) reaction measurements. The fact that thorium is monoisotopic makes this study particularly attractive.

4.3 THE PROMPT GAMMA RAYS FROM THERMAL NEUTRON ABSORPTION BY U^{235} AND Pu^{239}

4.3.1 Introduction

The spectrum of gamma rays that comes from the absorption of thermal neutrons with the fissile nuclei of U^{235} and Pu^{239} has contributions from the following three processes:

(a) The prompt gamma rays from the thermal neutron capture process ($U^{235}(\eta, \gamma) U^{236}$),

(b) The prompt fission gamma rays,

(c) The delayed gamma rays emitted by the decay of the fission fragments of earlier fissions in sample.

The fission process is the predominant reaction, with 85.1% compared to 14.9% of captures for U^{235} and 73.0% compared to 27% of captures for Pu^{239}. Studies done by Maienschein (M6) indicate that from every fission of U^{235}, about 7.4 photons are emitted promptly in the energy range from 0.3 MeV to 10 MeV. The total energy emitted is (7.2 ± 0.8) MeV/fission. Comparison of these data with the intensity of the capture gamma rays, which generally are less than a few percent per capture, indicates that at least in numbers the prompt fission gammas are expected to be overwhelmingly predominant over the capture gamma rays.

The study of the origin of the prompt gamma rays from the fission of U^{235} and Pu^{239} involves directly the knowledge of the mechanics of nuclear fission. A very extensive literature has been published about nuclear fission, but still rather little is understood about it. Its complexity comes from the very large amount of energy involved and the

participation of every nucleon during the cataclysmic rearrangement of one nucleus into two nuclei. Fraser and Milton have published a comprehensive review article on nuclear fission in reference F2.

Studies done by Wilson (W1) indicate that the properties of the prompt fission neutrons were consistent with their evaporation from the moving fission fragments, which was confirmed later by Fraser (F3) who also was able to set an upper limit of 4×10^{-14} sec for the time of emission of these neutrons after the scission of the uranium nucleus. According to Griffin (G4), the prompt gamma rays are emitted soon after the boil-off of the prompt neutrons, and Maienschein et al. (M6) concluded that nearly all of the gamma rays are emitted within 10^{-6} sec after the fission. Maier-Leibnitz has constructed a curve, Fig. 4.6(a), depicting the time dependence of the gamma-ray shield, and Griffin (G4) described the gamma-ray emission rate as 10^{-5} sec after the fission which is shown in Fig. 4.6(b).

From the published literature, the following summary picture is drawn of the prompt gamma-ray emission from the fission process. Soon after the fission occurs, the fission fragments are left in excited levels of high initial spin and the emission of the prompt neutrons is the most favorable decay process, which is completed within 4×10^{-14} sec after the nuclear scission. When the density of high-spin levels available for the prompt neutrons is sufficiently reduced, enhanced E2 gamma transitions can compete favorably with the neutron emission, and so within the next 10^{-6} sec nearly all the prompt gamma rays are emitted (see Fig. 4.6(a)), although up to 10^{-3} sec, prompt gammas are still emitted from (presumably) isomeric transitions (see

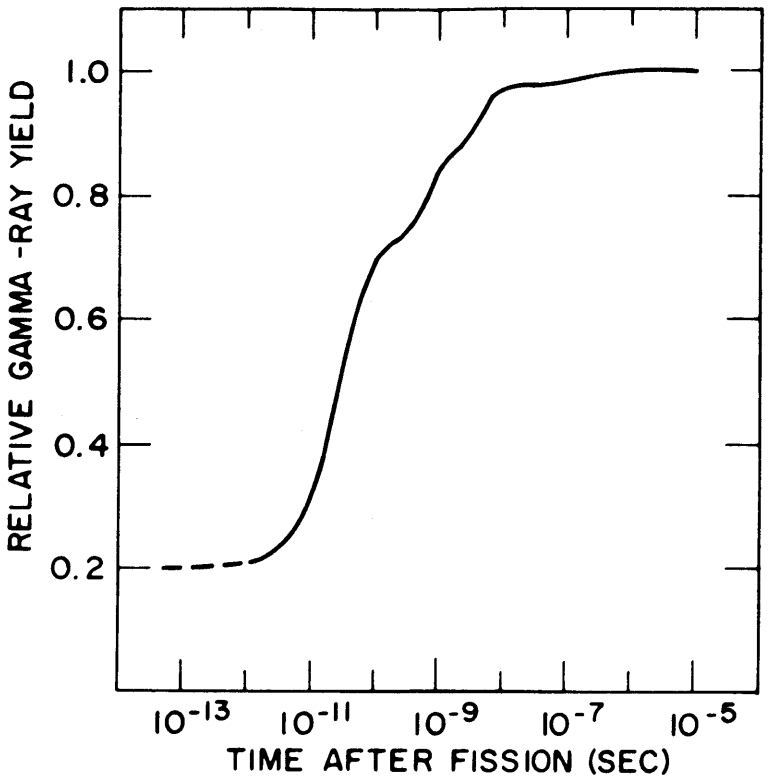

FIG. 4.6(a) RELATIVE NUMBER OF GAMMAS RELEASED AT TIME $\underline{t}$ AFTER FISSION (FROM REF. M7)

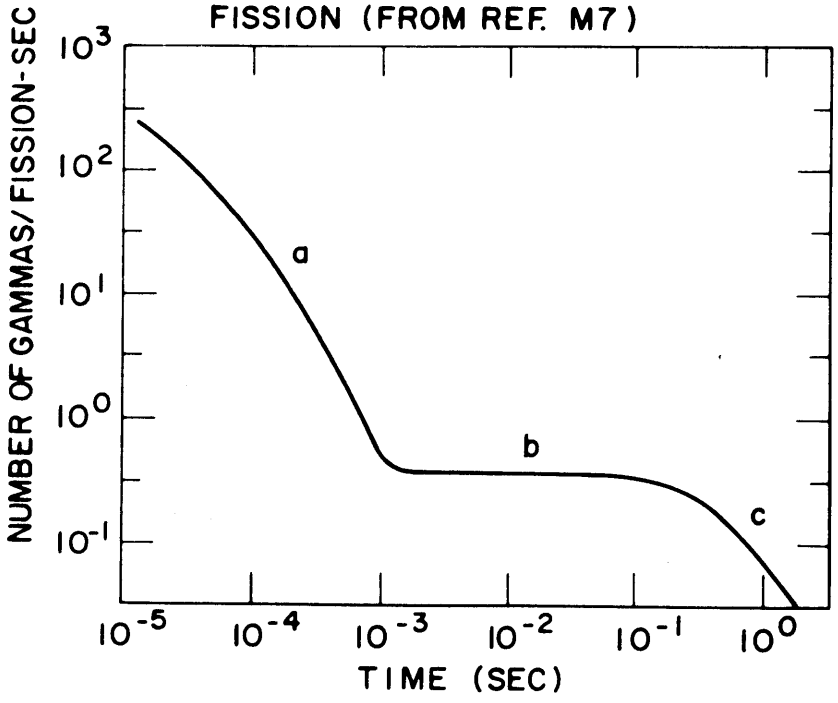

FIG. 4.6(b) NUMBER OF GAMMAS RELEASED PER FISSION AS A FUNCTION OF TIME AFTER THE FISSION (FROM REF. G4)

region a of Fig. 4.6(b)). After the emission of prompt gammas as the predominant process up to 10^{-3} sec after the fission, the next decay must come from the beta decay of the fission fragments which requires a time of the order of seconds. During this period, gamma emission occurs whenever the beta decay goes to an excited state of the daughter nucleus. From 10^{-3} sec to 10^{-1} sec, these decays are so few as to leave the populations of various fission products essentially unchanged, and so it is expected that the rate of decay will be constant as should also the rate of gamma emission (see region b of Fig. 4.6(b)). For times greater than 10^{-1} sec, the fast beta decays are replaced by slower ones and there is a consequent decrease in the delayed gamma emission rate (see region c of Fig. 4.6(b)).

In this present work the spectrum for U^{235} and for Pu^{239}, with 8.8% contamination of Pu^{240} and 1.1% contamination of Pu^{241}, was obtained in Compton suppression mode for the low energy portion and in triple coincidence mode for the energy region above 1.3 MeV. From the data obtained, it was concluded that no significant spectral structure can be obtained below 1.3 MeV, where the spectrum shows strong lines from the interaction of the fission neutrons with the germanium detector and also the background line of annihilation gammas.

All the significant structure was obtained from the triple coincidence mode spectrum shown in section 4.3.3. For U^{235}, 58 certain lines were found together with an additional 5 uncertain lines. For Pu^{239}, with a contamination of 8.8% of Pu^{240} and 1.1% of Pu^{241}, 51 certain and 17 uncertain lines were obtained.

On the basis of the above discussion, it is expected that the great majority of the observed gammas are prompt fission gammas. As further confirmation of this hypothesis, it is noted that more than 75% of the gamma rays that come from the decay of fission products are situated in the energy region of less than 900 keV. If any capture gammas are observed, they would be expected to be very weak. Also, some contribution is expected from the capture gamma rays for Pu^{240} in the spectrum for the plutonium sample. The results and comments are given in section 4.3.3.

4.3.2 Geometry for Irradiation and Counting

The samples of uranium and plutonium were the same as described previously in section 3.3.1. For uranium, a metal sheet 0.005 inch thick and 93.17% enriched in U^{235} with a total of 1.1448 grams of fissile material was used. For plutonium, a metal sheet 0.006 inch thick with 91% of Pu^{239}, 8% of Pu^{240} and 1% of Pu^{241}, having a weight of 1.388 grams of Pu^{239} plus Pu^{241}, and 0.1317 grams of Pu^{240}, was irradiated.

A plan view of the geometry for irradiation is shown in Fig. 4.7. Both samples were compressed between two sheets of LiF, 1.6 cm thick, with a through hole of 1-inch diameter and tilted about 15° to the line of the gamma beam, as shown in Fig. 4.7(a). The reason for using the sheets of LiF was to limit the irradiation portion of the available plutonium foil to 1-inch diameter because it contained more fissile material than the required amount. The use of the same arrangement for the uranium sample equalized the geometry of irradiation for both

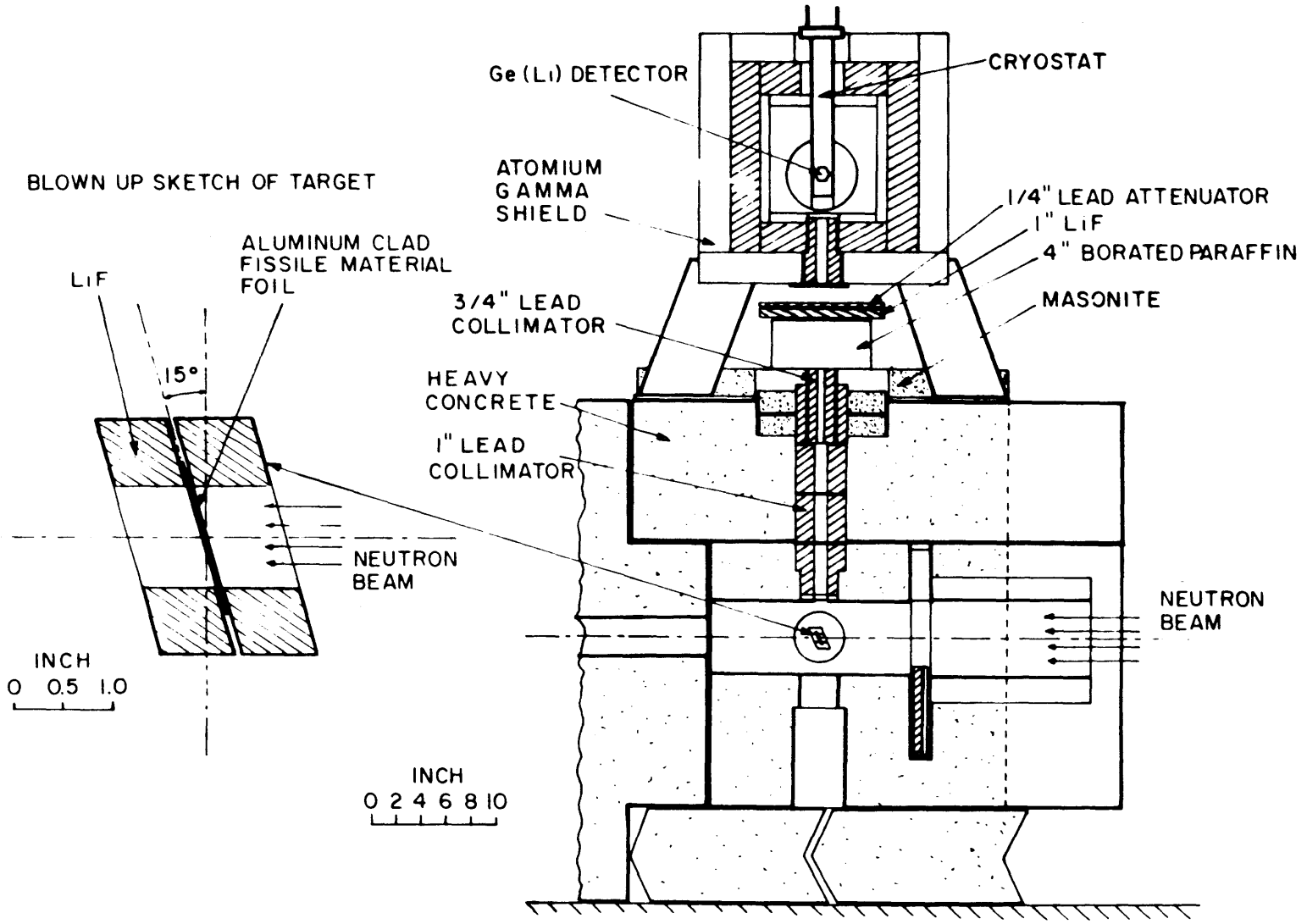

FIG. 4.7 GEOMETRY FOR IRRADIATION AND COUNTING SAMPLES OF U^{235} AND Pu^{239}

foils in order to make the comparison of the gamma yield between the two samples more precise.

One problem that arose during the preliminary phases of the experiments was the large contribution of background from the interaction of fission neutrons with the detector and surrounding materials. It proved necessary to insert a fast neutron scatterer in the gamma beam: borated paraffin with 5% boron in weight and a density of 0.92 grams/cc.

To establish a compromise between lowering the background due to the neutrons and not attenuating excessively the desired gamma rays, a preliminary experiment was performed in order to obtain the relative attenuation of fission neutrons as a function of the thickness of borated paraffin.

In this experiment, the fission neutrons coming from the irradiation of a uranium fuel rod enriched to 2% in U^{235} were attenuated by a plate of variable thickness of borated paraffin before they were counted. Two thicknesses were used, 2 inches and 4 inches, and the results were compared to the result for no scatterer in the neutron beam. Figure 4.8 shows the results.

For counting the fission neutrons, an unusual way of detecting fast neutrons was used. The 30-cc Ge(Li) detector operated in the free mode was used to take the prompt gamma spectrum for the fuel rod for each of the three experimental arrangements. In these spectra, the area under the peak of the 693-keV gamma which resulted from the inelastic scattering of fast neutrons by Ge^{72} inside the detector was proportional to the number of fast neutrons (neglecting any difference

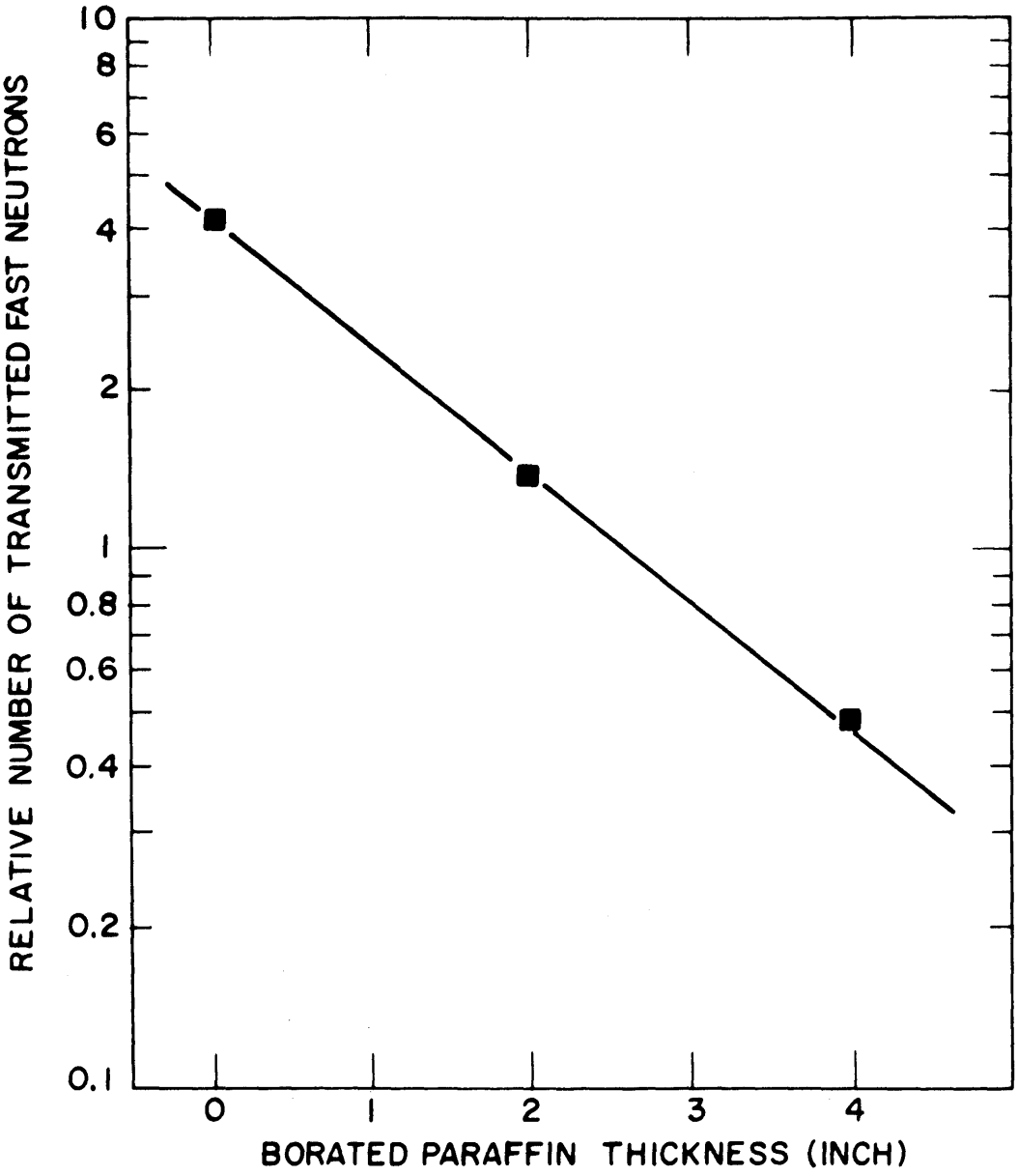

FIG. 4.8 RELATIVE NUMBER OF TRANSMITTED FAST NEUTRONS AS A FUNCTION OF BORATED PARAFFIN THICKNESS.

in the shape of neutron spectra) coming through the gamma beam as is shown in section 5.4. A typical example of a prompt gamma spectrum of a uranium rod taken in the free mode is shown in Fig. 2.10.

A filter thickness of 4 inches was chosen as a reference value for all subsequent runs. This thickness lowered the fast neutron flux to about 15% of that from the unscattered beam. The gamma attenuation factor for the 4 inches of borated paraffin was calculated to be about 2 for 2-meV gammas, down to 1.5 for 6-meV gammas, which was accepted as tolerable. A sheet of 1.6 cm of LiF was added over the borated paraffin in order to absorb further the moderated neutrons. Moreover, in order to lower the count rate of the electronics to a reasonable limit to avoid loss of resolution, a sheet of 1/4 inch of lead was added to cut down further the predominantly low energy gamma rays hitting the detector.

The ordering of these scatterers in the gamma beam is shown in Fig. 4.7(b).

In order to determine the energies of the lines, a spectrum of the uranium sample was taken with a large collimator to bring deliberately into the spectrum the lines of iron from the primary shielding structure. The prominent lines of 5920.5 keV and 6018.5 keV from the iron were shown clearly above the background, and they were used for the energy calibration together with the hydrogen line coming from the plastic material covering the LiF plates. The other lines of iron of lower energies and high intensities were used to further check the linearity of the energy calibration. The spectrum of the plutonium sample was taken with the same gain as that of uranium, and an

immediate identification of the peaks was possible through the comparison with the uranium spectrum. The line at 3575.2 keV was used for calibration together with the hydrogen line.

Once the energies of the lines were determined, a final spectrum for each of the samples was obtained with the 3/4-inch collimator. With this arrangement, only the hydrogen line is seen in the spectra with some trace of the two strongest lines of 5920.5 keV and 6018.5 keV of iron.

4.3.3 Results and Comments

Figures 4.9 and 4.10 show plots of the spectrum for uranium and plutonium, respectively, taken in the triple coincidence mode.

Table 4.4 shows the results of the data analysis. These spectra offered an interesting test of the capability of the GAMANL computer code due to the large number of lines and low statistics involved. At this point, it is interesting to consider the question as to the reliability of the peaks recognized by the data analysis. Currie (C1) has defined a limiting level of signal detection above which an observed signal may be reliably recognized as "detected." This critical level was established by Hamawi (H3) for the GAMANL analysis, and it was shown that it corresponds to a 60 percent error in the determination of the area under a peak for typical cases. In this present analysis, we set the error limit at 40 percent, below which the GAMANL would not print out the result of a peak. We noticed a remarkable agreement in energy of the peaks between the spectral analysis of uranium and plutonium which substantiates the power of the Fourier analysis of gamma spectra used in GAMANL.

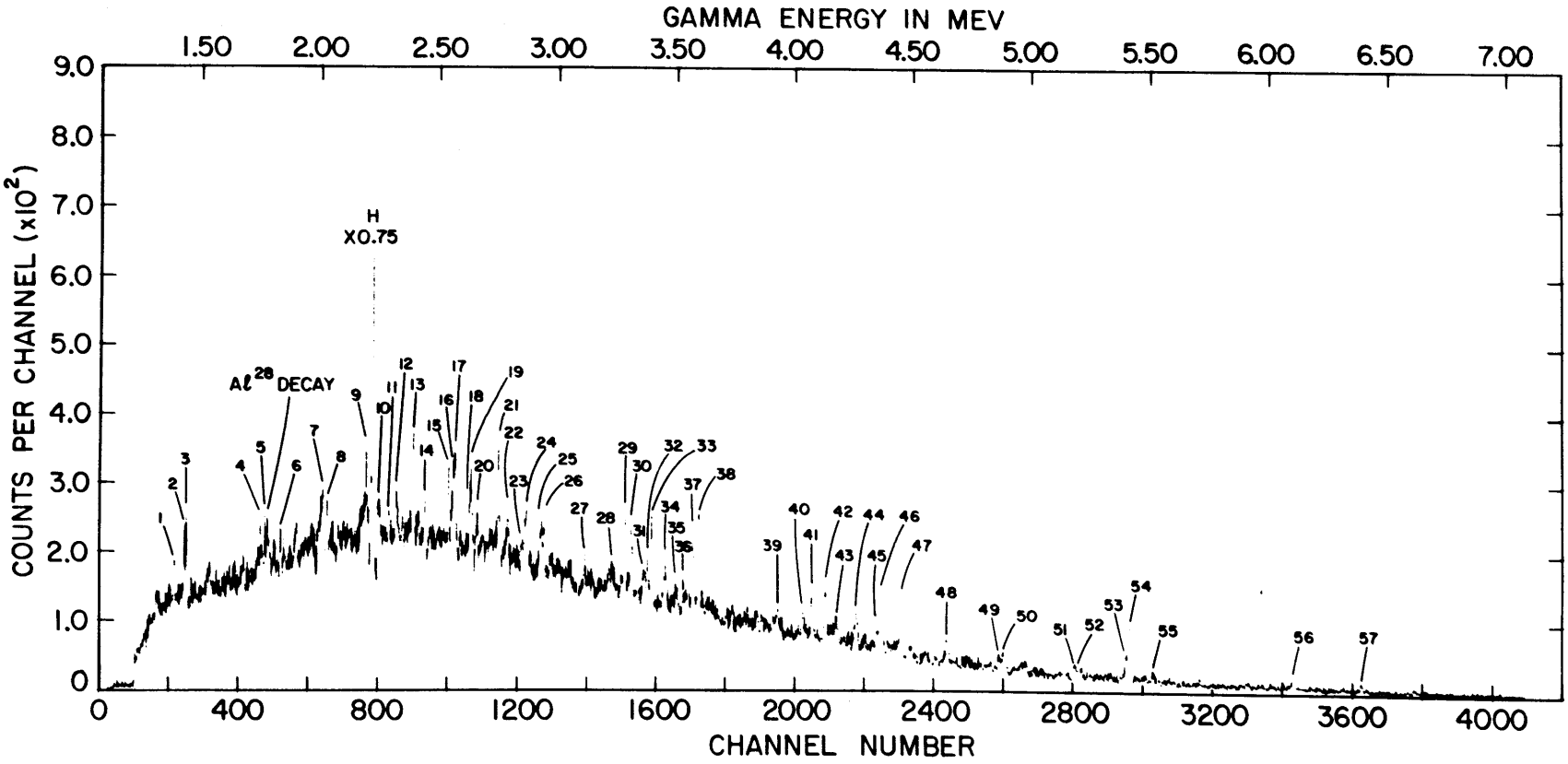

FIG. 4.9 THE PROMPT GAMMA-RAYS FOR U^{235} TAKEN IN TRIPLE COINCIDENCE MODE

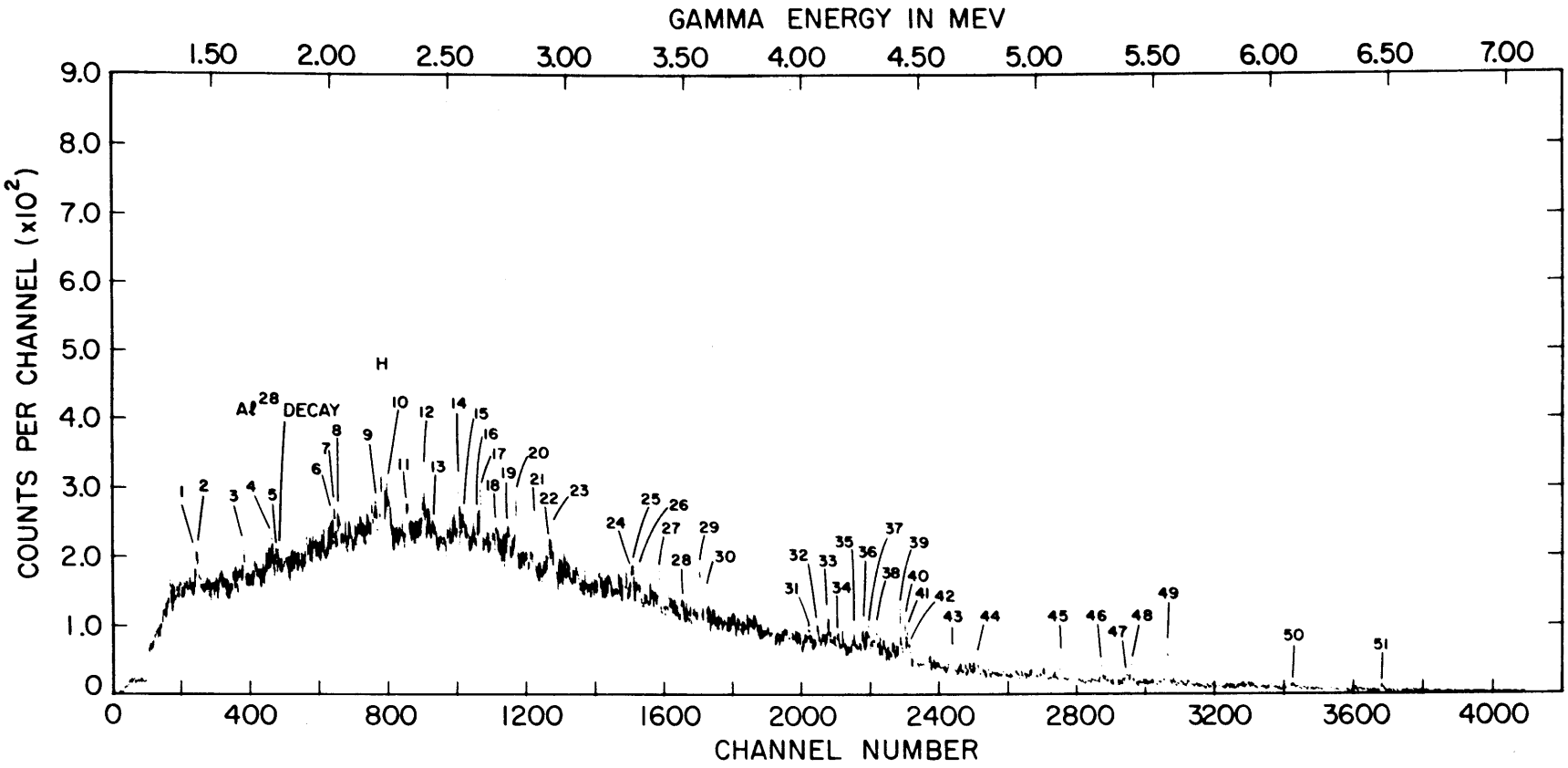

FIG. 4.10 THE PROMPT GAMMA-RAYS FOR PLUTANIUM TAKEN IN TRIPLE COINCIDENCE MODE

TABLE 4.4

The Energy and Intensity of Prompt Gamma Rays for U^{235} and Plutonium

U^{235}			Plutonium		
Line No.	Energy* (keV)	Intensity** (No./100 fissions)	Energy* (keV)	Intensity** (No./100 fissions)	Line No.
1	1383.9	–	inconlusive		
2	1427.7	–	1428.8		1
3	1435.4	–	1435.2		2
	inconclusive		1632.1		3
4	1750.9	1.80	1750.0	1.20	4
5	1769.2	1.46	1767.7	0.86	5
6	1835.1	1.57	inconclusive		
7		unresolved	2006.4	0.52	6
8	2016.0	1.34	2015.5	0.72	7
9	2032.2	1.15	2031.4	0.66	8
10	2196.3	1.15		unresolved	9
11	2252.4	0.33		unresolved	10
12	2294.1	0.29	definite no		
13	2322.6	0.52	2321.9	0.51	11
14	2394.3	1.63	2395.5	0.66	12
15	2443.1	0.70	2443.0	unresolved	13
16	2544.1	1.00	2544.3	0.61	14
17	2565.2	0.59	2565.2	0.20	15
18	2568.4	0.81	inconclusive		
19	2634.9	0.52	unresolved		16
20	2638.6	1.03	2638.0	0.62	17
21	2662.7	0.40		unresolved	18

* The standard deviation for energy determination is ±1 keV.

** The accuracy for intensity determination is better than ±30%. The live numbers correspond to the numbers shown in Figs. 4.9 and 4.10 for U^{235} and Pu^{239}, respectively.

TABLE 4.4 (continued)

U^{235}			Plutonium		
Line No.	Energy (keV)	Intensity (No./100 fissions)	Energy (keV)	Intensity (No./100 fissions)	Line No.
22	2753.4	1.35	2753.6	0.28	19
23	2791.7	0.41	2789.8	0.59	20
24	2853.3	0.21	inconclusive		
25	2868.8	0.61	2867.6	0.39	21
26	2933.1	0.36	2931.8	0.31	22
27	2942.9	0.37	2943.9	0.46	23
28	3115.9	0.30	inconclusive		
29	3231.3	0.30	inconclusive		
	inconclusive		3281.8	0.26	24
30	3288.1	0.80	3288.6	0.31	25
31	3312.3	0.61	3310.8	0.34	26
32	3370.8	0.27	inconclusive		
33	3383.4	0.33	inconclusive		
34	3400.4	0.80	3401.3	0.38	27
35	3458.3	0.41	inconclusive		
36	3502.6	0.18	3501.6	0.17	28
37	3532.8	0.24	inconclusive		
38	3575.2	0.78	3575.2	0.36	29
39	3600.0	0.88	3601.4	0.23	30
40	3934.1	0.20	inconclusive		
41	4040.3	0.24	4040.3	0.16	31
42	4079.0	0.38	4078.3	0.14	32
	definite no		4123.0	0.18	33
43	4135.7	0.43	definite no		
44	4184.1	0.20	4184.5	0.10	34
	inconclusive		4233.6	0.14	35
45	4263.1	0.29	definite no		

TABLE 4.4 (concluded)

U^{235}			Plutonium		
Line No.	Energy (keV)	Intensity (No./100 fissions)	Energy (keV)	Intensity (No./100 fissions)	Line No.
	inconclusive		4272.7	0.18	36
	inconclusive		4295.2	0.22	37
	inconclusive		4329.9	0.16	38
46	4351.2	0.20	inconclusive		
47	4364.9	0.46	definite no		
	definite no		4430.0	0.37	39
48	4453.5	0.54	4452.0	0.32	40
	definite no		4462.0	0.27	41
	definite no		4470.7	0.13	42
49	4646.9	0.17	inconclusive		
	definite no		4651.9	0.14	43
	definite no		4757.5	0.17	44
50	4885.7	0.10	inconclusive		
	definite no		5119.5	0.22	45
51	5185.7	0.11	inconclusive		
52	5188.4	0.08	inconclusive		
	definite no		5291.2	0.15	46
53	5405.2	0.24	5405.2	0.08	47
54	5418.2	0.52	5416.5	0.18	48
55	5520.8	0.13	inconclusive		
	definite no		5570.5	0.40	49
56	6102.0	0.13	6102.0	0.05	50
57	6389.0	0.12	inconclusive		
	definite no		6480.0	0.10	51

In Table 4.4 are shown the energies in units of keV, and the intensities of the observed gamma lines expressed as the number of photons per 100 fissions, assuming that they all come from the fission process. For the first few lines, the intensities were not calculated due to great uncertainty in the efficiency at the lower energy portion of the triple coincidence spectra. In the energy column, wherever inconclusive appears, it means that for that sample there might exist a line corresponding to the other sample hidden in the background but no certainty is assured. Wherever definite no appears, it means that there is definitely no evidence of a peak at that energy. Wherever unresolved appears, it means there is a peak but it is unresolved.

In the spectrum shown in Figs. 4.9 and 4.10, no evidence of capture gamma background peaks from the aluminum cladding nor from the 6.83% U^{238} in the uranium sample were noticed. The only background lines present were the 2223.3-keV line of hydrogen and the 1778.5-keV line from the decay of Al^{28}.

For the U^{235} sample, there are three lines for which there is no evidence of presence in the plutonium sample. There are two alternatives to explain their origin: either they are capture gammas or their presence in the plutonium spectrum is unnoticed due to excessively small yield in the fission of Pu^{239}. Table 4.5 presents the energies and the intensities of these gamma lines, considering them as capture gammas. Here, the intensities are in units of number of photons per 100 captures.

For the plutonium sample, there are 10 lines for which no evidence of their presence was noticed in the uranium sample. In this

TABLE 4.5
Probable Capture Gamma Rays for U^{235}

Line Number U^{235} Spectrum	Energy (keV)	Intensity (No./100 captures)
44	4135.7	2.5 ± 0.4
46	4263.1	1.7 ± 0.3
48	4364.9	2.6 ± 0.4

case, there are three possible origins: (a) they are capture gammas for Pu^{239} which amounts to 91% of total weight of the sample; (b) they are capture gammas for Pu^{240} which amounts to 8% of the sample, and (c) they are too weak to be observed in the U^{235} sample. All the lines with the exception of numbers 43 and 44 seem definitely not in category (c). They are most likely a combination of capture gammas for Pu^{239} and Pu^{240} nuclei. The influence of Pu^{241} is negligible because of its low percentage in the composition. Table 4.6 presents the energies and intensities of these lines. Here the intensities are presented in two columns, first in units of number of photons per hundred captures by Pu^{239} nuclei, and second in units of number of photons per hundred captures by Pu^{240}.

It was observed that no significant alteration in the relative intensities of the lines of the U^{235} sample is noticed for counting times of 15, 18 and 22 hours. Unfortunately, for shorter runs the count accumulation is too small to be useful in an analysis. On the basis of the discussion in section 4.3.1, it is believed that the great majority of the lines observed in both spectra are of prompt fission gammas.

TABLE 4.6

Probable Capture Gamma Rays for Either Pu^{239} or Pu^{240}

Line Number Pu Spectrum	Energy (keV)	Intensity (No./100 captures) By Pu^{239}	By Pu^{240}
34	4123.0	0.49 ± 0.19	4.9 ± 1.9
40	4430.0	1.00 ± 0.10	10.0 ± 1.2
42	4462.0	0.73 ± 0.10	7.3 ± 1.0
43	4470.7	0.35 ± 0.09	3.5 ± 0.9
44	4651.9	0.38 ± 0.09	3.8 ± 0.9
45	4757.5	0.46 ± 0.10	4.6 ± 1.0
46	5119.5	0.60 ± 0.09	6.0 ± 0.9
47	5291.2	0.40 ± 0.07	4.0 ± 0.7
50	5570.5	1.10 ± 0.14	11.0 ± 1.4
52	6480.0	0.27 ± 0.13	2.7 ± 1.3

Nevertheless, a small contribution from the decay gammas cannot be overlooked. It has been found that, after irradiating the uranium sample for 15 hours and with the operating system in triple coincidence, a sudden interruption of the incident neutron beam with the shutter does not decrease the count rate to zero instantaneously but rather to about ±5% of the original count rate with most of the counts coming in the lower energy portion of the triple coincidence spectrum, as expected. Thereafter, the count rate decreased rapidly and was down to about zero within a few minutes. There was no way, with the available experimental arrangement, to assign any of the lines of the spectra to the decay gammas coming from short-lived fission products due to the need of at least 15 hours of counting for a constant source in order to have significative counting statistics.

The prompt gamma rays reported in this chapter were used in the analysis of some typical fuels. This technique is discussed in Chapter V.

Chapter V

THE ASSAY OF FUEL RODS USING PROMPT GAMMA RAYS

5.1 INTRODUCTION

The potentiality of capture gamma rays for elemental analysis was recognized as early as 1963 by Greenwood et al. (G6). Isenhour et al. (I1) presented semi-empirical results on the sensitivity of capture gamma-ray analysis of natural elements. Rasmussen and Hukai (R4) used capture gamma rays for the analysis of coal samples using a pair spectrometer with Ge(Li) detector. An extensive evaluation of the potentiality of neutron capture gamma rays in elemental analysis using germanium detectors was studied recently by Hamawi (H3).

In this chapter the use of prompt fission gammas, together with capture gamma rays, for the analysis of fuel rods is described. Also, measurement of the fission neutron yield as detected through the Ge^{72} inelastic scattering conversion electrons is shown to be a powerful means to analyze uranium fuel rods.

5.2 THE PROMPT ACTIVATION ANALYSIS OF URANIUM FUEL RODS

5.2.1 Experimental Procedure

Figure 5.1 shows the plan view of the geometry for irradiation of the fuel rods. A hole of 3/4-inch diameter was drilled through the side steel access plugs of the front irradiation facility in order to insert the fuel rods into the irradiation position. Two sets of LiF plates surround

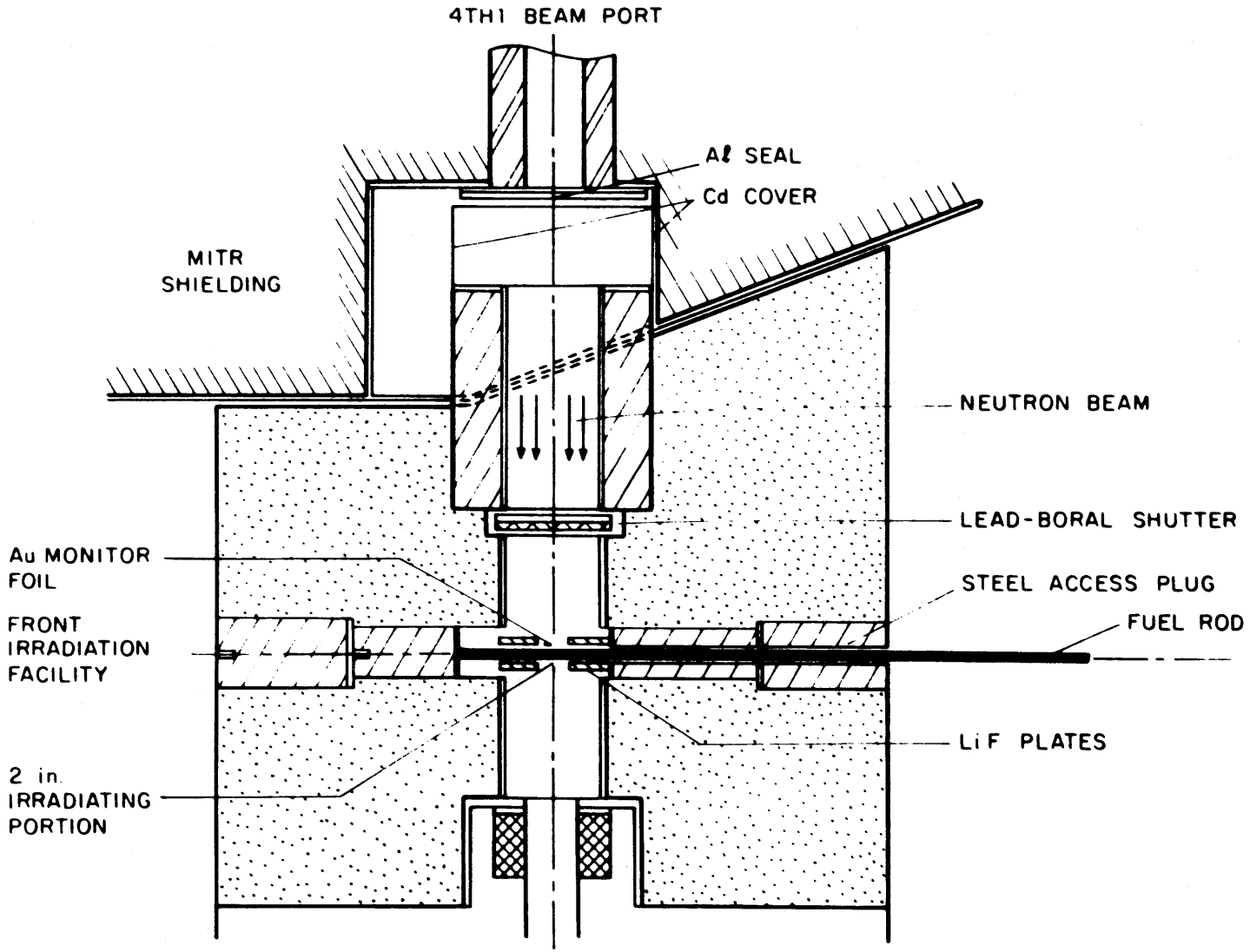

FIG. 5.1 THE GEOMETRY FOR IRRADIATION OF FUEL RODS AT THE FRONT FACILITY

the fuel rod at the irradiation position in order to limit the part of the sample exposed to the beam. This had the effect of reducing the fast neutron background at the detector. The irradiated length of the fuel rod was set at 2 inches, which is the portion viewed by the detector.

The geometry for counting the gammas coming from the fuel rod is the same as that used for the irradiation of fissile foils; it is shown in Fig. 4.1. A set of three shielding materials was placed in the gamma beam: (a) borated paraffin of 4-inch thickness; (b) 1.6-cm-thick LiF plate, and (c) 1/4-inch-thick lead plate. Their function was explained in section 4.3.2.

Five fuel rods of different enrichment were irradiated. Table 5.1 shows the characteristics of each rod. The triple coincidence mode of taking the gamma spectrum was used for the five rods. The same electronic settings were used for all the samples and also the same irradiation time of 18 hours. For each run, a gold monitor foil was attached to the fuel rod at the edge of the irradiated portion to measure the flux. A typical spectrum from the fuel rod is shown in Fig. 5.2, with the peaks from the contribution of U^{235}, U^{238} and Al identified.

5.2.2 Theory

The total number of gamma rays, G, of a given energy, produced from the interaction of uranium atoms with thermal neutrons, that are detected during t seconds of bombardment of a uranium fuel rod, is given by the following expressions:

TABLE 5.1

Uranium Oxide Fuel Rods Used in Enrichment Experiment

Enrichment Weight Percent	Pellet Diameter (Inch)	Cladding** Thickness (Inch)	Density (g/cc)	Cladding External Diameter (Inch)
0.711*	0.500	0.031	5.185	9/16
1.0999	0.446	0.025	10.11	1/2
1.30	0.500	0.030	10.11	9/16
1.61	0.500	0.030	10.11	9/16
1.999	0.446	0.025	10.11	1/2

* Made by compressing natural uranium oxide powder in aluminum tubing.

** Aluminum 1100 series.

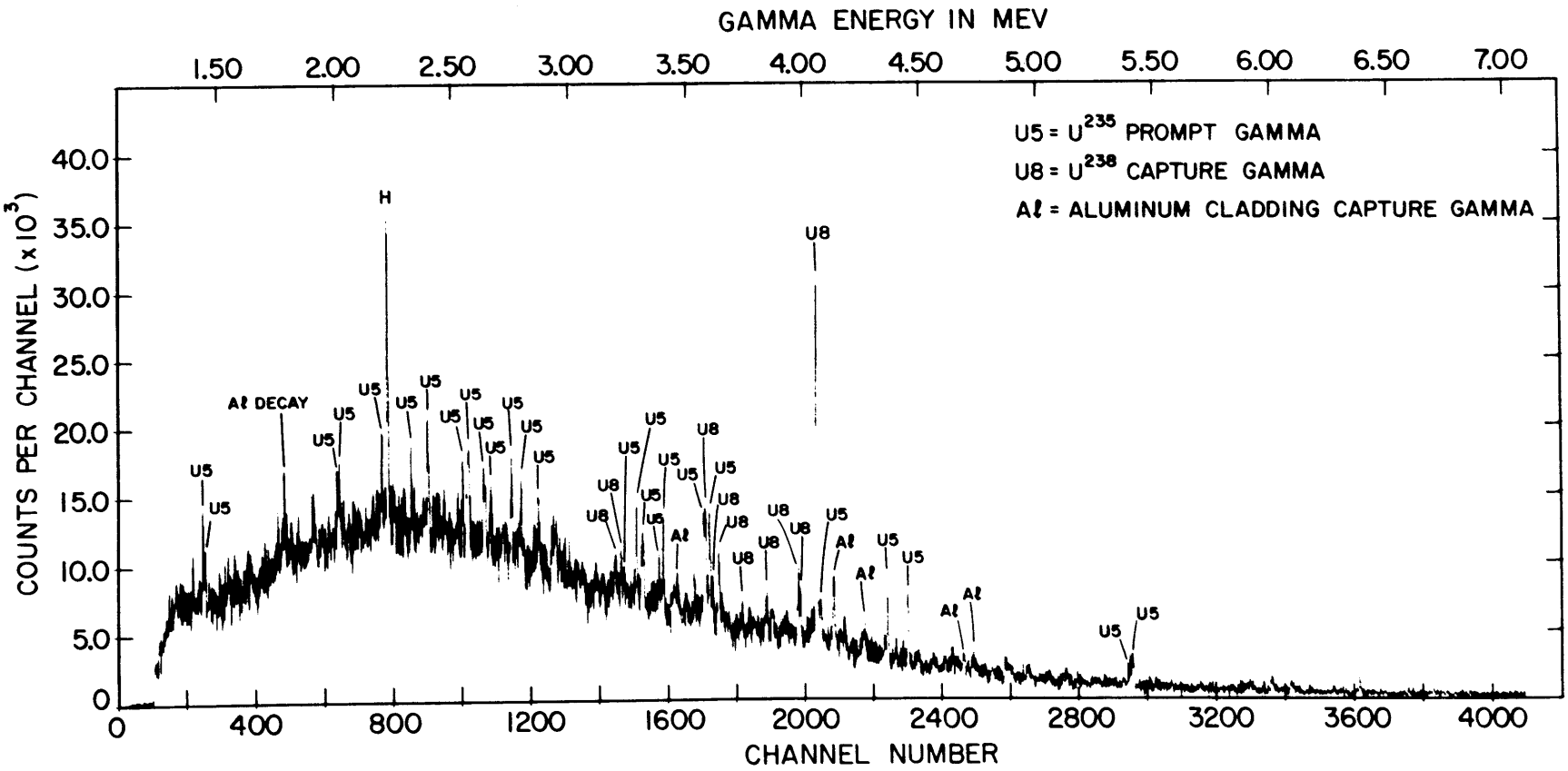

FIG. 5.2 THE GAMMA SPECTRUM OF A URANIUM OXIDE 1.61% ENRICHED ROD TAKEN IN TRIPLE COINCIDENCE MODE

For capture gammas:

$$G = N_c \sigma_c \phi t \epsilon I_c / 100 \tag{5.1}$$

where

N_c = total number of uranium atoms

ϵ = total detection efficiency at given energy

I_c = intensity in photons per 100 captures

σ_c = capture cross section

For fission gammas:

$$G = N_f \sigma_f \phi t \epsilon I_f / 100 \tag{5.2}$$

where

N_f = total number of fissile uranium atoms

I_f = intensity in photons per 100 fissions

σ_f = fission cross section

For fission product decay gammas:

$$G = N_f \sigma_f \phi \epsilon \int_0^t F \, dt \tag{5.3}$$

where

N_f = total number of fissile atoms

F = function defined in section 3.2.1, but in the present case, it is independent of decay time and dependent on the irradiation time.

For the analysis of capturing atoms, i.e., U^{238}, the Method of Comparison is used, in which a fuel rod is taken as the standard against which the "unknown" rods are compared. The number of atoms of U^{238} under irradiation in an unknown rod divided by the number of the same atoms in the standard rod is given by the expression:

$$\frac{N^x}{N^s} = \frac{G^x}{G^s} \frac{\phi^s t^s}{\phi^x t^x} \tag{5.4}$$

which is derived using Eq. 5.1. The superscripts x and s stand for the unknown and standard rods, respectively. It was assumed that the geometry for irradiation and counting for both rods was the same.

In a capture gamma spectrum, generally many peaks appear due to neutron capture by the same nuclei, and better statistics are obtained by summing up the areas under each peak for both the unknown and the standard rods. The expression (5.4) in this case is extended to the following form:

$$\frac{N^x}{N^s} = \frac{\sum_i G_i^x}{\sum_i G_i^s} \frac{\phi^s t^s}{\phi^x t^x} \tag{5.5}$$

where $\sum_i$ indicates the sum over the peaks i, each characterized by its energy.

The accuracy of the ratio N^x/N^s depends almost entirely on the statistics of counting because the flux and time ratios can be determined quite accurately.

For the fissile nuclei, the gamma spectra are composed of gammas from the three sources mentioned above, and the sum of all detected gammas from the fissile nuclei is given by the following general equation:

$$\sum_\ell G_\ell = N\phi t \left[\sigma_c \sum_i \epsilon_i I_i/100 + \sigma_f \left(\sum_j \epsilon_j I_j/100 + \sum_k \epsilon_k \frac{1}{t} \int_0^t F_k \, dt \right) \right] \tag{5.6}$$

where N is the total number of fissile nuclei under irradiation and the

summations are performed over the peaks due to each process, and $\ell = i+j+k$.

It is believed that the predominant contribution comes from the fission gammas, which is the first term in parentheses in Eq. 5.6. In fact, the gamma-ray lines used in the analysis of U^{235} content are believed to be due only to fission gammas. The complete expression (5.6) has the sole function of showing the independence of the method of analysis of the origin of the gamma rays.

The total number of fissile nuclei under irradiation can be rewritten in the following form:

$$N = E \frac{N_o}{M_5} \frac{W_t}{100} \tag{5.7}$$

where

E = percent enrichment of U^{235}

N_o = Avogadro's number

M_5 = atomic mass of U^{235}

W_t = total weight of fuel (fissile plus fertile) under irradiation.

Then, by denoting the expression inside brackets as the function B, Eq. 5.6 can be rewritten as:

$$\sum_{\ell} G_{\ell} = E \frac{N_o}{M_5} \frac{W_t}{100} \phi t B \tag{5.8}$$

where the function B depends on the cross sections for capture and fission, the detection efficiency and intensity of each gamma, the characteristics of the fission products involved and the time of irradiation. Thus, by irradiating several fuel rods of different enrichment for the

same amount of time and by normalizing the incident flux and the total weight of the fuel under irradiation, it is expected that the total number of counts from the fissile nuclei will be proportional to the enrichment of the fuel rods; and Eq. 5.8 can be used for the determination of the enrichment of an unknown rod. This method is independent of the origin of the gammas because the number of gammas is proportional to the number of the fissile element atoms independently of the process of interaction.

5.2.3 Analysis of U^{238} Content

In Table 5.2 are shown the principal capture gamma-ray lines for U^{238} that can be seen in the spectrum of the fuel rods of different enrichment. Also given is the area under each line as calculated by the computer code GAMANL with the error due only to the statistics of counting.

In order to use Eq. 5.5, the fuel rod of 1.61% enrichment was used as the standard. The correction due to the difference in the attenuation of the incident neutron flux inside the fuel rods was calculated using the subroutine "Flux Attenuation" of the computer program FUEL ASSAY. This correction was smaller than ±5% for all the rods. The self-absorption of the gamma rays was assumed the same for all the rods with the exception of the natural uranium oxide rod for which the density was only half as large as the others. For this latter case, the correction was estimated to be 1.107.

Table 5.3 shows the results of the analysis of U^{238} content by taking the rod of 1.61% enrichment as the standard. The experimental results agree with the calculated results within ±6% in all cases.

TABLE 5.2

The Capture Gamma Rays for U^{238} in Fuel Rods of Different Enrichment

Energy (keV)	Total Number of Counts				
	2%	1.61%	1.30%	1.1%	0.711%
3220.9	185 ± 52	259 ± 39	243 ± 66	191 ± 26	
3583.3	386 ± 58	350 ± 84	341 ± 56	245 ± 37	
3639.8	156 ± 30	308 ± 49	209 ± 51	168 ± 26	
3981.6 / 3990.1	310 ± 30	435 ± 57	501 ± 56	450 ± 60	224 ± 55
4059.7	1125 ± 144	1455 ± 87	1450 ± 92	1412 ± 91	936 ± 80
Total	2162 ± 154	2807 ± 148	2744 ± 148	2466 ± 121	1160 ± 96
Flux relative to 1.61%	1.01	1.00	0.993	1.128	1.06

TABLE 5.3

Results of the Analysis of U^{238} Content

Rod	N^x/N^s	
	Experimental	Calculated*
2.0%	0.770 ± 0.068	0.793
1.3%	0.977 ± 0.074	1.003
1.1%	0.816 ± 0.060	0.800
0.711%	0.526 ± 0.052	0.518

*Calculated from the data given by the fuel supplier, General Electric Company, except for the natural uranium rod which was made by the author.

5.2.4 Analysis of U^{235} Content

In Table 5.4 are shown the lines and the areas under each peak of the gamma rays coming from the interaction of thermal neutrons with U^{235}, as given by GAMANL. Unfortunately, the statistics of count accumulation for the rod of 0.711% enrichment were not significant and were therefore omitted from further analysis.

It was observed that the total number of counts under each peak was quite small with a large relative error; nevertheless, with the summation of all the peaks a significant improvement was noticed.

A normalization of the total weight of the fuel rods under irradiation was performed relative to the rod of 1.61% enrichment due to the difference in the diameter of the uranium oxide pellets between the 1.61% and the 2.0% and 1.1% rods, as shown in Table 5.1. This diameter factor was calculated as 1.2569, which was then used to multiply the total number of counts for both the 2.0% and 1.1% enriched rods. The incident flux correction and the flux attenuation correction are the same as for U^{238} analysis.

The final results are shown in Fig. 5.3. From the curve, the estimated accuracy is about ±10% for 2% enriched rods.

The accuracy of this method, as well as that for measuring U^{238} content, was limited by counting statistics due to low total efficiency of the spectrometer, and not due to the count rate saturation of the electronics. For all the rods counted, less than 800 counts per second were detected. By noticing that 4000 counts per second is the threshold for loss of resolution with the present setup, the count rate could be increased by a factor of 5, either by decreasing the distance between

TABLE 5.4

The Principal Prompt Gamma Rays from the Interaction of Thermal Neutrons with U^{235} in Fuel Rods

Energy (keV)	Total Number of Counts			
	2.0%	1.61%	1.3%	1.1%
1435.4	287 ± 34	227 ± 27	203 ± 54	113 ± 18
2394.3	503 ± 60	474 ± 94	512 ± 80	383 ± 98
2568.4	375 ± 56	429 ± 60	312 ± 68	164 ± 25
2634.9 2638.6	532 ± 85	452 ± 72	403 ± 98	337 ± 53
2753.4	430 ± 64	453 ± 63	374 ± 75	277 ± 46
2792.3	288 ± 54	340 ± 54	367 ± 80	175 ± 42
3288.1	359 ± 54	522 ± 68	335 ± 73	206 ± 48
3312.3	310 ± 69	340 ± 68	390 ± 60	214 ± 44
3401.0	340 ± 56	332 ± 46	252 ± 42	158 ± 17
3575.2	386 ± 54	379 ± 49	340 ± 35	198 ± 24
3600.0	313 ± 78	345 ± 48	209 ± 57	191 ± 40
4364.9	282 ± 42	294 ± 38	212 ± 37	226 ± 66
4453.5	300 ± 36	292 ± 38	206 ± 41	250 ± 42
5405.2 5418.2	406 ± 41	473 ± 51	317 ± 67	264 ± 42
Total	5112 ± 220	5352 ± 232	4432 ± 233	3032 ± 177
Normalized total counts*	6425 ± 275	5352 ± 232	4401 ± 231	3501 ± 203

*The normalization was done relative to the 1.61% enriched rod and takes account of the incident flux, flux attenuation in the fuel, and the slight difference in diameter of fuel pellets of the rods.

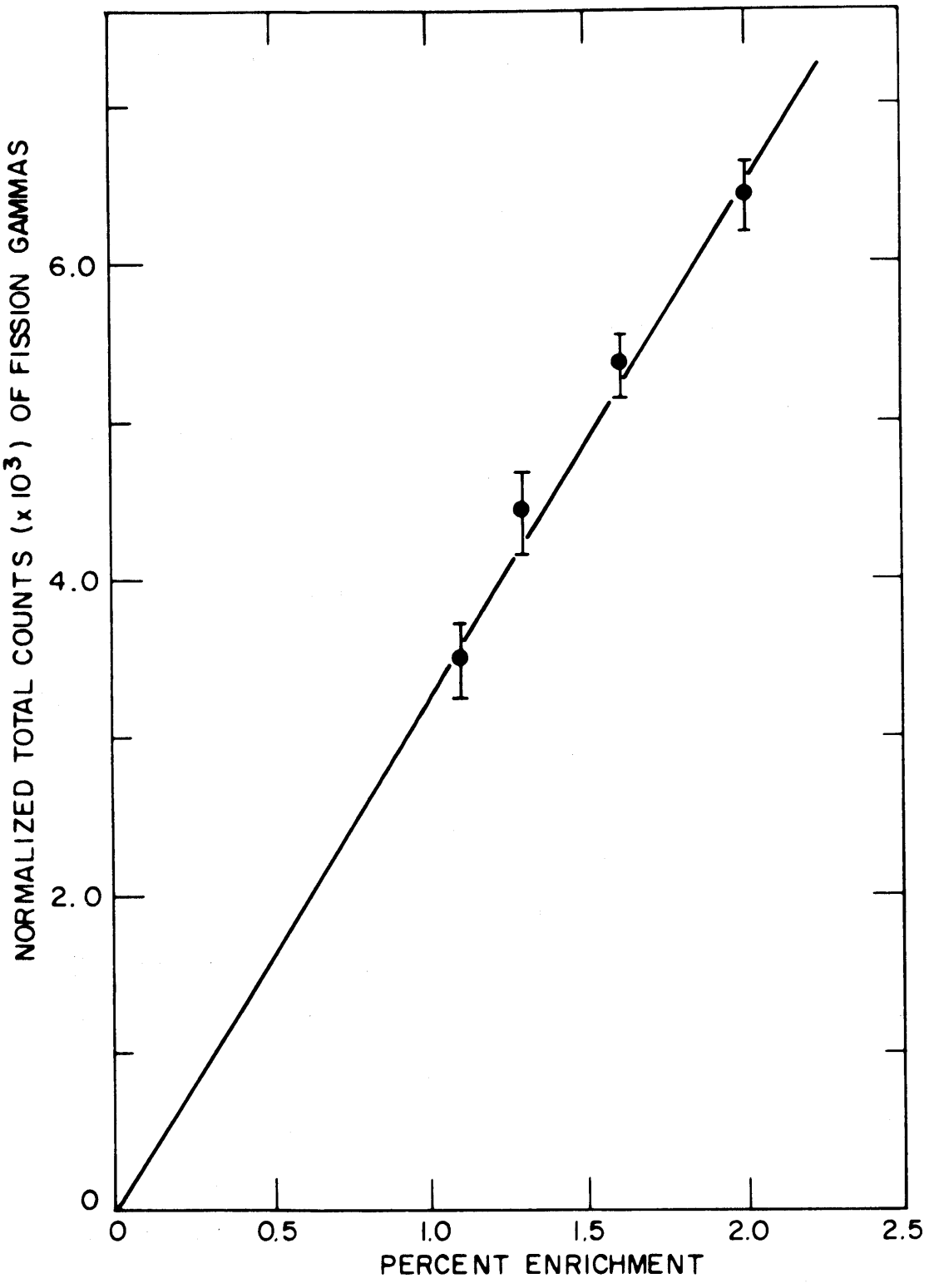

FIG. 5.3 THE VARIATION OF FISSION GAMMA COUNTS WITH FUEL ROD ENRICHMENT

the detector and the sample or increasing the neutron flux. An improvement could also be accomplished by using a larger detector of higher intrinsic efficiency.

5.3 THE PROMPT ACTIVATION ANALYSIS OF PLUTONIUM-URANIUM RODS

5.3.1 Experimental Procedure

For the purpose of investigating the possibility of assaying fuel rods of mixed fissile composition by using the prompt gammas, a fuel rod of the type B-Gold was irradiated with the same experimental arrangement of the uranium rods as described in section 5.2.1. The composition of the oxide fuel rod of type B-Gold, as given by the fabricators and listed in Table 3.2, is 0.30% U^{235}, 0.25% Pu^{239} and 0.016% Pu^{240} as the major components, with U^{238} making up the remaining weight percentage. The gamma spectrum was taken in triple coincidence mode with the same experimental arrangement as well as the same electronic settings as for the uranium rods. Figure 5.4 shows the resulting gamma spectrum. Although the statistics are poor, there can be distinguished in the spectrum 17 peaks due to the contribution of the fission gammas from plutonium together with uranium; 1 peak due only to U^{235}; 5 peaks due only to plutonium; and 9 peaks from U^{238} captures. Also shown are several aluminum lines from the cladding, including the strong line at 1778.8 keV due to the decay of Al^{28}, and the usual hydrogen line. The low statistics are due mainly to the geometrical arrangement, to low detection efficiency and the small magnitude of the incident neutron flux. The count rate could be increased by

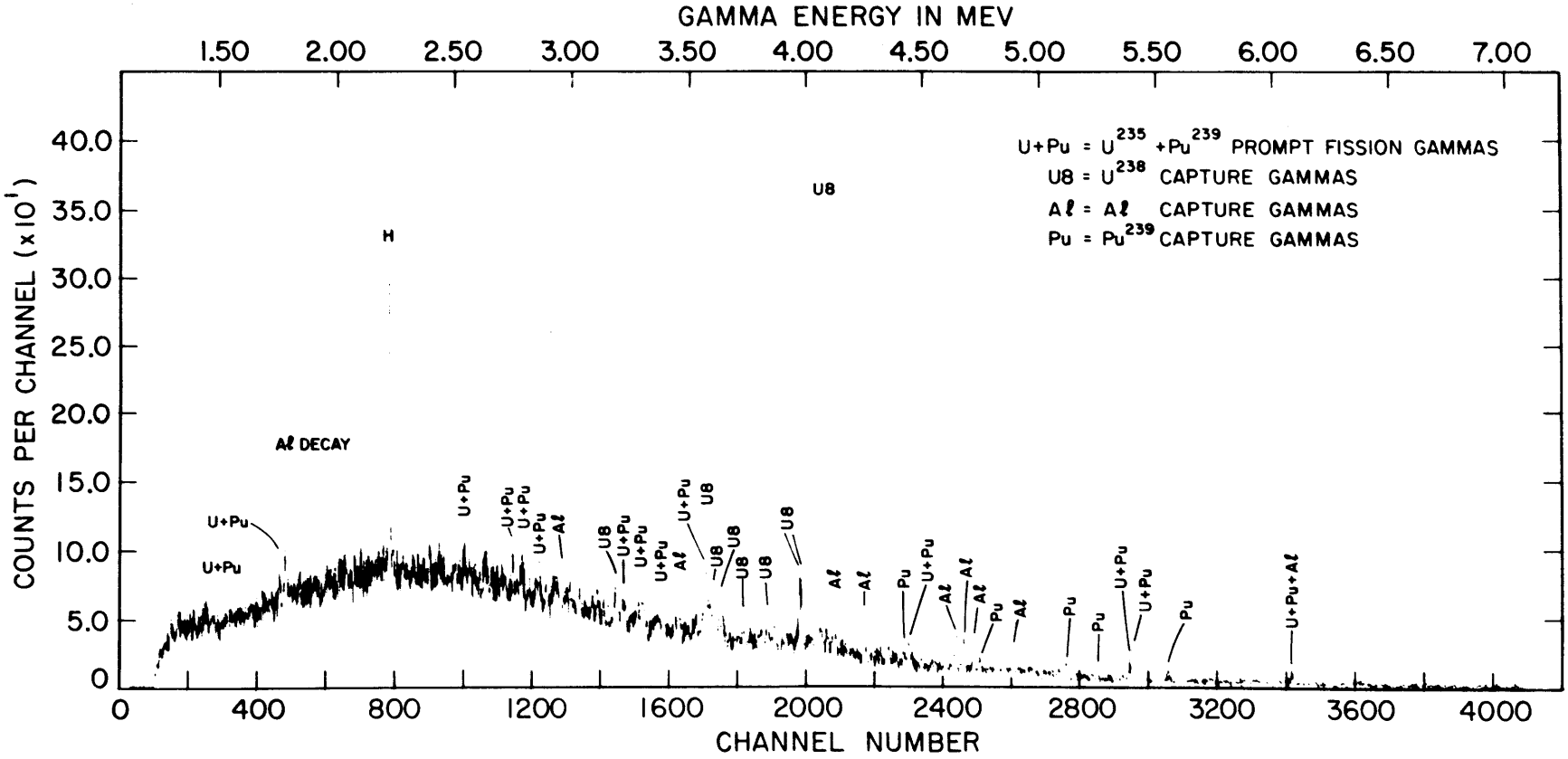

FIG.5.4 THE GAMMA SPECTRUM OF PLUTONIUM-URANIUM ROD, TYPE B-GOLD, TAKEN IN TRIPLE COINCIDENCE MODE

a factor of 6 without endangering the resolution of the system. If this count rate is somehow achieved by improving a combination of the above mentioned factors, a significantly better accuracy could be expected.

5.3.2 Theory

Theoretically, there are several different ways of treating the problem of analyzing the content of the fissile elements starting from the spectral data shown in Fig. 5.4. The method developed in Chapter III could be applied in this case also, because of the difference in the yield of the fission gammas from Pu^{239} compared with the same gammas from U^{235}, as shown in section 4.3.3. But, in practice, this involves differences of small magnitudes due to the low statistics and it would result in very poor accuracy. On the other hand, the use of the single U^{235} peak observable in the spectrum at 4364.9 keV is also impractical for the same reason. Nevertheless, in order to separate the contribution of U^{235} from that of plutonium, at least one piece of information must be extracted from the spectrum which is a characteristic of only one of them. Considering the statistics of counting, the best choice for this differential characteristic is the total area under the 5 peaks due only to plutonium, although this total number of counts is still low.

Once this empirical conclusion is taken into consideration, there are many ways to follow the mechanics of handling the data and equations. Basically, in Fig. 5.4 there are three kinds of peaks to be considered: One due only to captures by U^{238}, another due only to plutonium, and a third due to the combination of fissile plutonium and U^{235} fission gammas which will be called from now on the mixed lines.

For the sake of simplifying the notation, these three distinct kinds of lines are treated here as lumped together into three distinct peaks. Also, a notation is adopted in which the gammas from the fission process are assumed to be due only to prompt fission gammas, although the results are independent of the origin of these gammas since the corresponding equations are of the same basic form. And it is recalled that besides the data from the spectrum of the mixed rod, there is also available information from the uranium and plutonium foils and also from the uranium rods, each one of them able to serve as a standard rod for calibration purposes.

Thus, the total number of counts for each of the three kinds of peaks in the spectrum of Fig. 5.4, i.e., due to plutonium, U^{238} and the combination of U^{235} and plutonium, are given, respectively,by the following expressions:

$$G_9 = N_9 \phi \sigma_9 t \epsilon_9 I_9 / 100 \tag{5.9}$$

$$G_8 = N_8 \phi \sigma_8 t \epsilon_8 I_8 / 100 \tag{5.10}$$

$$G_{59} = N_5 \phi \sigma_5 t \epsilon_{59} I'_5 / 100 + N_9 \phi \sigma_9 t \epsilon_{59} I'_9 / 100 \tag{5.11}$$

The final objective is to find the ratios N_5/N_9 and N_5/N_8 in order to obtain the enrichment of each fissile element. The immediate objective is to cancel out the main sources of intrinsic inaccuracy which are the efficiency, intensity and possibly the cross sections.

By dividing Eq. 5.11 by Eq. 5.9, the following expression is obtained:

$$\frac{G_{59}}{G_9} = \frac{N_5 \sigma_5 \epsilon_{59} I'_5}{N_9 \sigma_9 \epsilon_9 I_9} + \frac{\epsilon_{59} I'_9}{\epsilon_9 I_9} \tag{5.12}$$

The ratios on the right-hand side of Eq. 5.12, other than N_5/N_9, are obtained from the data on prompt gammas from the fissile foils of U^{235} and Pu^{239} taken from the experiments described in section 4.3.

From the uranium and plutonium foils, there results

$$\frac{G_5^F}{G_9^F} = \frac{N_5^F \sigma_5 \epsilon_{59} I'_5 t_5^F \phi_5^F}{N_9^F \sigma_9 \epsilon_9 I_9 t_9^F \phi_9^F} \tag{5.13}$$

where N_5^F and N_9^F are the number of fissile atoms of U^{235} and Pu^{239} in the respective foils, which are easily obtained from the weight of the foils given in section 3.3.1. Thus,

$$\frac{\sigma_5 \epsilon_{59} I'_5}{\sigma_9 \epsilon_9 I_9} = \frac{G_5^F N_9^F \phi_9^F t_9^F}{G_9^F N_5^F \phi_5^F t_5^F} = R_3 \tag{5.14}$$

And, from the plutonium foil,

$$\frac{G_9^{F'}}{G_9^F} = \frac{N_9^F \sigma_9 \phi^F \epsilon_{59} I'_9/100}{N_9^F \sigma_9 \phi^F \epsilon_9 I_9/100} = \frac{\epsilon_{59} I'_9}{\epsilon_9 I_9} = R_4 \tag{5.15}$$

where $G_9^{F'}$ is the total number of counts under the peaks for the Pu foil corresponding to the mixed lines in the spectrum of Fig. 5.4. It is important to assert that in the determination of the ratios R_3 and R_4 the intensities of the lines given in Table 4.4 are not used, but rather the total counts under the peaks given by GAMANL, which is shown in Tables 5.5, 5.6 and 5.7 in the next section.

Thus, from Eq. 5.13 and the expressions for the ratios R_3 and R_4, the ratio N_5/N_9 in the "mixed" rod is determined by:

$$\frac{N_5}{N_9} = \frac{1}{R_3}\left(\frac{G_{59}}{G_9} - R_4\right) \tag{5.16}$$

which is the fundamental expression for obtaining the ratio N_5/N_9.

On the other hand, in order to obtain an expression for the ratio N_5/N_8, Eq. 5.12 is rewritten in the following form:

$$\frac{G_{59}}{G_9} = \frac{N_5 \sigma_5 \epsilon_{59} I'_5}{N_8 \sigma_8 \epsilon_8 I_8} \frac{N_8 \sigma_8 \epsilon_8 I_8}{N_9 \sigma_9 \epsilon_9 I_9} + R_4 \tag{5.17}$$

in which the first ratio in the right-hand member of Eq. 5.12 was multiplied and divided by G_8.

From the data for the 1.61% enriched uranium rod which was irradiated with the same experimental arrangement and now is taken as a standard rod, the following ratio can be obtained:

$$\frac{G_5^R}{G_8^R} = \frac{N_5^R \sigma_5 \epsilon_{59} I'_5}{N_8^R \sigma_8 \epsilon_8 I_8} \tag{5.18}$$

where G_5^R is the total number of counts under the peaks for the standard rod corresponding to the mixed lines in the spectrum of Fig. 5.4.

From Eq. 5.18 there results the ratio,

$$\frac{\sigma_5 \epsilon_{59} I'_5}{\sigma_8 \epsilon_8 I_8} = \frac{G_5^R N_8^R}{G_8^R N_5^R} = R_5 \tag{5.19}$$

Then, going back to Eq. 5.17 and taking Eq. 5.19 into account, the ratio N_5/N_8 can be determined by the following expression:

$$\frac{N_5}{N_8} = \frac{1}{R_5} \frac{G_9}{G_8} \left(\frac{G_{59}}{G_9} - R_4 \right) \tag{5.20}$$

5.3.3 Results

Tables 5.5, 5.6 and 5.7 present the experimental data to be used in Eqs. 5.16 and 5.20 in order to determine the ratios N_5/N_9 and N_5/N_8.

The calculated values of the ratios R_3, R_4 and R_5 are the following:

$$\begin{aligned} R_3 &= 1.345 \pm 0.081 \\ R_4 &= 3.614 \pm 0.153 \\ R_5 &= (0.922 \pm 0.060) \times 10^2 \end{aligned} \tag{5.21}$$

And the ratios given by Eqs. 5.14 and 5.18 are:

$$\begin{aligned} \frac{N_5}{N_9} &= 1.369 \pm 0.292 \\ \frac{N_5}{N_8} &= (0.314 \pm 0.096) \times 10^{-2} \end{aligned} \tag{5.22}$$

TABLE 5.5

The Total Number of Counts of the Fission Gamma Lines
Which Are Common in the Spectra for the Mixed Rod,
U-Foil, Pu-Foil, and the 1.61% Enriched U-Rod

Energy (keV)	Mixed Rod (18 hrs. run)	U^{235} Foil (15 hrs. run)	Pu^{239} Foil (15 hrs. run)	U-Rod 1.61% Enriched (18 hrs. run)
1427.7	91 ± 14	265 ± 31	289 ± 43	184 ± 27
1435.4	117 ± 14	324 ± 35	254 ± 42	227 ± 27
1750.5	283 ± 42	170 ± 24	199 ± 36	127 ± 34
2394.3	146 ± 23	640 ± 64	497 ± 90	474 ± 74
2544.1	174 ± 20	307 ± 42	330 ± 53	364 ± 54
2662.7	242 ± 41	305 ± 54	336 ± 92	247 ± 52
2753.4	151 ± 30	553 ± 55	334 ± 92	453 ± 63
2792.3	188 ± 21	151 ± 40	511 ± 71	340 ± 54
2868.8	130 ± 14	307 ± 54	281 ± 53	275 ± 54
3231.3	155 ± 12	113 ± 20	160 ± 43	118 ± 23
3288.1	138 ± 14	449 ± 54	573 ± 102	522 ± 68
3401.0	142 ± 16	508 ± 60	498 ± 75	332 ± 46
3575.2	216 ± 26	509 ± 56	346 ± 51	379 ± 49
4453.5	195 ± 32	425 ± 50	324 ± 42	292 ± 38
5405.2	105 ± 17	172 ± 42	81 ± 20	147 ± 27
5418.2	156 ± 17	381 ± 80	163 ± 29	326 ± 42
6102.7	93 ± 9	95 ± 12	72 ± 16	63 ± 12
Total	$G_{59} = 2722 \pm 96$	$G_5^F = 5674 \pm 200$	$G_9^F = 5248 \pm 253$	$G_5^R = 4870 \pm 202$

TABLE 5.6

Total Counts for the Pu Lines in the Mixed Rod Spectrum and the Corresponding Values for the Pu-Foil

Energy (keV)	Mixed Rod (18 hrs. run)	Pu-Foil (18 hrs. run)
4430.0	125 ± 20	461 ± 50
4757.5	99 ± 18	294 ± 45
5119.5	99 ± 16	273 ± 37
5291.2	42 ± 13	209 ± 32
5570.5	134 ± 24	505 ± 60
Total	$G_9 = 499 \pm 42$	$G'_9 = 1452 \pm 272$

TABLE 5.7

Total Counts for the U^{238} Lines Which Are Common to the Mixed Rod and to the 1.61% Enriched Uranium Standard Rod

Energy (keV)	Mixed Rod (18 hrs. run)	U-Rod 1.61% Enriched (18 hrs. run)
3220.9	181 ± 18	259 ± 39
3583.3	422 ± 97	350 ± 84
3639.8	206 ± 22	308 ± 49
3739.6	148 ± 31	228 ± 23
3846.4	153 ± 31	203 ± 16
3982.6	192 ± 25	435 ± 57
3990.1	164 ± 24	
4059.7	1704 ± 68	1455 ± 87
Total	$G_8 = 3170 \pm 136$	$G_8^R = 3238 \pm 151$

From the values given in Tables 5.5, 5.6 and 5.7, the ratios between the weights of the fissile components were determined and compared to the data calculated from the specifications given by the fuel supplier, E. I. DuPont. The results are given in Table 5.8 below:

TABLE 5.8

Experimental Results of the Analysis of a Plutonium-Uranium Rod Type B-Gold

Weight Percent Ratio	Experimental Result	Calculated Result
W_5/W_9	1.346 ± 0.287	1.190
W_5/W_8	$(0.314 \pm 0.096) \times 10^{-2}$	0.301×10^{-2}
W_9/W_8	$(0.233 \pm 0.087) \times 10^{-2}$	0.253×10^{-2}

In this problem, the presence of about 1% of Pu^{241} relative to the total weight of Pu^{239} in both the plutonium fuel and the mixed rod was treated by adding the Pu^{241} to the total Pu^{239} content. This assumption is reasonable because of the small amount of Pu^{241} involved and the similarity between both nuclei with respect to fission properties.

It was also assumed that the lines assigned only to plutonium in the spectrum of the mixed rod were due solely to Pu^{239} and not to other isotopes of plutonium present both in the mixed rod and the plutonium-foil. This assumption is justified for two reasons: (a) The only important isotope beside Pu^{239} is Pu^{240}, which is present in the amount of 8.8% in weight relative to Pu^{239} in the plutonium foil and 6.4% in the mixed rod. If there are, in fact, any gamma lines from Pu^{240},

their effect would be felt with about the same intensity for both the "unknown" mixed rod and the standard plutonium foil because the percent in both is very close, and their effect will tend to cancel out in the ratio calculations. (b) The relative intensities of the three principal lines due only to plutonium are approximately the same in the spectrum of two types of mixed rods, one containing four times more Pu^{240} than the other, and both having about the same amount of Pu^{239}, which indicates strongly that at least those three lines are due solely to the presence of Pu^{239}.

The table of results indicates that, although the accompanying error is large, there is a sound agreement between the experimental result and the specifications given by the fabricators.

It is believed that with a drastic improvement in the statistics of counting, by changing the present experimental arrangement, the method could be used for the analysis of mixed rods with an accuracy of better than ±10%. It is also expected that this method could be applied in the analysis of burned fuel elements for measurement of Pu buildup after a long cooling time.

5.4 ANALYSIS OF FUEL RODS USING THE FISSION NEUTRON YIELD

5.4.1 Introduction

Fission neutrons are potentially a good indicator for analysis of fissile material. A process of analysis based upon the difference in the fission cross section of uranium isotopes, and using the fission neutrons, has been developed by Jones et al. (J1). The main problem for the detection of the fission neutrons is the need to discriminate

against the source neutrons that induce the fission and against the background gammas. Generally, it is preferred to detect and count the fission neutrons of energies above those of the neutrons used to irradiate the sample, and for this purpose one needs an energy-sensitive detector.

Jones et al. used a recoil proton scintillation counter which used the technique of pulse-shape discrimination to reject pulses induced in the detector by gamma rays. An analyzer was used to record the pulse-height spectrum produced by the recoiling protons in the scintillator, and the number of fission neutrons above a given energy was counted as being proportional to the sum of the recoil proton pulses above that energy in the collected spectrum.

Both these functions of discriminating against the gamma background and the source neutrons can be performed by a single Ge(Li) detector operating in the free mode and acting now as a fast neutron detector. This method is based on the inelastic scattering of fission neutrons by Ge^{72} in the crystal: the fission neutrons striking the 27.37% abundant Ge^{72} isotope inside the germanium detector excite it to a level at 693 keV. The level at 693 keV has spin zero and it de-excites directly to the ground state which also has zero spin. For a transition $0 \rightarrow 0$, the only possible de-excitation mechanism is internal conversion. The internal conversion electrons will loose their energy in the detector and produce a strong peak in the spectrum. The intensity of the inelastic transition at 693 keV is proportional to the fission neutron yield because this transition occurs only through inelastic scattering. There is no Ge^{71} in the natural state, which makes

impossible any contribution from the thermal neutron capture process, and therefore the thermal neutrons are automatically discriminated out.

About 77% of the fission neutrons have energy above 693 keV and therefore are capable of producing the 693-keV peak. The detection efficiency for the conversion electrons is believed to be almost 100% because they are produced inside the detector itself.

5.4.2 Experimental Procedure

Figure 5.5 shows the plan view of the experiments for the measurement of the yield of fission neutrons. The fuel rod is placed vertically, and it is held tightly between two frames of masonite, one of which is adjustable according to the diameter of the fuel rod; the other is fixed in place and has a V-notch against which the rod is held by the adjustable piece. The neutron beam passes through a 1-1/2-inch hole in the fixed masonite frame and hits the rod as seen in Fig. 2.3(b). The 35-cc Ge(Li) detector views the fuel through a lead collimator, 11 inches long and 1/2 inch in hole diameter. Five fuel rods, described in Table 5.1, with different enrichments were irradiated. Two of these rods had 1/2-inch external cladding diameter and the remaining three were of 9/16-inch diameter. The gamma beam alignment was set with the 9/16-inch external cladding diameter rods. In order to have the center line of the fuel rods of 1/2-inch external cladding diameter also line up with respect to the collimator and the detector, a sheet of aluminum was used to wrap the 1/2-inch o.d. fuel rod, to increase the total external diameter of the cladding to 9/16 inch at the place where the rod is held by the masonite frames.

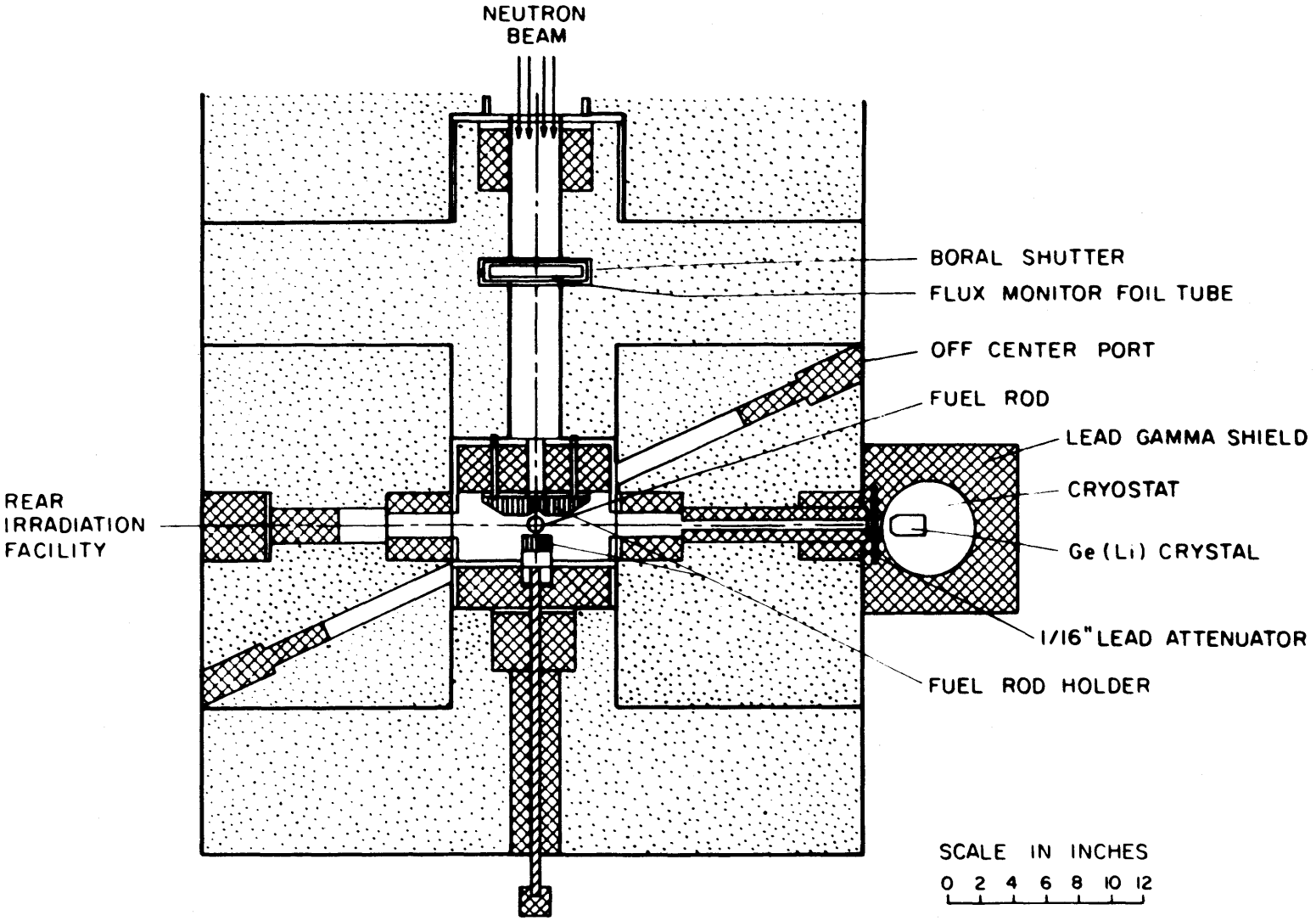

FIG. 5.5 EXPERIMENTAL ARRANGEMENT FOR THE MEASUREMENT OF THE FISSION NEUTRON YIELD

A 1/4-inch-thick sheet of masonite was placed in the gamma beam in order to attenuate the scattered thermal neutrons reaching the detector. It also shielded against very low energy gammas. Figure 2.10 shows a typical spectrum of the prompt gammas from the fuel rods taken in free mode. The annihilation gamma is shown together with thermal neutron capture gammas from germanium and iron. The strong line at 693 keV is from Ge^{72}. This line was first identified by Hoffman (H7), and it has a smooth tail on the upper side of the peak. No explanation for this strange shape of the peak has been found.

All the spectra were obtained by irradiating for 160 minutes live time as counted by the 4096 channel analyzer. For each run the incident neutron flux was monitored and taken into account.

The total number of fission neutrons detected by the germanium detector is given by the following expression:

$$G_N = \nu_5 N_5 \sigma_f \phi_N \epsilon_N t_N \tag{5.23}$$

where

ν_5 = average number of fission neutrons produced per fission of U^{235}

ϵ_N = total detection efficiency for fission neutrons

t_N = total live irradiation time, 160 minutes.

Equation 5.23 can be rewritten as an explicit function of the enrichment E in the same fashion as Eq. 5.8 in the following form:

$$G_N = E \nu_5 \frac{N_8}{M_5} \frac{W_t}{100} \sigma_f \phi_N \epsilon_N t_N \tag{5.24}$$

Therefore, by assuming that ν_5 is the same for distinct fuel rods, and by normalizing by the values of the total weight, W_t, of the fuel rods and the values of ϕ_N, the total number of detected fission neutrons is proportional to the enrichment of the fuel rod, and Eq. 5.24 can be used for analytical purposes to examine the content of U^{235} in a uranium fuel rod.

5.4.3 Results

Figure 5.6 shows the experimentally obtained peaks in the region of 400 keV to 800 keV for the spectra of prompt gammas from the irradiation of fuel rods.

Table 5.9 shows the total counts obtained under the peaks for each rod, and also the normalized number of counts with respect to the 2.0% enriched fuel rod.

TABLE 5.9

Total Number of Counts Under 693-keV Ge^{72} Transition Peak

Rod Enrichment	Experimental Data	Normalized* Data
2.0%	73,973 ± 975	73,973 ± 975
1.61%	76,026 ± 948	60,462 ± 853
1.3%	64,349 ± 896	48,433 ± 674
1.1%	44,465 ± 861	40,748 ± 790
0.711%	9,228 ± 434	23,447 ± 1402

*The normalization was performed relative to the 2.0% enriched rod and took account of the incident flux, the neutron attenuation in the fuel, the slight difference in diameter of the fuel pellets in the rods, and the density of the 0.711% enriched rod.

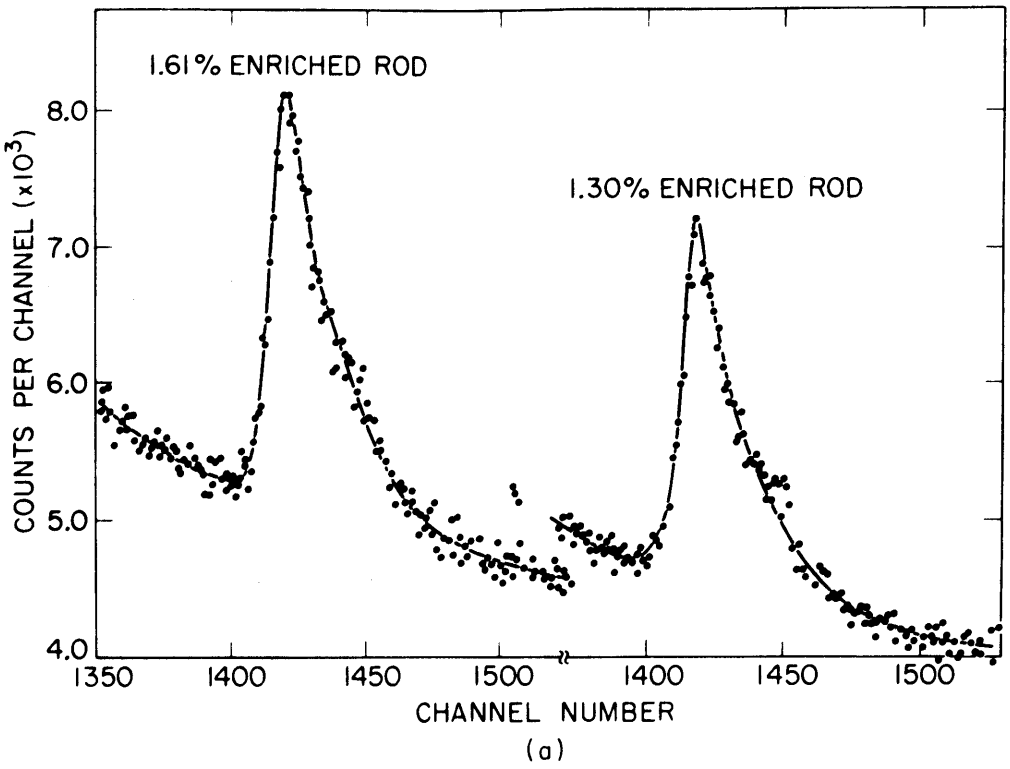

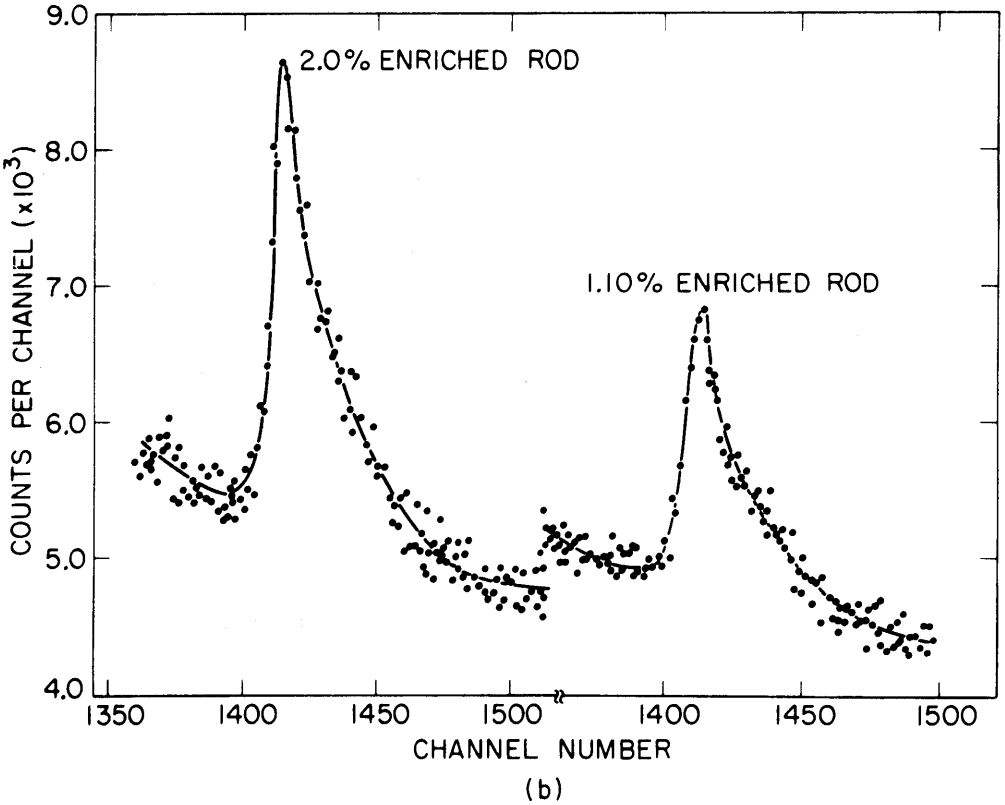

FIG. 5.6 THE VARIATION OF THE 693 keV Ge PEAK WITH THE ENRICHMENT OF FUEL ROD

Figure 5.7 shows the linear relation between the enrichment and the normalized number of counts. The experimental point for the natural uranium fuel rod is accompanied by a relatively much higher error due to the poorer statistics of counting. There was a much lower quantity of fissile material in this fuel rod due to the density of its uranium oxide, which was about half of that of the other rods. A different experimental arrangement would be helpful for enrichments lower than 1% with the detector closer to the fuel rod. A much longer counting time would be another alternative.

From Fig. 5.7 it is concluded that the accuracy of determination of enrichment of fuel rods using this method is about 2% for 1% enriched rods, decreasing to about 1% accuracy for 2% enriched rods.

This method could be used also for the determination of the relative amount of Pu^{239} in a mixed rod, if the U^{235} amount is a known quantity, together with the fission cross section and the average number of fission neutrons per fission for both nuclei. The equation to be used would be:

$$\frac{N_9}{N_5} = \frac{G_9}{G_5} \frac{\sigma_5 \nu_5}{\sigma_9 \nu_9} \tag{5.25}$$

where ν is the average number of neutrons emitted per fission; $G_9 + G_5$ is the total number of counts under the 693-keV peak for the mixed rod; and G_5 is determined by using Fig. 5.7, once the U^{235} enrichment is assumed as known. This was done for the mixed rod B-Gold using the same ν for both fissile elements and the fission cross sections, 741 barns for Pu^{239} and 577 barns for U^{235}.

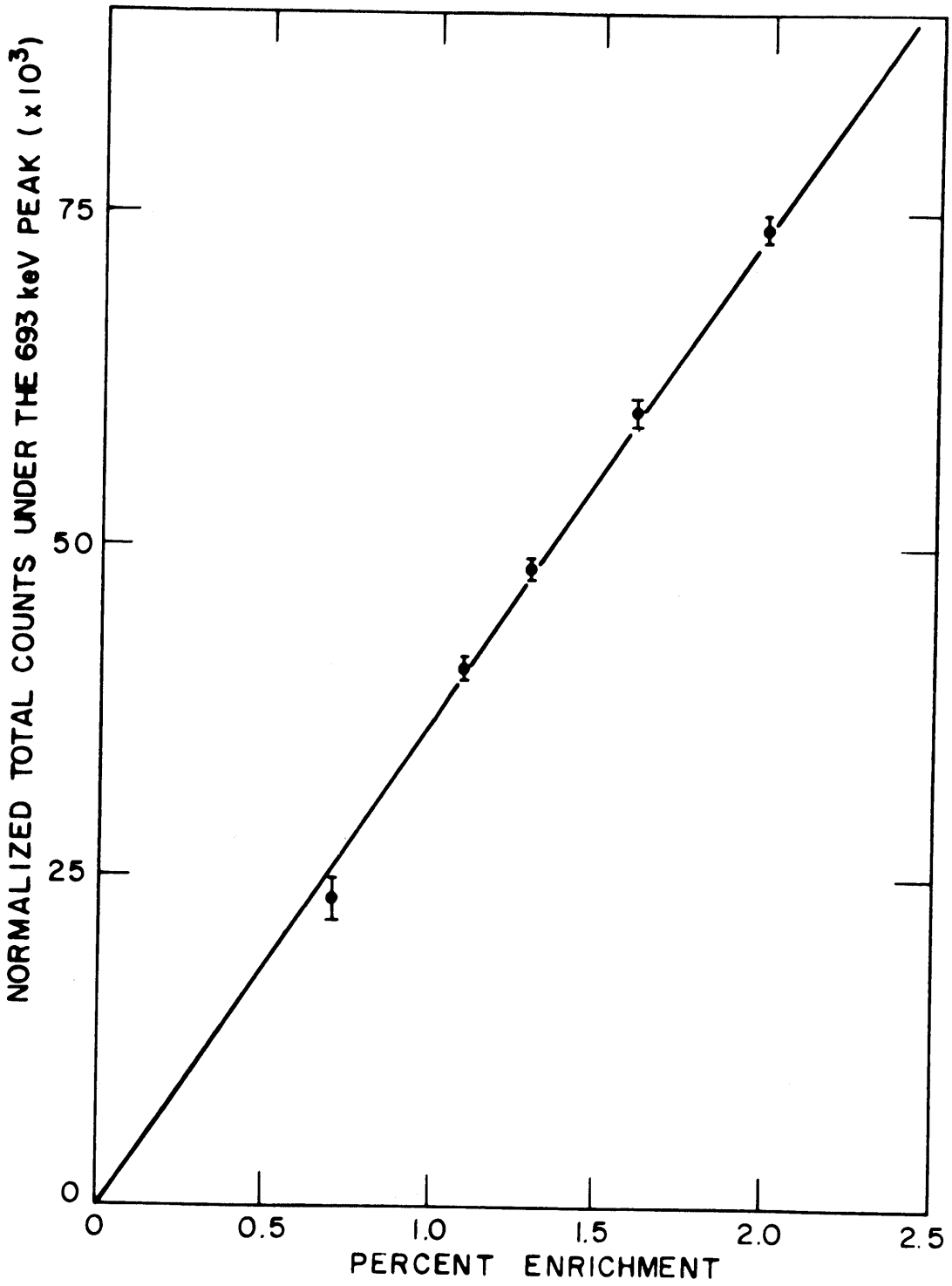

FIG. 5.7 RELATION OF THE MEASURED FISSION NEUTRON YIELD TO THE FUEL ENRICHMENT

Agreement between the experimental data and the calculated result was observed within ± 10% error. The use of germanium detectors for fast neutron detection has a potential drawback, that of radiation damage to the crystal. Studies done by Kraner et al. (K2) indicate that a Ge(Li) detector bombarded by fast neutrons loses energy resolution for high values of total neutron exposure. According to his work, the tolerable fast neutron exposure is about 10^{10} neutrons per cm^2 of germanium crystal. During the experiments involved in this section, a total of 5×10^7 fast neutrons hit the 35-cc coaxial detector in an area of about 1 cm^2. No observable radiation damage was noticed. Kraner has reported that the degraded resolution of the detector caused by fast neutron bombardment can be recovered through a thermal cycling process in which the damaged crystal is annealed by the thermal agitation of the atoms within the defective atomic arrangement.

In conclusion, both active methods of using either prompt gammas or fission neutron yield proved to be sound techniques for fuel analysis.

A weak point for the technique using the prompt gammas is the low counting rate. Nevertheless, this drawback is not an intrinsic disadvantage, and with improvements in geometric configuration and detection techniques, such as fast counting systems allied with close detector-sample distance, much better accuracy is expected than obtained in this work. Using this technique (as it now stands, without improvements), an average of about 30 hours would be necessary to assay a fuel rod.

On the other hand, the use of Ge(Li) crystals as energy threshold fast neutron detectors offers a new prospect for rapid assay (about 4

hours) of uranium fuel rods with great accuracy. Also, as a fission neutron detector, the germanium detector could be used in techniques for analysis of mixed fuel rods based upon the difference in the fission cross section of the fissile elements constituting the fuel rods.

In the following chapter, consideration is given to the use of prompt gammas for measuring reactor physics parameters.

Chapter VI

THE MEASUREMENT OF η AND C AND SOME CONSIDERATIONS ON THE FEASIBILITY OF AN IN-CORE GAMMA-RAY SPECTROMETER FOR THE MIT EXPONENTIAL FACILITY

6.1 INTRODUCTION

In this chapter are presented some considerations pertinent to the development of new techniques for measuring reactor physics parameters based on high resolution gamma-ray spectroscopy of fuel elements. The motivation for this analysis came about when it was proposed to study the physics of burned fuel elements at the Department of Nuclear Engineering at M.I.T. A burned fuel element, due to the presence of decaying fission product radioactivity, presents new problems and requires new methods for measuring the reactor physics parameters.

The classical method of inserting activation foils in between the fuel pellets of fuel elements, for measuring the reactor physics parameters of lattices composed of fresh fuel elements located in critical or exponential facilities, is well established and widely used. However, the use of the same techniques for burned fuel would involve cutting into the fuel and would obviously present severe problems such as the release of fission products and plutonium from the burned fuel during the cutting process. Thus, any method that could provide information on the neutronic behavior of a fuel rod by means of external measurements would be valuable. Such a method could be also applied

profitably to fresh fuel. The emission of capture and fission gammas and fission neutrons by a fuel element during irradiation in an exponential facility suggested this study of the potential applicability of gamma-ray spectroscopy to this problem.

Recent developments in experimental reactor physics (P1, Z1) indicate that measurements made on single fuel elements can be used to compute quantities ordinarily found by means of measurements on assemblies containing many fuel elements, and with comparable accuracy. This means that use of only one burned fuel rod in an exponential facility could yield the needed information. Donovan et al. (D3) have shown that three parameters, Γ = heterogeneous thermal constant, η = fission neutron yield, and A = resonance absorption parameter, can uniquely determine the infinite medium multiplication constant. The heterogeneous thermal constant Γ can be uniquely determined by measuring the radial location of the thermal flux peak in a single rod experiment performed in an exponential tank. Thus, it is an externally measurable parameter. In this chapter the possibility of measuring η by external means, through gamma-ray spectroscopy measurements performed by an in-core spectrometer operating in an exponential facility, is investigated.

In the following two sections, a method of measuring two parameters for the fuel rods with the experimental configuration shown in Fig. 5.1 is proposed, which <u>if</u> performed for the fuel rod inserted in an exponential facility would yield the parameter η and the initial conversion ratio. Following these two sections, a preliminary conceptual design is presented for an in-core gamma-ray spectrometer for the

MIT Exponential Facility. The actual development and construction of such a spectrometer is left as a recommendation for future work.

6.2 THE INITIAL CONVERSION RATIO

The initial conversion ratio C is defined as the ratio of the rate at which Pu^{239} is produced to the rate at which U^{235} is destroyed. This parameter is measurable through gamma spectrometry for fuel rods irradiated with the experimental configuration shown in Fig. 5.1. It is observed that the initial conversion ratio is meaningful only for fuel rods installed in a reactor or exponential facility. In this sense, the measurement of the above ratio for the experimental arrangement shown in Fig. 5.1 is merely demonstrative, but it is still valuable to show as a prototype for a similar measurement made by an in-core gamma spectrometer detecting gammas from a single rod in the center of an operating exponential facility.

The actual measurement of C with the present experimental arrangement involves no new data other than that taken in Chapter V. Only the handling of the pertinent data is different.

The rate at which Pu^{239} is produced is proportional to the rate at which U^{238} captures neutrons, and the rate at which U^{235} is destroyed is proportional to the total fission gamma emission rate if one assumes that for all the uranium fuel rods under consideration the ratio of the capture to fission cross section is the same.

Thus,

$$C = \text{constant} \cdot \frac{N_8 \sigma_{c8}}{N_5 \sigma_f (1 - \alpha_{25})} \tag{6.1}$$

where the constant is intrinsically dependent on the irradiation time, the decay constant of U^{239} and N_p^{239}, which are the same for all four rods of varying enrichment described in Chapter V and considered here.

The total number of detected capture gamma rays for a fuel element is given by the following expression:

$$\sum_i G_{8i} = N_8 \sigma_{c8} \phi t \sum_i \epsilon_i I_{ci}/100 \tag{6.2}$$

and for the fission gammas,

$$\sum_j G_{5i} = N_5 \sigma_f \phi t \sum_j \epsilon_j I_{fj}/100 \tag{6.3}$$

with the same notation as used in the preceding chapter.

Thus, C is given by the following expression:

$$C = \text{constant} \cdot \frac{\sum_i G_{8i}}{\sum_j G_{5j}} \frac{\sum_j \epsilon_j I_{fj}}{\sum_i \epsilon_i I_{ci}} \frac{1}{1+\alpha_{25}} \tag{6.4}$$

The parameter C is independent of the incident flux and the flux attenuation inside the fuel rod. The dependence on the gamma self-absorption in the fuel, due to the difference in energy between the capture gammas for U^{238} and the fission gammas, is negligible.

Here again, we use the method of comparing one fuel rod against a standard, for which it is assumed that the parameter C is well known. In this case, there results the expression:

$$\frac{C^x}{C^s} = \frac{\sum_i G_{8i}^x}{\sum_i G_{8i}^s} \frac{\sum_j G_{5j}^s}{\sum_j G_{5j}^x} \tag{6.5}$$

It is observed that for the measurement of this parameter by using the above equation for fuel rods in an exponential facility, some correction factors may be required due to the neutron spectral difference for each fuel. The epithermal neutrons alter the intensities of the capture gamma rays for U^{238}, and possibly the intensity of the fission gammas. Thus, the neutron spectral difference will require corrections to the intensities of the gammas, and also to the capture to fission cross section ratio.

For the present experimental arrangement, the first ratio of Eq. 6.5 is obtained by using the results given in Table 5.4. The results for the parameter C are presented in Table 6.1 below.

TABLE 6.1
The Relative Initial Conversion Ratio

	C Relative to 1.61% Enriched Fuel Rod	
Fuel Rod	Measured	Calculated*
2%	0.806 ± 0.106	0.802
1.3%	1.180 ± 0.102	1.242
1.1%	1.551 ± 0.103	1.471

*Calculated from $(N_5^S/N_5^X)(N_8^X/N_8^S)$, where the values of N were taken from the data given by the fuel fabricator: this assumes all microscopic nuclide cross sections are identical for the rods irradiated.

6.3 THE FISSION NEUTRON YIELD PARAMETER

Here, the fission neutron yield parameter η is defined as the ratio of the rate at which fission neutrons are produced to the rate at which neutrons are absorbed in the uranium of the fuel rod. The same observation about the meaning of η as remarked for the parameter C is applicable.

From the definition, η is given by the expression:

$$\eta = \frac{\nu N_5 \sigma_f}{N_5\sigma_f + N_5\sigma_{c5} + N_8\sigma_{c8}} \tag{6.6}$$

By inverting Eq. 6.6, the following expression is obtained:

$$\frac{1}{\eta} = \frac{N_5\sigma_f(1+\alpha_{25})}{\nu N_5 \sigma_f} + \frac{N_8 \sigma_{c8}}{\nu N_5 \sigma_f} \tag{6.7}$$

By representing the first ratio of the above equation as $1/\eta_5$ and the second as $1/\eta_8$, there results,

$$\frac{1}{\eta} = \frac{1}{\eta_5} + \frac{1}{\eta_8} \tag{6.8}$$

where η_5 is the ratio of the rate at which fission neutrons are produced to the rate at which neutrons are absorbed in U^{235}, and η_8 is the ratio of the rate at which fission neutrons are produced to the rate at which neutrons are absorbed in U^{238}.

By using Eqs. 6.2, 6.3 and 5.23, the following relations are obtained:

$$\eta_5 = \frac{G_N}{\phi_N \epsilon_N t_N} \frac{\phi t \sum_j \epsilon_j I_{fj}/100}{\sum_j G_{5j}(1+\alpha_{25})} \tag{6.9}$$

$$\eta_8 = \frac{G_N}{\phi_N \epsilon_N t_N} \frac{\phi t \sum_i \epsilon_i I_{8i}/100}{\sum_i G_{8i}} \tag{6.10}$$

Here also, the method of comparison is used in which it is assumed that the values of η_5 and η_8 are well known for a standard rod against which the others are compared. Whence, although the geometrical arrangement for the determination of the yield of fission neutrons as described in section 5.4 is different from the configuration used to determine the yield of the fission and capture gammas as it is shown in Fig. 5.1, this data can be used because in the calculation of ratios the geometrical factor is cancelled out.

Therefore,

$$\frac{\eta_5^x}{\eta_5^s} = \frac{G_N^x}{G_N^s} \frac{\phi_N^s}{\phi_N^x} \frac{\phi^{x}t^{x}}{\phi^{s}t^{s}} \frac{\sum_j G_{5j}^s}{\sum_j G_{5j}^x} \tag{6.11}$$

and

$$\frac{\eta_8^x}{\eta_8^s} = \frac{G_N^x}{G_N^s} \frac{\phi_N^s}{\phi_N^x} \frac{\phi^{x}t^{x}}{\phi^{s}t^{s}} \frac{\sum_i G_{8i}^s}{\sum_i G_{8i}^x} \tag{6.12}$$

By using the data in Table 5.2 for U^{238} captures, the data in Table 5.4 for U^{235} fission gammas and the data in Table 5.9 for the

yield of fission neutrons, the results for Eqs. 6.11 and 6.12 are shown, respectively, in Tables 6.2 and 6.3.

TABLE 6.2

The Relative Values of η_5

Fuel Rod	η_5 Relative to 1.61% Enriched Fuel Rod	
	Measured	Calculated*
2%	1.019 ± 0.063	1.00
1.3%	0.974 ± 0.070	1.00
1.1%	1.030 ± 0.075	1.00

*Calculated by assuming the same ν and α_{25} for all the rods.

TABLE 6.3

The Relative Values of η_8

Fuel Rod	η_8 Relative to 1.61% Enriched Fuel Rod	
	Measured	Calculated*
2%	1.264 ± 0.089	1.247
1.3%	0.820 ± 0.049	0.805
1.1%	0.657 ± 0.052	0.680

*Calculated from $(N_5^x/N_5^s)(N_8^s/N_8^x)$ where the values of N were taken from the data given by the fuel fabricator.

6.4 FEASIBILITY OF AN IN-CORE GAMMA-RAY SPECTROMETER FOR THE MIT EXPONENTIAL FACILITY

Based on the results of the last three sections, it is strongly suggested to explore further the applicability of using in-core gamma-ray spectroscopy in order to measure the fission neutron yield parameter and the initial conversion ratio for a single rod located at the center of an exponential facility.

Technical difficulties in the past have resulted in neglecting this field in favor of external measurement of an emergent beam. The only accessible literature on in-core gamma-ray spectroscopy was the work of Andrews et al. (A1) who investigated the identification of several gammas coming from a heavy water lattice by using a small NaI crystal. With the improvement in the detection methods by using Ge(Li) detectors and pair-spectrometers, there is now a much better prospect of making meaningful measurements of this type.

In this section is presented a conceptual design of a gamma-ray spectrometer capable of operating in the triple coincidence mode to detect prompt gammas coming from a single fuel element placed in an exponential facility.

6.4.1 The Present MIT Exponential Facility

The MITR exponential facility has been amply described in several previously published reports (P1, D2). The primary source of neutrons for the exponential facility is the MIT Research Reactor, presently operating at a nominal power level of 5 MW. The exponential facility assembly consists of a cylindrical aluminum tank which may be

filled with heavy water and into which any number of fuel rods, up to a complete subcritical reactor lattice, may be inserted. Figure 6.1 is a cross section view of the exponential facility. The exponential assembly is fed from the bottom by neutrons which originate in the MIT Reactor, pass through its horizontal thermal column, and thence into a graphite-lined cavity or "hohlraum" beneath the exponential tank. The hohlraum serves both to direct the horizontal current of neutrons upward into the exponential tank and to assure that the energy spectrum of the source neutrons is highly thermal. The main body of the exponential facility consists of a cylindrical tank 70 inches high and 4 feet in diameter, and its sides are covered with cadmium sheet, 0.020 inch thick in order to reduce the thermal flux to zero at the (extrapolated) outer boundary. An 8-foot-diameter movable lid above the tank prevents contamination of the heavy water by the moisture in the air, and it is also cadmium-lined. The exponential tank is removable so that different sized tanks may be used, and it is contained in a 72-inch-diameter outer tank fixed to the external biological shield of the facility. The space between the exponential tank and the outer tank can be filled to permit eventual use of radial reflectors or external poison regions, but so far it has been maintained as a 1-foot-thick voided annulus.

It is quickly realized that the main problem for the proposed gamma spectrometer would be the high ambient background in the tank and vicinity. A survey of the gamma-ray dose inside the exponential tank and in the empty region between the exponential tank and the outer tank during the operation of the facility was carried out by Sicilian (S2). He identified also the main sources of these backgrounds. In brief,

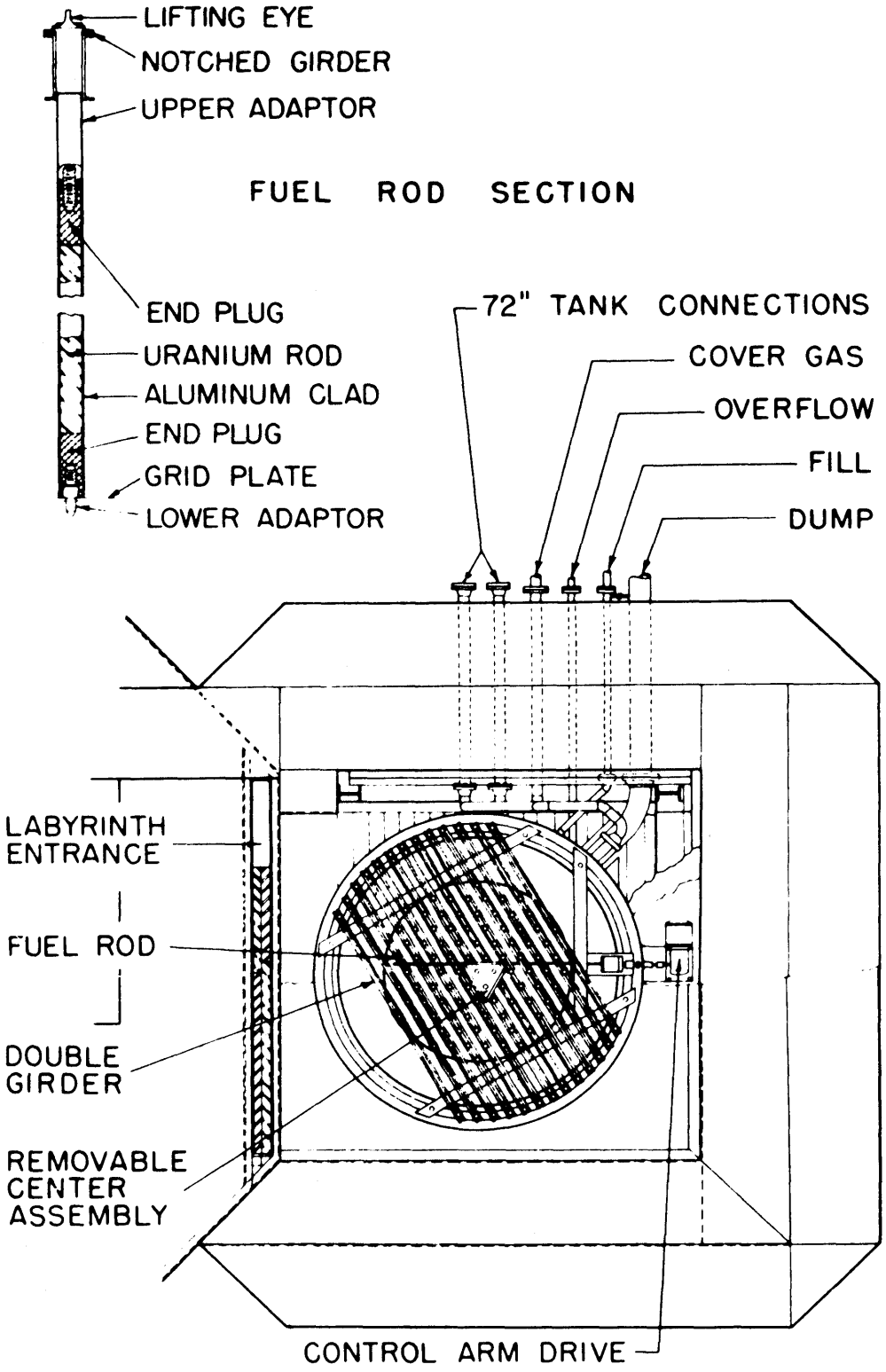

FIG. 6.1 PLAN VIEW OF THE PRESENT EXPONENTIAL FACILITY OF M.I.T. RESEARCH REACTOR

there are three gamma background sources. In order of decreasing importance, they are: hohlraum gammas, cadmium capture gammas, and moderator capture gammas. The sum of the effects from all three sources gave a dose of 500 to 1000 Roentgens per hour in the annulus region, halfway between the bottom and the top of the tank. The dose inside the hohlraum was measured to be about 6000 R/hr. Inside the exponential tank, close to its center, when filled with heavy water and under normal operating conditions the measured dose was about 10 R/hr with the dosimeter encased inside a lead block with 2-inch-thick walls.

6.4.2 The Proposed Gamma Spectrometer

In this conceptual design of a gamma spectrometer operating in connection with the exponential facility, economic boundaries, or optimization, have not been considered. The proposed design takes into account the experience gained from the external and internal sample irradiation facilities designed and operated during the last four years at the MIT Reactor facility. Obviously, there are many alternative conceptual designs that could be proposed.

The first measure for consideration is to lower to a minimum the source strength of the background gammas. In order to accomplish this, it is necessary to substitute all the cadmium absorber sheets in the exponential facility by 1.6-cm-thick LiF sheets wherever possible and by 1/4-inch-thick boral sheets in the remaining places. The LiF sheets are by far the best neutron absorbers with respect to gamma-ray production. A sheet of 1.6-cm-thick LiF, viewed by the Ge(Li) detector and placed in the irradiation position, attenuates thermal

neutrons by a factor of about 10^5, yielding almost no gammas. Only a weak contribution from the 7246.7-keV gamma from Li is visible. Boral has a disadvantage over LiF, since it produces an extremely strong gamma ray of 480 keV with a 755-barn cross section, which comes from the excited level of Li resulting from the thermal neutron interaction with B^{10}. Nevertheless, because of the low energy of these gammas, it is relatively easy to attenuate them by using lead.

The best gamma shielding material for gamma spectroscopy purposes is lead. It has one strong capture gamma at a well-established energy of 7367.7 keV which could eventually be used for energy calibration purposes. Bismuth also is a good material, considering its capture cross section which is five times smaller than that of lead, but it has several prominent lines in the region of 4 MeV and is more expensive than lead.

Figure 6.2 presents the plan view of the proposed conceptual design. The spectrometer itself is encased in a "gun barrel" gamma shield that fits in one corner of the present exponential facility room.

The height of the proposed gamma beam is 2 feet above the bottom level of the 4-foot-diameter exponential tank. The estimated thermal neutron flux at the bottom of the tank is 5×10^9 n/cm^2-sec, and it decreases exponentially roughly as $e^{-0.05h}$, where h is the distance in centimeters from the bottom when the tank is filled with heavy water and in operation. Thus, at 2 feet from the bottom, the thermal neutron flux is estimated to be 4×10^8 n/cm^2-sec which is the same as the flux available at the external front irradiation facility described in Chapter II.

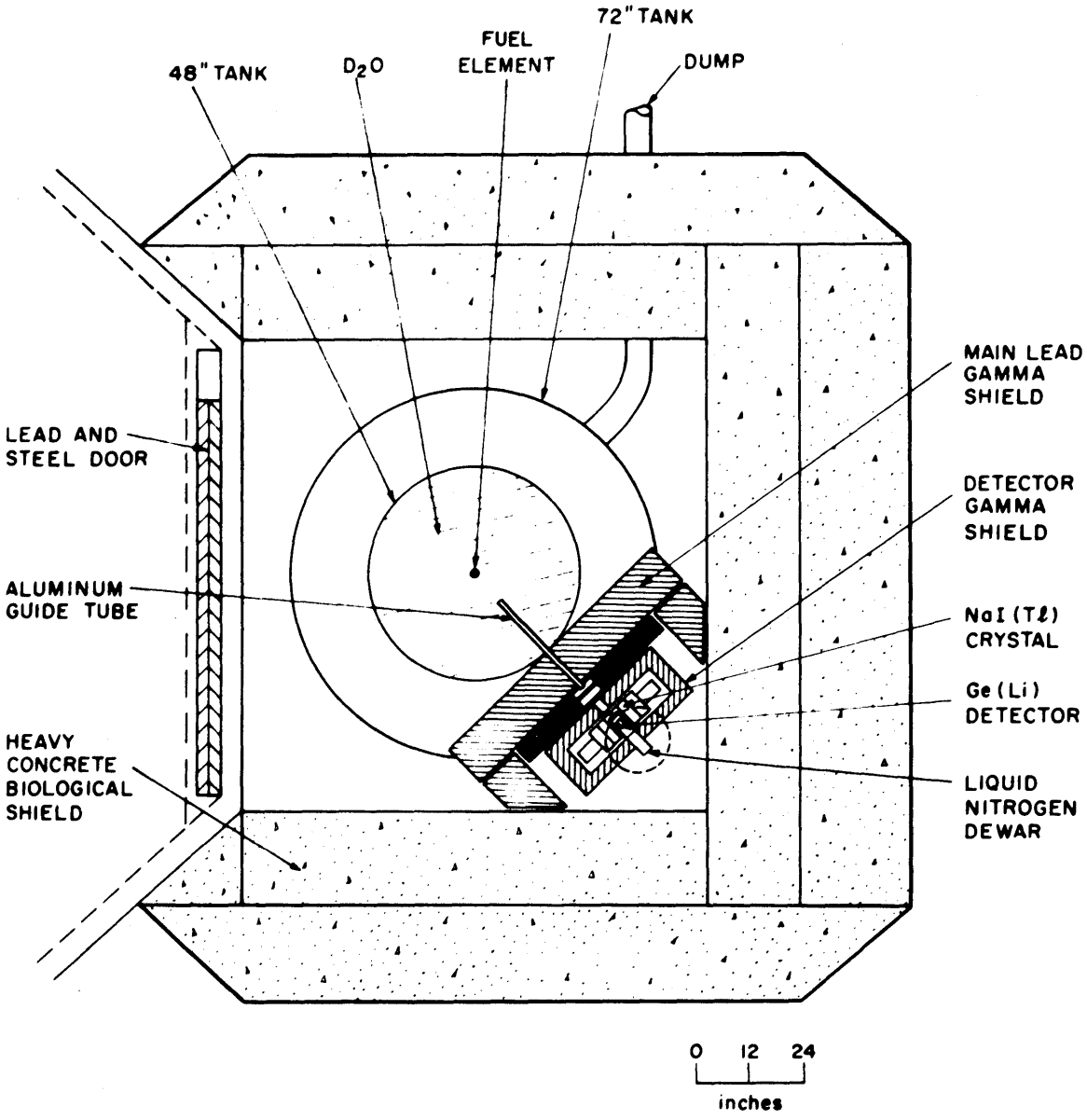

FIG. 6.2 PLAN VIEW OF THE PROPOSED GAMMA SPECTROMETER OPERATING IN THE M.I.T. EXPONENTIAL FACILITY

The distance between the single fuel element and the Ge(Li) detector is 38 inches which is about the same as for the external facility. It is suggested, nevertheless, that this distance could be varied by mounting the entire spectrometer on a movable table with wheels on fixed tracks, in order to keep open the possibility for changing the total detection efficiency according to the fuel gamma strength and the background. The two NaI(Tl) crystals of 6-inch diameter are mounted inside a 6-1/2-inch i.d. and 12-inch o.d. gun barrel that serves as a gamma shield and as a rigid base for mounting and aligning the sodium crystals and the Ge(Li) detector snout. At one side of the gun barrel there is a 2-1/8-inch hole through which the Ge(Li) detector snout is inserted horizontally. The crystal has a vertical liquid nitrogen (LN) container, and it is designed to provide a hollow LN-filled bent finger that has a detector-mount assembly that lies in the horizontal plane. In this fashion, the head of the preamplifier can be connected close to the detector at the corner region of the bent snout.

A long and thin aluminum guide tube with low pressure inside and sealed on both ends conducts the gamma beam from the fuel element to the detector. It penetrates the heavy water tank, leaving a few inches of heavy water in the path of the gamma beam between one end of the tube and the fuel rod under irradiation. This amount of heavy water in the gamma beam would play the same role as borated paraffin, described in section 4.3. The thickness of this shield can be determined from preliminary feasibility experiments performed at the external irradiation facility by measuring the attenuation of fission neutrons and gamma rays as a function of the thickness of heavy water in the gamma

beam. Close to the detector and still in the gamma beam, there is an opening into which can be inserted extra shielding plates such as lead and LiF to protect the detector from thermal neutrons and undesired gammas. A series of lead collimators defining the gamma beam restrict the view of the detector only to a portion of the fuel rod.

The gun barrel containing the detector assembly is located close to the edge of the 72-inch tank, which was cut out to fit the gun barrel. The detector assembly has a gamma shield made up of 7-inch-thick lead to give further protection against the gammas from the 48-inch tank. Below the detector, 1 foot of heavy concrete plus 1 foot of lead serve as a shield against the hohlraum gammas.

The signals from the detector, after preamplification, are sent through a set of cables to the outside of the exponential facility where the electronic assembly is located.

It is felt that an in-pile spectrometer of the type suggested above would be capable of interrogating a fuel element during irradiation and could therefore serve as the basis for a new approach to experimental reactor physics studies.

Chapter VII

CONCLUSIONS AND RECOMMENDATIONS

7.1 CONCLUSIONS

This present work was a study of the gamma rays emitted by the products of the interaction of thermal neutrons with the nuclei of U^{238}, Th^{232}, U^{235} and Pu^{239}, during and after the irradiation. The use of these gammas for fuel rod assay was also explored.

A method of assaying fuel rods containing a mixture of plutonium (about 0.25% of Pu^{239}) and uranium oxide (0.30% of U^{235}), based on the difference in the observable yield of the fission products I^{135} and Sr^{92}, was developed. This method required the use of a standard rod (1.30% of U^{235}) and a set of two calibrating foils, one containing only plutonium and another only uranium; an accuracy ranging from ±6% to ±10% was proven to be possible for determining the Pu and U content in a day of work.

The energies and intensities of the thermal neutron capture gamma rays for U^{238} and Th^{232} were determined. Compton suppression and triple coincidence modes of operation were used in low and high energy regions, respectively. A few new lines have been found for U^{238} in the energy region previously unexplored. In the case of Th^{232}, 66 lines were observed compared to the 7 lines reported in the literature.

The prompt gammas emitted by the highly excited fission products following the fission of U^{235} and Pu^{239} were resolved in the energy

region above 1.4 MeV. For U^{235} fissions, 57 certain lines were found, and for Pu^{239}, 51 certain lines were recorded. Most of these gammas were present in both the spectra of U^{235} and Pu^{239}. It was concluded that the majority of these gammas are fission gammas emitted soon after the boil-off of the prompt neutrons, within 10^{-6} sec after the fission by the de-excitation of the fission fragments. The number of prompt gammas per fission, above 1.4 MeV, was found to be 35% greater for U^{235} fissions than for Pu^{239} fissions. A few of these gammas might come from short-lived fission product decays; however, the transitions found in the spectrum of one fissile nuclei but not found in the spectrum of another were assigned tentatively as due to capture gammas (3 lines for U^{235} and 10 lines for Pu^{239}).

Fission gammas were used for assaying a plutonium-uranium oxide rod containing 0.25% of Pu^{239} and 0.30% of U^{235} in weight. An accuracy of ±7% was obtained for the analysis of U^{238} content, and 10% to 20% accuracy was obtained for U^{235} and Pu^{235} compared to the manufacturing analysis.

It was found that Ge(Li) detectors can be used as energy threshold neutron detectors, and by operating as such they could be used to determine the relative fission neutron yield. With this method, the enrichment of uranium rods can be found with an accuracy of ±1% to ±2% in the range of 1% to 2% enrichment.

The feasibility of using prompt gammas for the measurement of the initial conversion ratio C and the neutron yield parameter η in an exponential facility was studied. The results obtained suggest strongly that an in-core gamma spectrometer operating in an exponential facility could yield these reactor physics parameters.

7.2 RECOMMENDATIONS

(1) It is suggested that future work investigate the possibility of using the Rh^{103}-La^{140} gamma rays instead of the I^{135}-Sr^{92} gamma rays. This new pair of fission products would be preferable because of their yield difference which is of the order of a factor of 10 compared to 2 for I^{135} and Sr^{92}. However, in this case a longer cooling time, of a few days, would be required.

For quicker analysis, it is recommended that a study of the use of all prominent peaks of the short-lived fission product spectra, as obtained in this present work, be undertaken in order to improve the statistics of counting and consequently the accuracy of the present method. A careful analysis of the correction factors would be necessary.

It is suggested that the use of the present method for detecting nonuniform distribution of fissile elements in plutonium-uranium rods be investigated.

It is also recommended that the present method be investigated for use in analyzing burned fuel rods. However, a neutron flux of the order of 10^{10} n/cm^2-sec would be necessary for reirradiation and analysis of a typical burned fuel rod.

(2) It is recommended that a study of the energy level structure for Th^{233} be undertaken by complementing the data found in this work with a $Th^{232}(d, p)Th^{233}$ reaction study.

(3) It is recommended that the data of Pu^{239} prompt gammas be improved by using a sample containing a smaller amount of Pu^{239} than the present work in order to lower the count rate, and so increase the resolution.

(4) The poor accuracy of the method of analysis of fuel rods using prompt gammas was due mainly to the small count rate, and consequently the poor statistics. It is recommended that this method be used with a more favorable geometrical arrangement, with a larger detection solid angle and a greater detector efficiency in order to improve the statistics of counting.

(5) It is recommended that consideration be given to the use of Ge(Li) detectors as fission neutron detectors for the determination of Pu^{239} content of spent fuel. This method would require incident neutrons of two different energies in order to distinguish U^{235} from Pu^{239} by differences in the fission cross section as a function of energy.

(6) It is recommended that the feasibility study of an in-core gamma spectrometer be followed by actual construction of a spectrometer to operate in the MITR Exponential Facility.

Finally, it is recommended that the use of gamma-ray spectroscopy of fuel elements be extended to many still unexplored applications for the measurement of reactor physics parameters and that special consideration be given to the use of prompt gammas for measurements involving burned fuel rods.

Appendix A

REFERENCES

A1 D. G. Andrews and T. A. Khan, "Gamma-Ray Measurements Inside a Natural Uranium Heavy-Water Lattice," Trans. Am. Nucl. Soc., Vol. 8, No. 1, 279 (1965).

B1 G. A. Bartholomew and P. J. Campion, "Symposium on Physics Research with Pile Neutrons," IAEA, Vienna (1960).

B2 G. A. Bartholomew, A. Doveika, K. M. Eastwood and S. Monaro, "Compendium of Thermal-Neutron-Capture Gamma-Ray Measurements," Part I, Nucl. Data, Section A, Vol. 3, Nos. 4-6 (December 1967).

B3 N. P. Bauman et al., "Lattice Experiments with Simulated Burned Fuel for D_2O Power Reactors," DP-1122 (February 1968).

C1 L. A. Currie, "Limits of Qualitative Detection and Quantitative Determination," Anal. Chem., Vol. 40, No. 3, 586 (1968).

D1 F. Depisch, H. Hick and P. Weinzierl, "Neutronen-Transmissionsmethode zur zerstorungsfreien Bestimmung von Pu-Isotopen in Brennelementen," Acta Physica Austriaca, 25.Band, 3.Heft, 279 (1967).

D2 W. H. D'Ardenne, T. J. Thompson, D. D. Lanning and I. Kaplan, "Studies of Epithermal Neutrons in Uranium Heavy Water Lattices," MIT-2344-2, MITNE-53, Dept. of Nucl. Eng., M.I.T. (August 1964).

D3 R. D. Donovan, "Determination of the Heterogeneous Parameters Γ, A and η by Measurements on Single Fuel Element," M.S. Thesis, Dept. of Nucl. Eng., M.I.T. (1967).

E1 R. R. Edwards, "A Review of Recent Studies of Non-Destructive Assay Methods for Irradiated Nuclear Fuels," Nucl. Applications, Vol. 4 (April 1968).

F1 R. S. Forsyth and N. Ronqvist, "Burnup Determination by High Resolution Gamma Spectroscopy: Spectra from Slightly Irradiated Uranium and Plutonium Between 400-830 keV," AE-241 (August 1966).

F2 J. S. Fraser and J. C. D. Milton, "Nuclear Fission," Ann. Rev. Nucl. Sc., Vol. 16 (1966).

F3 J. S. Fraser, "The Angular Distribution of Prompt Neutrons Emitted in Fission," Phys. Rev., Vol. 88, 536 (1952).

G1 G. E. Gordon, J. W. Harvery and H. Nakahara, "Measuring Fission Spectra with Semiconductor Detectors," Nucleonics, No. 12, 62 (December 1966).

G2 L. V. Groshev et al., "Atlass of Gamma-Ray Spectra from Radiative Capture of Thermal Neutrons," English translation by J. B. Sykes, Pergamon Press, London (1959).

G3 R. C. Greenwood and J. H. Reed, "Prompt Gamma-Rays from Radiative Capture of Thermal Neutrons," Report No. IITRI-1193-53 (1965).

G4 J. J. Griffin, "Beta Decay and Delayed Gammas from Fission Fragments," Phys. Rev., Vol. 134, No. 4B, 817 (May 1964).

G5 L. V. Groshev et al., "Compendium of Thermal-Neutron-Capture Gamma-Ray Measurements," Part III for $Z = 68$ to $Z = 94$, Nucl. Data, Section A, Vol. 5, No. 3-4 (February 1969).

G6 R. C. Greenwood and J. Reed, "Scintillation Spectrometer Measurements of Capture Gamma-Rays from Natural Elements," Proc. Mod. Trends in Act. Anal., 1961, International Conference, College Station, Texas (December 1961).

H1 R. L. Heath, "The Potential of High Resolution Gamma-Ray Spectrometry for the Assay of Irradiated Reactor Fuel," Proceedings of Symp. Safeguards Res. Devel., WASH-1076, 115 (1967).

H2 T. L. Harper and N. C. Rasmussen, "Determination of Thermal Neutron Capture Gamma Yields," MITNE-104, Subcontract No. 6017, GGA Contract No. DASA 01-69-C-0151, Vol. 1 (1969).

H3 J. N. Hamawi and N. C. Rasmussen, "Investigation of Elemental Analysis Using Neutron-Capture Gamma-Ray Spectra," MITNE-107, U.S. Bureau of Mines Contract No. H0180895 (1969).

H4 J. N. Hanson, "Investigation of High Resolution Gamma-Ray Spectrometer," S.M. Thesis, Dept. of Nucl. Eng., M.I.T. (1965).

H5 R. Heath et al., "Instrumental Requirements for High-Resolution Gamma-Ray Spectrometry Using Lithium-Drifted Germanium Detectors," IEEE Trans. Nucl. Sc., NS-13, 445 (June 1966).

H6 T. L. Harper, T. Inoue and N. C. Rasmussen, "GAMANL, A Computer Program Applying Fourier Transforms to the Analysis of Gamma Spectral Data," MIT-3944-2, MITNE-97 (August 1968).

H7 F. Hoffman, "The Application of Pulsed Neutron Techniques to the Measurement of Inelastic Scattering Cross Sections," Ph. D. Thesis, Dept. of Nucl. Eng., M.I.T. (1966)

I1 T. L. Isenhour and G. H. Morrison, "Modulation Technique for Neutron Capture Gamma-Ray Measurement in Activation Analysis," Anal. Chem., Vol. 38, 2, 162 (February 1966).

J1 D. W. Jones, P. R. Malmberg, T. H. May and C. V. Strain, "Nondestructive Assay of Fissionable Materials," Nucl. Appl. and Tech., Vol. 8, No. 1 (January 1970).

K1 G. R. Keepin, "Nondestructive Detection, Identification and Analysis of Fissionable Materials," Proc. Symp. Safeguards Res. Dev., WASH-1076, 150 (1967).

K2 H. W. Kraner, C. Chasman and K. W. Jones, "Effects Produced by Fast Neutron Bombardment of Ge(Li) Gamma-Ray Detectors," Nucl. Instr. and Meth., Vol. 62, 173 (1968).

M1 B. P. K. Maier, "Bestimmung des (631) K=1/2, I=1/2-Zustendes im U-239," Zeits. fur Physik 184, 143 (1965).

M2 W. J. McGonnagle, "Nondestructive Reactor Fuel Assay," Proc. Symp. Safeguards Res. Dev., WASH-1076, 96 (1967).

M3 C. E. Miner, "A Semiconductor Detector Cryostat," Nucl. Instr. and Meth., 55, 125 (1967).

M4 C. Maples, G. W. Goth and J. Cerny, "Nuclear Reaction Q-Values," Nucl. Data, Section A, Vol. 2, Nos. 5-6 (December 1966).

M5 J. H. E. Mattauch, W. Thiele, "Consistent Set of Q-Values," Nucl. Phys., 67, 32 (1965).

M6 F. C. Maienschein et al., "Gamma Rays Associated with Fission," Proc. Intern. Conf. Peaseful Uses of At. Energy, 2nd, Geneva, 15, 366 (1958).

M7 H. Maier-Leibnitz et al., Symp. Phys. and Chem. of Fission, IAEA, II, 113 (1965).

M8 J. B. Marion, "Gamma-Ray Calibration Energies," Nucl. Data, A4, 301 (1968).

N1 F. Netter et al., "Origine d'un Rayonnement Gamma Intense Lié à l'Absorption de Neutrons Lents par l'Uranium 235," Comptes Rend., 252, 1759 (1961).

O1 N. Oi et al., "Gamma-Ray Spectra of Fission Products Observed with Li-Drifted Germanium Detectors (II), Journ. Nucl. Sc. and Tech., 4, No. 7, 372 (July 1967).

O2 V. J. Orphan and N. C. Rasmussen, "Study of Thermal Neutron Capture Gamma-Rays Using a Lithium-Drifted Germanium Spectrometer," Contract No. AF19(628)5551, MITNE-80, Dept. of Nucl. Eng., M.I.T. (1965).

P1 E. E. Pilat, M. J. Driscoll, I. Kaplan and T. J. Thompson, "The Use of Experiments on Single Fuel Element to Determine the Nuclear Parameters of Reactor Lattices," MIT-2344-10, MITNE-81, Dept. of Nucl. Eng., M.I.T. (1967).

R1 N. C. Rasmussen, Y. Hukai, T. Inoue, and V. J. Orphan, "Thermal Neutron Capture Gamma-Ray Spectra of the Elements," MITNE-85 (1969).

R2 N. C. Rasmussen, "The Nondestructive Analysis of Spent Reactor Fuel by Gamma-Ray Spectroscopy," Proc. Symp. Safeguards Res. Dev., WASH-1076, 130 (1967).

R3 B. F. Rider et al., "A Survey and Evaluation of Thermal Fission Yields for U-235, Pu-239, U-233, and Pu-241," GEAP-5356 (March 1967).

R4 N. C. Rasmussen and Y. Hukai, "The Prompt Activation Analysis of Coal Using Neutron Capture Gamma-Rays," Trans. Am. Nucl. Soc., Vol. 10, No. 1, 29 (June 1967).

S1 R. K. Sheline, W. N. Shelton, T. Udagawa, E. T. Turney and H. T. Motz, "Levels in U^{239}," Phys. Rev., 151, No. 3, 1011 (November 1966).

S2 J. M. Sicilian, "The Feasibility of Gamma-Ray Spectroscopy in an Exponential Facility," B.S. Thesis, M.I.T., Dept. of Nucl. Eng. (1969).

S3 J. A. Sovka and N. C. Rasmussen, "Nondestructive Analysis of Irradiated MITR Fuel by Gamma-Ray Spectroscopy," Ph. D. Thesis, Dept. of Nucl. Eng., M.I.T. (1965).

S4 S. S. Seth, L. N. Price and M. J. Driscoll, "Measurement of Integral Parameters," Heavy Water Lattice Project Annual Report, MIT-2344-9, MITNE-79, Chapter 3 (September 1966).

T1 J. Turkstra, W. M. Steyn and W. T. DeWett, "The Rapid Determination of U^{235}/U^{238} Ratios by Activation Analysis Utilizing High Resolution Gamma-Spectrometry," Nucl. Instr. Meth., No. 63, 269 (1968).

T2 M. R. Trammel and W. A. Henninger, "Nuclear Data Library for the Fission Product Program," Astronuclear Lab., Westinghouse, WANL-TME-574 (November 1966).

W1 R. R. Wilson, "Directional Properties of Fission Neutrons," Phys. Rev. 72, 189 (1947).

Z1 J. W. Zink and G. W. Rodeback, "The Determination of Lattice Parameters by Means of Measurements on a Single Fuel Element," Nucl. Sc. Eng., 9, 16 (1961).

Appendix B

COMPUTER CODE FUEL ASSAY

FUEL ASSAY performs the calculation of Eqs. 3.27 and 3.28 which gives the ratio of the number of Pu^{239} and U^{235} atoms in an unknown fuel rod to the number of U^{235} atoms in the standard rod according to the method described in Chapter III. It also gives the enrichment in weight percent according to Eqs. 3.22 and 3.23. The correction factors are calculated and taken into account. The values of the ratios R_1 and R_2 defined in Chapter III are assumed as known data.

```
      DIMENSION AX(20),EAX(20),AS(20),EAS(20),RSUM(2),D(2),RDT(2),
     1SIGMA(2),SUM(2),V(2),ERSUM(2)
      READ (5,106) R1,ER1,R2,ER2
C     R1=RATIO GIVEN BY EQ.3.16
C     ER1=ERROR CORRESPONDING TO R1
C     R2=RATIO GIVEN BY EQ.3.17
C     ER2=ERROR CORRESPONDING TO R2
      DO 1000 J=1,2
      READ (5,100) N
  100 FORMAT (I5)
C     N=NUMBER OF PEAKS FOR A FISSION PRODUCT
C     J=1 CORRESPONDS TO FISSION PRODUCT NUMBER 1
C     J=2 CORRESPONDS TO FISSION PRODUCT NUMBER 2
      READ (5,101) (AX(I),EAX(I),AS(I),EAS(I),I=1,N)
  101 FORMAT (4F10.1)
C     AX(I)=AREA OF PEAK FOR UNKNOWN ROD
C     EAX(I)=ERROR ACCOMPANYING AX(I)
C     AS(I)=AREA OF PEAK FOR STANDARD ROD
C     EAS(I)=ERROR ACCOMPAYING AS(I)
      SUMAX=0
      DO 102 I=1,N
  102 SUMAX=SUMAX+AX(I)
      SUMAS=0
      DO 103 I=1,N
  103 SUMAS=SUMAS+AS(I)
      RSUM(J)=SUMAX/SUMAS
      SUMQX=0
      DO 10 I=1,N
   10 SUMQX=SUMQX+EAX(I)**2
      SUMQS=0
      DO 11 I=1,N
   11 SUMQS=SUMQS+EAS(I)**2
      ESUMAX=SQRT(SUMQX)
      ESUMAS=SQRT(SUMQS)
      ERSUM(J)=RSUM(J)*SQRT((ESUMAX/SUMAX)**2+(ESUMAS/SUMAS)**2)
      READ (5,104) TL,TX,TS,D(J)
```

```
  104 FORMAT (3F10.3,F6.4)
C     CORRECTION DUE TO DEADTIME
C     TL=LIVETIME OF COUNTING (HOUR)
C     TX=ACTUAL COUNTING TIME FOR UNKNOWN ROD (HOUR)
C     TS=ACTUAL COUNTING TIME FOR STANDARD ROD (HOUR)
C     D(J)=DECAY CONSTANT (PER HOUR)
      A=-0.022
      B=0.223
      C1=TL/TX-A/3.*TX**2-B/2.*TX
      C2=TL/TS-A/3.*TS**2-B/2.*TS
      X1=2.*A+D(J)*B+C1*D(J)**2
      X2=2.*A+D(J)*B+C2*D(J)**2
      Y1=A*(1.+(1.+D(J)*TX)**2)+D(J)*B*(1.+D(J)*TX)+C1*D(J)**2
      Y2=A*(1.+(1.+D(J)*TS)**2)+D(J)*B*(1.+D(J)*TS)+C2*D(J)**2
      RDT(J)=(X2-Y2*EXP(-D(J)*TS))/(X1-Y1*EXP(-D(J)*TX))
      WRITE (6,105) RDT(J),J
  105 FORMAT ('1','CORRECTION FACTOR DUE TO DEADTIME=',F10.5,5X,'J=',I5)
  106 FORMAT (2(F10.4,F5.3))
      RSUM(J)=RSUM(J)*RDT(J)
      ERSUM(J)=ERSUM(J)*RDT(J)
 1000 CONTINUE
      RXS1=(RSUM(1)-RSUM(2))/(R1-R2)
      ENUM1=SQRT(ERSUM(1)**2+ERSUM(2)**2)
      EDEN1=SQRT(ER1**2+ER2**2)
      NUM1=RSUM(1)-RSUM(2)
      DEN1=R1-R2
      ERXS1=RXS1*SQRT((ENUM1/NUM1)**2+(EDEN1/DEN1)**2)
C     CORRECTION DUE TO NEUTRON MONITOR FOILS
      READ (5,107) FLUXS,FLUXX
  107 FORMAT (2E10.8)
C     FLUXS=INCIDENT FLUX FOR STANDARD ROD
C     FLUXX=INCIDENT FLUX FOR UNKNOWN ROD
C     PHISX=CORRECTION FACTOR
      PHISX=FLUXS/FLUXX
      WRITE (6,108)PHISX
  108 FORMAT ('1','CORRECTION FACTOR DUE TO NEUTRON MONITOR=',F10.5)
```

```
C      CORRECTION FACTOR DUE TO FLUX DEPLETION IN FUEL ROD
       READ (5,109) R,(SIGMA(K),K=1,2)
  109  FORMAT (3F10.4)
C      K=1 CORRESPONDS TO UNKNOWN ROD
C      K=2 CORRESPONDS TO STANDARD ROD
C      R=RADIUS OF FUEL ROD (CM)
C      SIGMA(1)=MACROSCOPIC ABSORPTION CROSS SECTION FOR UNKNOWN ROD
C      SIGMA(2)=MACROSCOPIC ABSORPTION CROSS SECTION FOR STANDARD ROD
       DO 1002 K=1,2
       NI=210
       SUM(K)=0
       DELY=R/NI
       NI=NI+1
       DO 1001 M=1,NI
       A1=SQRT(R**2-((M-1)*DELY)**2)
       SUM(K)=SUM(K)+EXP(-2.*SIGMA(K)*A1)*DELY
 1001  CONTINUE
       V(K)=2./SIGMA(K)*R-2./SIGMA(K)*SUM(K)
       NI=NI-1
 1002  CONTINUE
       F=V(2)/V(1)
       WRITE (6,110) F
  110  FORMAT ('1','CORRECTION DUE TO NEUTRON DEPLETION=',F10.5)
C      RATIO OF NUMBER OF ATOMS OF PU-239 IN UNKNOWN ROD TO THE
C     1NUMBER OF ATOMS OF U-235 IN STANDARD ROD
       RPUXS=RXS1*PHISX*F
       ERPUXS=ERXS1*PHISX*F
       WRITE (6,111) RPUXS,ERPUXS
  111  FORMAT ('1','NX9/NS5=',F10.5,2X,'ERROR=',F7.5)
       RXS2=(R1*RSUM(2)-R2*RSUM(1))/(R1-R2)
       EP1=SQRT((ER1/R1)**2+(ERSUM(2)/RSUM(2))**2)*R1*RSUM(2)
       EP2=SQRT((ER2/R2)**2+(ERSUM(1)/RSUM(1))**2)*R2*RSUM(1)
       ENUM2=SQRT(EP1**2+EP2**2)
       NUM2=R1*RSUM(2)-R2*RSUM(1)
       ERXS2=SQRT((ENUM2/NUM2)**2+(EDEN1/DEN1)**2)*RXS2
       WRITE (6,2000) ERXS2
```

```
C      RATIO OF NUMBER OF ATOMS OF U-235 IN UNKNOWN ROD TO THE
C     1NUMBER OF ATOMS OF U-235 IN STANDARD ROD
       RUXS=RXS2*PHISX*F
       ERXS=ERXS2*PHISX*F
       WRITE (6,112) RUXS,ERXS
  112  FORMAT ('1','NX5/NS5=',F10.5,3X,'ERROR=',F7.5)
C      ENRICHMENT OF UNKNOWN ROD IN WEIGHT PERCENT
       READ (5,113) ES,DS,DX
  113  FORMAT (3F10.4)
C      ES=ENRICHMENT IN WEIGHT PERCENT OF STANDARD ROD
C      DS=DENSITY OF STANDARD ROD
C      DX=DENSITY OF UNKNOWN ROD
       EX9=ES*RPUXS*239./235.*DS/DX
       EX5=ES*RUXS*DS/DX
       EEX5=ES*DS/DX*ERXS
       EEX9=ES*239./235.*DS/DX*ERPUXS
       WRITE (6,114) EX9,EEX9,EX5,EEX5
  114  FORMAT ('1','ENRICHMENT IN WEIGHT PERCENT DUE TO PU=',F6.3,
      13X,'ERROR=',F6.3,/'ENRICHMENT IN WEIGHT PERCENT DUE TO U-235=',
      1F6.3,3X,'ERROR=',F6.3)
       CALL EXIT
       END
```